Shannon-Kotel'nikov Mappings for Analog Point-to-Point Communications

Pål Anders Floor, Tor A. Ramstad,

***Abstract*—In this paper an approach to joint source-channel coding (JSCC) named Shannon-Kotel'nikov (S-K) mappings is discussed. S-K mappings are continuous, or piecewise smooth direct source-to-channel mappings operating on amplitude-continuous and discrete-time signals, and they encompass several existing JSCC schemes as special cases. Many existing approaches to analog- or hybrid discrete-analog JSCC provide both excellent performance as well as robustness to variable noise level at both low and arbitrary complexity and delay. However, a general theory explaining their performance and behaviour, as well as guidelines on how to construct well-performing mappings, do not exist. Therefore, such mappings are often based on educated guesses inspired by configurations that are known in advance to produce good solutions through numerical optimization methods. The objective of this paper is to develop a theoretical framework for analysis of analog- or hybrid discrete-analog S-K mappings which enables calculation of distortion when applying them on point-to-point links, reveal more about their fundamental nature, and provide guidelines for their construction at low as well as arbitrary complexity and delay. Such guidelines will likely help constrain solutions to numerical approaches and help explain why deep learning approaches obtain the solutions they do. The overall task is difficult and we do not provide a complete framework at this stage: We focus on high SNR and memoryless sources with an arbitrary continuous unimodal density function and memoryless Gaussian channels. We also provide example mappings based on surfaces which are chosen, or constructed, based on the provided theory.**

***Index Terms*—Joint source channel coding, analog mappings, distortion analysis, differential geometry, OPTA.**

I. Introduction

OVER the last decades attention has been directed towards miniature devices, for example in-body sensors and miniature electronic modules replacing neural network function in the brain. For this reason, and several others, it has become important to study communication systems with low complexity and delay with the highest possible performance.

In this paper we investigate a broad set of analog or *hybrid discrete-analog* (HDA) joint source-channel coding (JSCC) schemes named *Shannon-Kotel'nikov mappings* (S-K mappings). S-K mappings operate directly on analog information sources and are known to perform well at low complexity and delay when carefully constructed [4], [5], [6], [7], [8].

Shannons' *separation theorem* or *information transmission theorem* (see [9, pp. 224-227]) for communication of a single source over a point-to-point link states that source- and channel coding can be performed separately, without any loss compared to a joint technique. To prove that separation is optimal, arbitrary complexity and delay is assumed. With a constraint on complexity and delay, separate source and channel coding (SSCC) does not necessarily result in the best possible performance, as some examples illustrate: It was shown in [10], [11] that for an independent and identically distributed (i.i.d.) source and an additive white Gaussian noise (AWGN) channel, both of the same bandwidth, the information theoretical bound[1], *optimal performance theoretically attainable* (OPTA), is achieved by a simple linear source-channel mapping operating on a symbol-by-symbol basis. This result was generalized in [11], [12] to special combinations of correlated sources and channels with memory. Furthermore, it was shown in [13], that with an ideal feedback channel, OPTA is achieved when the channel-source bandwidth ratio is an integer. This was extended to simple sensor networks in [14] as well as noisy feedback in [15]. However, with limited or no feedback, the asymptotic bounds cannot be obtained at finite complexity and delay when source and channel are of different bandwidth or dimension, or in general, when the source and channel are not *probabilistically matched* [16]. An open question is what the best possible performance is under complexity and delay constraints. Efforts dealing with this issue are Kostina and Verdú [17] and Merhav [18], [19].

Several analog and semi-analog JSCC schemes for the bandwidth mismatch case, operating at low and arbitrary complexity and delay, have been suggested in the literature: The *analog matching* scheme in [20] is a structured semi-analog approach built on *lattices* that achieves OPTA in the limit of infinite complexity and delay for any colored Gaussian source transmitted on any colored Gaussian channel. However, the performance of analog matching scheme in the finite complexity and delay regime is, to our knowledge, unknown at present. Efforts dealing with this problem using HDA schemes are [21] and [22], the latter considering the broadcast problem. Schemes that are known to perform well at low complexity and delay are the HDA approaches in [4], [23], [24], [25], certain analog mappings like the *Archimedes Spiral* [26], [27], [28] and mappings found by deep learning in [8], [29].

The approach to JSCC studied in this paper, namely S-

NOTE: The final printed version of this paper appears in IEEE Transactions on Information Theory, Vol. 70, No. 4, April 2024, and can be found here: https://ieeexplore.ieee.org/document/10189867

This work was supported by NTNU via the project CUBAN and the Research Council of Norway (NFR) via the projects MELODY no. 187857/S10 and CAPSULE no. 300031.

P. A. Floor is with the Colourlab, Department of Computer Science, Norwegian University of Science and Technology (NTNU), Gjøvik, Norway (e-mail: paal.anders.floor@ntnu.no). T. A. Ramstad is Prof. Emeritus at the Department of Electronic Systems, Norwegian University of Science and Technology (NTNU), Trondheim, Norway (e-mail: torramstad@gmail.com).

Parts of this paper have previously been presented at SPAWC 2006 [1], NORSIG 2006 [2] and ITW 2007 [3].

[1]By *information theoretical bound* we refer to a bound derived assuming no restriction on complexity and delay.

K mappings, is inspired by many earlier efforts: First of all, Shannon suggested using continuous mappings through space-curves as a way of getting close to the information theoretical bounds [30]. Simultaneously, Kotel'nikov developed a theory for analyzing distortion of amplitude-continuous and time-discrete systems realized as parametric curves in N dimensions in [31]. These are basically bandwidth- or dimension expanding systems with *pulse-position modulation* as a special case. The efforts of Goblick [10], Berger et al. [11] Ziv [32] and Vaishampayan [33], [34] are pioneering works on the subject. The effort by Gastpar et. al. [16] is another important contribution and Merhav's efforts [18], [19] provides insight into the workings of such schemes through analysis based on statistical mechanics. Other important works include *power-constrained channel-optimized vector quantizers* (PCCOVQ) [33], [35], [36], the HDA schemes in [4], [23], [24], the linear *block pulse-amplitude modulation* (BPAM) scheme in [37] and the use of parametric curves for both bandwidth expansion [34] and compression [26], [27]. Other efforts dedicated to analog or semi-analog mappings 'are [5], [6], [7], [8], [38], [39], [40], [41], [42]. These efforts illustrate that such schemes perform well at low complexity and delay, some providing excellent performance not matched by any other known scheme.

Besides Goblikc's [10], Ziv's [32], Gastpar's [16] and Merhav's approaches [18], [19], there are, as far as we know, no theory to analyze such mappings nor guideline their construction on a general basis. The objective of this paper is to introduce a theoretical framework based on *differential geometry*, encompassing most analog and HDA schemes. This approach seeks to complement the above mentioned approaches. The proposed framework facilitate calculation and analysis of the overall distortion in order to reveal the fundamentals of S-K mappings, as well as guideline their construction towards well performing mappings. The reason for developing a theory is to gain knowledge on how to optimally construct such mappings, not having to rely solely on educated guesses, numerical optimization sensitive to initial conditions, or deep learning approaches in which little is known about why certain results are produced.

Treating nonlinear mappings on a general basis is difficult, and we do not present a complete framework at this point, rather introduce a set of necessary tools providing insights into the construction of S-K mappings. We limit the treatment to memoryless, independent analog sources drawn from an arbitrary unimodal density function. The sources are transmitted on memoryless, independent Gaussian point-to-point channels. Most of the results provided are proven under the assumption of *high* signal-to-noise ratio (SNR). Generally, S-K mappings apply when the channel-source dimension (or bandwidth) ratio is a positive rational number. We focus on low complexity and delay but also consider how S-K mappings perform when their *dimensionality* increase. That is, what gains may be obtained if we increase the mappings dimension to code blocks of samples, ultimately by letting mapping dimensionality go to infinity. When analysing distortion behaviour of such mappings, we also consider how mapping curvature affects their performance. To keep the treatment as general as possible, all results are provided without reference to a specific mapping realization. Finally, we consider mapping construction by providing specific examples focusing on surface-based mappings chosen or constructed based on the provided theory. We also illustrate the gain obtained by increasing mapping dimensionality for a particular type of piecewise smooth (HDA) mapping for dimension expansion.

The paper is organized as follows: In Section II the problem is formulated, *OPTA* is introduced, S-K mappings are defined and key concepts from differential geometry are presented. In Section III a distortion framework for S-K mappings based on concepts from differential geometry is developed and guidelines for their construction are given. In Section IV asymptotic analysis is considered and it is shown under which conditions S-K mappings may achieve OPTA for Gaussian sources. Section V deals with construction of S-K mappings to illustrate some of the theory developed in preceding sections. In Section VI a discussion is given.

II. Problem formulation and preliminaries

Fig. 1 shows the communication systems under consideration. The terminology will be explained throughout this section and in Section III.

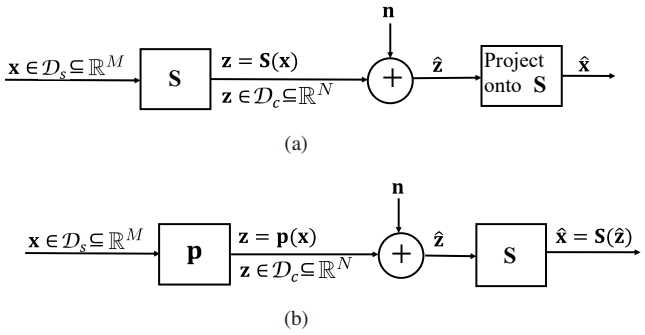

Fig. 1. Communication systems under consideration: (a) Dimension expansion ($M < N$). (b) Dimension reduction ($M > N$).

Assume a source $\mathbf{x} \in \mathcal{D}_s \subseteq \mathbb{R}^M$, drawn from a continuous unimodal probability density function (pdf) $f_{\mathbf{x}}(\mathbf{x})$, with i.i.d. components x_i. $\mathbf{x}$ is encoded to a vector $\mathbf{z} \in \mathcal{D}_c \subseteq \mathbb{R}^N$, which is transmitted on a memoryless channel with average power P, i.e., $1/N \sum_{i=1}^{N} E\{z_i^2\} \leq P$, and additive Gaussian noise $\mathbf{n} \in \mathbb{R}^N$ with pdf $f_{\mathbf{n}}(\mathbf{n})$ and i.i.d. components $n_i \sim \mathcal{N}(0, \sigma_n^2)$. The operation where a source of dimension M is mapped onto a channel of dimension N is an M:N mapping. The channel output, $\hat{\mathbf{z}} = \mathbf{z} + \mathbf{n}$, is mapped through the decoder to reconstruct $\mathbf{x}$. As the focus is high SNR, *maximum likelihood* (ML) decoding is assumed, producing an estimate $\hat{\mathbf{x}}$ of $\mathbf{x}$. Ideally, MMSE decoding should be considered, but as we seek analytical results, ML decoding is more convenient, and as high SNR is considered, the loss is small [43, pp. 216-219]. Both encoder and decoder contain an S-K mapping, $\mathcal{S}$, defined in Section II-B. How $\mathcal{S}$ is applied for *dimension expansion* ($M < N$) and *dimension reduction* ($M > N$) will be explained in Section III.

Definition 1: Source- and channel domains:
The source domain, $\mathcal{D}_s$, is a simply connected, M-dimensional

subset of $\mathbb{R}^M$, $\mathcal{D}_s \subseteq \mathbb{R}^M$. The channel domain, $\mathcal{D}_c$, is a simply connected, N-dimensional subset of $\mathbb{R}^N$, $\mathcal{D}_c \subseteq \mathbb{R}^N$.

Whenever $M < N$, we consider the sub-division of $\mathcal{D}_c$ into two orthogonal subsets, an M dimensional simply connected domain $\mathcal{D}_{cc}$ and an $N - M$ dimensional simply connected domain $\mathcal{D}_{cd}$, so that $\mathcal{D}_c = \mathcal{D}_{cc} \times \mathcal{D}_{cd}$. Let $\mathcal{D}_{cc_i}$ and $\mathcal{D}_{cd_i}$ denote subsets of these two domains.

Whenever $M > N$ we consider the division of $\mathcal{D}_s$ into two orthogonal subsets, an N dimensional simply connected domain $\mathcal{D}_{sc}$ and an $M - N$ dimensional simply connected domain $\mathcal{D}_{sd}$, so that $\mathcal{D}_s = \mathcal{D}_{sc} \times \mathcal{D}_{sd}$. Let $\mathcal{D}_{sc_i}$ and $\mathcal{D}_{sd_i}$ denote subsets of these two domains. □

Remark 1: Subscripts c and d are short for *continuous* and *discrete* (as clarified later). Simply connected domains are considered as unimodal pdf's are assumed. $\mathcal{D}_s$ is usually unbounded if $f_{\mathbf{x}}(\mathbf{x})$ does not have compact support, but can be bounded if $f_{\mathbf{x}}(\mathbf{x})$ has compact support, or if $\mathbf{x}$ is limited for the purpose of code design. Typically, $\mathcal{D}_s$ is limited to contain the *significant probability mass*, referring to all $\mathbf{x}$ except those with very low probability. For Gaussian pdf one typically limit $\|\mathbf{x}\|$ at four standard deviations (like "4σ loading" assumed when construction scalar quantizers [44, pp. 124-125]). Similarly, $\mathcal{D}_c$ may be bounded due to code design or a power constraint.

As a measure of performance, the end-to-end mean squared error per source-sample between the input- and reconstructed vector, $D_t = (1/M)E\{\|\mathbf{x} - \hat{\mathbf{x}}\|^2\}$, is considered and compared to the *optimal performance theoretically attainable* (OPTA) [11].

A. OPTA

OPTA in the i.i.d. case is obtained by equating the rate-distortion function for the relevant source with the relevant channel capacity. The equation is solved with respect to the signal-to-distortion ratio (SDR), which becomes a function of the channel signal-to-noise ratio (SNR) [11]. For the case of Gaussian sources and channels, OPTA is explicitly given by

$$\frac{\sigma_x^2}{D_t} = \left(1 + \frac{P}{\sigma_n^2}\right)^{N/M}, \tag{1}$$

where σ_x^2 is the source variance, σ_x^2/D_t is the SDR and P/σ_n^2 is the channel SNR. Assuming Nyquist-sampling and an ideal Nyquist-channel, with equal duration of both source- and channel signal, the ratio between channel signalling rate f_c, and source sampling rate f_s, can be obtained by combining M source samples with N channel samples. That is, $f_c/f_s = N/M = r$, where r is a positive rational number, $r \in \mathbb{Q}_+$, named *dimension change factor*. If $r > 1$, the channels dimension is higher than that of the source and this can be utilized for noise reduction. If $r \in [0, 1)$, the source dimension, and hence its information, has to be reduced before transmission in general. Note that (1) is an *asymptotic bound*, which is generally obtained as $M, N \to \infty$ while $r = N/M \in \mathbb{Q}^+$ is kept constant. There are exceptions to this, like when $M = N$ [16].

B. Shannon-Kotel'nikov mappings

S-K mappings operate directly on amplitude-continuous, discrete-time signals. Let $\mathcal{S}$ denote a general S-K mapping and $\mathbf{S}$ a specific realization. Generally, $\mathcal{S}$ is a M- or N dimensional smooth (hyper) surface, or a set of M- or N dimensional smooth surface patches, $\mathcal{S}_i$. In the latter case, $\mathcal{S}$ may provide a mixture of discrete and continuous representations (a HDA system). Let $N_b(\mathcal{S}_i)$ denote set of indices for all nearest neighboring patches of $\mathcal{S}_i$ (in $\mathcal{D}_c$ or $\mathcal{D}_s$).

Definition 2: Piecewise smooth source-to-channel mapping:
Consider k (M- or N dimensional) smooth surface patches, $\mathcal{S}_i$, so that $\mathcal{S} = \cup_{i=1}^k \mathcal{S}_i$, and where $\mathcal{S}_i \cap \mathcal{S}_j = \emptyset, \forall j \neq i$, to assure uniqueness for all points on $\mathcal{S}$.

For $M < N$: Consider a sub-division of source domain, $\mathcal{D}_s$, into k M-dimensional subsets, $\mathcal{D}_{s_i}$, so that $\cup_{i=1}^k \mathcal{D}_{s_i} = \mathcal{D}_s$, and $\mathcal{D}_{s_i} \cap \mathcal{D}_{s_j} = \emptyset$, $\forall j \neq i$. To each $\mathcal{D}_{s_i}$ there is a corresponding M-dimensional $\mathcal{S}_i \subset \mathcal{D}_c \subseteq \mathbb{R}^N$, giving every point in $\mathcal{D}_s$ a unique representation in $\mathcal{D}_c$. Consider the sub-division of $\mathcal{D}_c$ in Definition 1, and let $\mathcal{D}_{cc_i}$ and $\mathcal{D}_{cd_i}$ be sets of (vector) values $\mathcal{S}_i$ takes in these subsets. Then $\mathcal{S}_i$ should be chosen so that $\cup_{i=1}^k \mathcal{D}_{cc_i} = \mathcal{D}_{cc}$, and $\mathcal{D}_{cc_i} \cap \mathcal{D}_{cc_j} \neq \emptyset$, $\forall i, j \in \{1, \cdots, k\}$. Further, $\mathcal{D}_{cd}$ may contain disjoint subsets so that $\cup_{i=1}^k \mathcal{D}_{cd_i} \subseteq \mathcal{D}_{cd}$.

For $M > N$: Consider a sub-division of channel domain, $\mathcal{D}_c$, into k N-dimensional subsets, $\mathcal{D}_{c_i}$, so that $\cup_{i=1}^k \mathcal{D}_{c_i} \subseteq \mathcal{D}_c$ and $\mathcal{D}_{c_i} \cap \mathcal{D}_{c_j} = \emptyset$, $\forall j \neq i$. To each $\mathcal{D}_{c_i}$ is a corresponding N-dimensional $\mathcal{S}_i \subset \mathcal{D}_s \subseteq \mathbb{R}^M$, giving every point of $\mathcal{S}$ a unique representation in $\mathcal{D}_c$. Consider the sub-division of $\mathcal{D}_s$ in Definition 1, and let $\mathcal{D}_{sc_i}$ and $\mathcal{D}_{sd_i}$ be the set of (vector) values $\mathcal{S}_i$ takes in these subsets. Then $\mathcal{S}_i$ should be chosen so that $\cup_{i=1}^k \mathcal{D}_{sc_i} = \mathcal{D}_{sc}$ and $\mathcal{D}_{sc_i} \cap \mathcal{D}_{sc_j} \neq \emptyset, \forall i, j \in \{1, \cdots, k\}$. $\mathcal{D}_{sd}$ may contain disjoint subsets so that $\cup_{i=1}^k \mathcal{D}_{sd_i} \subseteq \mathcal{D}_{sd}$.

In both cases the neighbours to $\mathcal{S}_i$, $\mathcal{S}_j$, $j \in N_b(\mathcal{S}_i)$, should, as far as possible, correspond to neighbouring subsets in $\mathcal{D}_s$ ($M < N$) or $\mathcal{D}_c$ ($M > N$), to avoid large decoding errors.□

Remark 2: For $M < N$, the condition $\mathcal{D}_{cc_i} \cap \mathcal{D}_{cc_j} \neq \emptyset$, $\forall i, j \in \{1, \cdots, k\}$ ensures a continuous representation in $\mathcal{D}_{cc}$ and that the channel space is properly utilized. Ideally, at high SNR, each $\mathcal{D}_{cc_i}$ should cover $\mathcal{D}_{cc}$. In low SNR range, or if there is significant correlation among the source variables [45], it may be convenient to relax this to $\mathcal{D}_{cc_i} \cap \mathcal{D}_{cc_j} \neq \emptyset$, $\forall j \in N_b(\mathcal{S}_i)$. This condition, together with $\mathcal{S}_i \cap \mathcal{S}_j = \emptyset, \forall j \neq i$, ensures a nonzero distance among the $\mathcal{S}_i$'s. The same goes for the $M > N$ case relating to $\mathcal{D}_s$. In $M > N$ case, $\cup_{i=1}^k \mathcal{D}_{c_i} \subseteq D_c$, to allow some space between subsets in $\mathcal{D}_c$, avoiding large decoding errors.

Remark 3: Generally, the number of $\mathcal{S}_i$'s, k, increases with SNR. There is some flexibility in placement of the $\mathcal{S}_i$'s in $\mathcal{D}_c$ (or $\mathcal{D}_s$) though *index assignment*. To avoid large decoding errors, one should choose an assignment where neighbours to $\mathcal{S}_i$ in $\mathcal{D}_c$ (or $\mathcal{D}_s$) corresponds to neighboring subsets in $\mathcal{D}_s$ (or $\mathcal{D}_c$). However, if quantized values are transmitted directly, this issue is usually resolved.

Definition 3: Shannon-Kotel'nikov (S-K) mapping
An S-K mapping, $\mathcal{S}$, is a continuous- or piecewise smooth mapping between source domain $\mathcal{D}_s \subseteq \mathbb{R}^M$ and channel domain $\mathcal{D}_c \subseteq \mathbb{R}^N$. There are three cases to consider:

1. Equal dimension M=N: $\mathcal{S}$ is a bijective mapping.

2. Dimension expansion $M < N$: $\mathcal{S} \subset \mathcal{D}_c$, an M-dimensional subset of the channel space $\mathbb{R}^N$, realized by a continuous or piecewise smooth M-dimensional surface, so that each source vector $\mathbf{x} \in \mathcal{D}_s$ has a unique representation on $\mathcal{S}$ in $\mathcal{D}_c$. In the continuous case, a particular $\mathbf{S} \in \mathcal{S}$ can be represented by the parametrization

$$\mathbf{S}(\mathbf{x}) = [S_1(\mathbf{x}), S_2(\mathbf{x}), \cdots, S_N(\mathbf{x})]. \tag{2}$$

In the piecewise smooth case, $\mathcal{S}$ is as in Definition 2.

3. Dimension reduction $M > N$: $\mathcal{S} \subset \mathcal{D}_s$, an N-dimensional subset of the source space $\mathbb{R}^M$, realized by a continuous or piecewise smooth N-dimensional surface, so that each point $P \in \mathcal{S}$ has a unique representation in $\mathcal{D}_c$. The map $\mathcal{D}_s \to \mathcal{S}$ is generally not bijective. In the continuous case, a particular $\mathbf{S} \in \mathcal{S}$ can be represented by the parametrization

$$\mathbf{S}(\mathbf{z}) = [S_1(\mathbf{z}), S_2(\mathbf{z}), \cdots, S_M(\mathbf{z})]. \tag{3}$$

In the piecewise smooth case, $\mathcal{S}$ is as in Definition 2. □

Remark 4: The parametrization is of mathematical convenience, not a restriction on the set of mappings. I.e., $\mathcal{S}$ does not need to have a parametrization. Note that when $M > N$ with continuous $\mathcal{S}$, large decoding errors are completely avoided (see Section III-B). Then it is not crucial that $\mathcal{S}$ does not intersect itself. I.e., this condition may be relaxed for that case.

We are concerned with cases 2 and 3 as case 1 was dealt with in [10], [6]. We will in the rest of the paper refer to S-K mappings as either *S-K mapping*, *signal surface* or simply $\mathcal{S}$.

Example 1: Throughout the paper we give several examples of S-K mappings satisfying Definition 3 above: The 3:2 mappings in Figs. 9(a) and 10(a) are continuous mappings with parametric equations where both $\mathcal{D}_s$ and $\mathcal{D}_c$ can be unbounded as the structures can be extended indefinitely. The 1:2 mappings in Fig. 8 (also potential 2:1 mappings), are valid mappings, one satisfying the conditions for a piecewise smooth S-K mapping. In Fig. 2, we give more examples of piecewise smooth source-to-channel mappings for $M < N$, i.e., with $\mathcal{S} \subset \mathcal{D}_c$. The same examples are valid for $M > N$ mappings in which $\mathcal{S} \subset \mathcal{D}_s$. To the upper left we have a 2:3 (or 3:2)

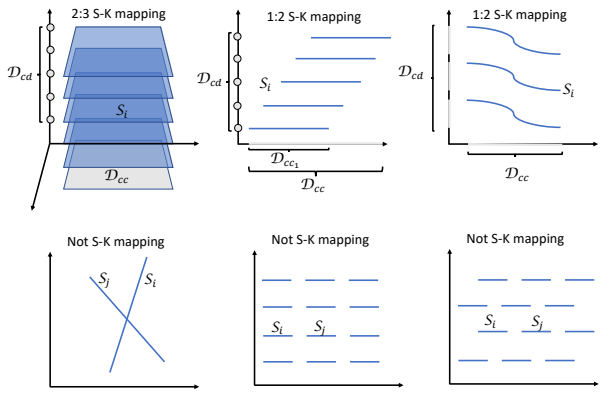

Fig. 2. Examples of piecewise smooth source-to-channel mappings. Upper left: 2:3 (or 3:2) S-K mapping. Upper center and upper right: 1:2 (or 2:1) S-K mappings. The bottom row shows structures that are not S-K mappings.

S-K mapping where $\mathcal{S}_i$ are parallel planes, a mapping we will exemplify throughout. In the upper middle figure is a 1:2 (or 2:1) S-K mapping where $\mathcal{S}_i$ are line segments. Both satisfies the condition $\mathcal{D}_{cc_i} \cap \mathcal{D}_{cc_j} \neq \emptyset$, $\forall i, j \in \{1, \cdots, k\}$ of Definition 2, but the first satisfies a stricter condition where each $\mathcal{D}_{cc_i}$ covers all of $\mathcal{D}_{cc}$. Both take on discrete values in $\mathcal{D}_{cd}$ (or $\mathcal{D}_{sd}$). The 1:2 (or 2:1) S-K mapping to the upper right, where $\mathcal{S}_i$ are curve segments, takes on continuous values in $\mathcal{D}_{cd}$ (or $\mathcal{D}_{sd}$), but each $\mathcal{S}_i$ represents a disjoint set in $\mathcal{D}_{cd_i} \subset \mathcal{D}_{cd}$. Note that all these S-K mappings have bounded $\mathcal{D}_{cc}$ (or $\mathcal{D}_{sc}$). The three mappings in bottom row does not comply with Definition 2: To the bottom left $\mathcal{S}_i \cap \mathcal{S}_j \neq \emptyset$. In the bottom middle figure, $\cup_{i=1}^{k} \mathcal{D}_{cc_i} = \mathcal{D}_{cc}$ is violated. To the bottom left, $\mathcal{D}_{cc_i} \cap \mathcal{D}_{cc_j} \neq \emptyset$, $\forall i, j \in \{1, \cdots, k\}$ is violated.

C. Relevant concepts from differential geometry

The theory of S-K mappings is based on concepts from differential geometry. A brief introduction of the concepts we apply are given here with more details provided in Appendix A and in [46] (available online). All concepts are taken from Kreyszig's book [47]. We use variables $u \in \mathbb{R}$ and $u_i \in \mathbb{R}$ here to keep the discussion general, avoiding reference to source- or channel variables.

Consider a curve, $\mathcal{C} : \mathbf{S}(u) = [S_1(u), S_2(u), \cdots, S_n(u)] \in \mathbb{R}^n$. We will denote the derivatives with respect to (w.r.t) a general parameter, u, as $\mathbf{S}'$, $\mathbf{S}''$ etc. In the special case of the parameter being *arc-length* of $\mathcal{C}$, we denote the derivatives $\dot{\mathbf{S}}$, $\ddot{\mathbf{S}}$ etc. That is, when we parameterize by

$$\ell(u) = \int_{u_l}^{u} \sqrt{\mathbf{S}' \cdot \mathbf{S}'} \mathrm{d}u = \int_{u_l}^{u} \|\mathbf{S}'\| \mathrm{d}u. \tag{4}$$

Then $\|\dot{\mathbf{S}}\| = \|\mathbf{t}\| = 1$, $\forall u$, with $\mathbf{t}$ the curves tangent vector(s) (See Appendix A-A).

For a curve, $\mathbf{S}(u)$, one can define the *principal curvature* w.r.t. arc-length at u_0 as $\kappa_0 = \kappa(u_0) = \|\ddot{\mathbf{S}}(u_0)\|$ [47, p. 34]. Consider arc-length parametrization with an amplification α, which we name *scaled arc-length parametrization*. Then $\|\mathbf{S}'(u_0)\| = \alpha\|\dot{\mathbf{S}}(u_0)\| = \alpha$, $\forall u_0$, and as $\dot{\mathbf{S}} \perp \ddot{\mathbf{S}}$, then $\kappa(u_0) = \|\mathbf{S}_0''\|/\|\mathbf{S}_0'\|^2$ according to (63) in Appendix A-A. Here and in the following, the notation $\mathbf{S}_0' = \mathbf{S}'(u_0)$ and $\mathbf{S}_0'' = \mathbf{S}''(u_0)$ is often used.

For surfaces, $\mathcal{S}$, with parametric representation as in (2), (3), we denote partial derivatives as

$$\mathbf{S}_\alpha = \frac{\partial \mathbf{S}}{\partial u^\alpha}, \quad \mathbf{S}_{\alpha\beta} = \frac{\partial^2 \mathbf{S}}{\partial u^\alpha \partial u^\beta}. \tag{5}$$

The use of sub- and superscripts in this section relate to *Einstein's summation convention* [46, p.2].

The curvature of a surface, $\mathcal{S}$, depends on the choice of *coordinate curves* on $\mathcal{S}$. For simplicity, consider a 2-dimensional surface in $\mathbb{R}^3$ in the following. A curve, $\mathcal{C}$, on surface $\mathbf{S}(u^1, u^2) \in \mathcal{S}$ is represented by the parametrization $\mathcal{C} : u^1 = u^1(t)$, $u^2 = u^2(t)$, which is in C^1 (the set of differentiable functions), where $t \in \mathbb{R}$. The coordinate curves, u^1 =constant and u^2 =constant, corresponds to parallel curves in the u^1, u^2-plane. One must always choose *allowable coordinates* which conditions are provided in [46, p.2]. The *normal curvature*, κ_n, of $\mathcal{S}$ at point P is given by $\kappa_n = b_{\alpha\beta}\mathrm{d}u^\alpha \mathrm{d}u^\beta / g_{\alpha\beta}\mathrm{d}u^\alpha \mathrm{d}u^\beta$ (see Appendix A-B2,

Eqn. (67)), where $g_{ij} = \mathbf{S}_i \cdot \mathbf{S}_j$ are the components of the *metric tensor* G, or *first fundamental form* (FFF) of $\mathcal{S}$, and $b_{\alpha\beta} = \mathbf{S}_{\alpha\beta} \cdot \mathbf{N}$ are components of the *second fundamental form* (SFF) of $\mathcal{S}$, with $\mathbf{N}$, the *unit normal* to $\mathcal{S}$ at P (see Appendix A-B1). A special case of particular interest is the extremal values of κ_n, named *lines of curvature* (LoC). If one chooses LoC as coordinate curves then the curvature of $\mathcal{S}$ in those directions, the *principal curvatures*, are given by $\kappa_i = b_{ii}/g_{ii}$, $\forall i$ (see Appendix A-B2 for details). For general coordinate curves, κ_i are the roots of (69) in Appendix A-B. The normal curvature, κ_n, for any (tangent) direction can be represented in terms of κ_1 and κ_2 according to *theorem of Euler* [47, p. 132] as $\kappa_n = \kappa_1 \cos^2\alpha + \kappa_2 \sin^2\alpha$, with α the angle between an arbitrary direction at P and the direction corresponding to κ_1. For m-dimensional surfaces in $\mathbb{R}^n$, the same concepts exist. However, the definition of $b_{\alpha\beta}$ is more elaborate (see for example [48]).

III. Distortion analysis for S-K mappings

In this section we quantify distortion for S-K mappings.

A. Dimension expanding S-K mappings.

In this section Kotel'nikovs theory from [31, pp.62-99] on $1{:}N$ mappings is generalized to include vector sources, enabling analysis of more general mappings. The results presented in this section are extensions of [1].

Fig. 1(a) depicts the block diagram for a dimension expanding communication system. Consider source vector $\mathbf{x} \in \mathcal{D}_s \subseteq \mathbb{R}^M$, which is represented on the channel as $\mathbf{x} \mapsto \mathbf{S}(\mathbf{x}) \in \mathcal{S} \subset \mathcal{D}_c \subseteq \mathbb{R}^N$, (see Definition 3). Applying a specific realization $\mathbf{S} \in \mathcal{S}$, the likelihood-function of the received vector $\hat{\mathbf{z}} = \mathbf{S}(\mathbf{x}) + \mathbf{n}$ is

$$f_{\hat{\mathbf{z}}|\mathbf{x}}(\hat{\mathbf{z}}|\mathbf{x}) = \left(\frac{1}{2\pi\sigma_n^2}\right)^{N/2} e^{-\frac{\|\hat{\mathbf{z}}-\mathbf{S}(\mathbf{x})\|^2}{2\sigma_n^2}}. \tag{6}$$

The ML-estimate is then defined as [49]

$$\hat{\mathbf{x}} = \max_{\mathbf{x}\in\mathbb{R}^M} f_{\hat{\mathbf{z}}|\hat{\mathbf{x}}}(\hat{\mathbf{z}}|\mathbf{x}), \tag{7}$$

and is maximized by the $\mathbf{x}$ minimizing $\|\hat{\mathbf{z}} - \mathbf{S}(\mathbf{x})\|$. I.e., the ML-estimate is the $\mathbf{x}$ in which $\mathbf{S}(\mathbf{x})$ is closest to $\hat{\mathbf{z}}$ in Euclidean distance. That is, a projection of $\hat{\mathbf{z}}$ onto $\mathcal{S}$.

Ideally one could formulate the exact distortion for any such scheme once a specific $\mathbf{S} \in \mathcal{S}$ is chosen. This is inconvenient when it comes to analysis of the general behavior of such mappings as it is usually very hard, if at all possible, to find closed form solutions. Therefore we use the approach by Kotel'nikov [31, pp.62-99], which reasoned that there are two main contributions to the total distortion using such mappings: *low-intensity noise* and *strong noise*. Low-intensity noise refers to errors in the reconstruction varying gradually with the magnitude of $\mathbf{n}$. Distortion due to low-intensity noise can be analyzed without reference to a specific $\mathbf{S}$ whenever the noise can be considered *weak*. The resulting distortion is named *weak noise distortion*, denoted by $\bar{\varepsilon}^2_{wn}$, as defined in Definition 4, section III-A1. Strong noise is known as *anomalous errors* in the literature, and results from a *threshold effect* [30], [19]. The resulting distortion is named *anomalous distortion* and denoted by $\bar{\varepsilon}^2_{an}$.

1) Weak noise distortion: To analyze non-linear mappings without reference to a chosen structure, the Taylor expansion and the concepts introduced in Section II-C apply. Let $\mathbf{S}_{lin}(\mathbf{x})$ denote 1st order Taylor approximation of $\mathbf{S}(\mathbf{x}) \in C^1$ at $\mathbf{x}_0$

$$\mathbf{S}_{lin}(\mathbf{x}) = \mathbf{S}(\mathbf{x}_0) + J(\mathbf{x}_0)(\mathbf{x} - \mathbf{x}_0), \tag{8}$$

where $J(\mathbf{x}_0)$ denotes the *Jacobian* (see Appendix A-B) of $\mathbf{S}$ evaluated at $\mathbf{x}_0$. Under (8) one can, for mathematical convenience, approximate the ML-decoder as a projection onto the tangent (hyper) plane of $\mathbf{S}$ at $\mathbf{S}(\mathbf{x}_0)$, as depicted in Fig. 3(a) for the 2:3 case. We have the following proposition providing the exact distortion under linear approximation:

Proposition 1: Minimum weak noise distortion
For any continuous i.i.d. source $\mathbf{x} \in \mathbb{R}^M$ with unimodal pdf $f_{\mathbf{x}}(\mathbf{x})$ sent on an i.i.d. Gaussian channel of dimension N using a continuous dimension expanding S-K mapping $\mathbf{S}$ as in (2) where $S_i \in C^r,\ r \geq 1,\ i = 1, .., N$, the minimum distortion under the approximation in (8) is

$$\bar{\varepsilon}^2_{wn} = \frac{\sigma_n^2}{M} \iint \cdots \int_{\mathcal{D}_s} \sum_{i=1}^{M} \frac{1}{g_{ii}(\mathbf{x})} f_{\mathbf{x}}(\mathbf{x}) \mathrm{d}\mathbf{x}, \tag{9}$$

obtained when the metric tensor G (or FFF) of $\mathbf{S}$ is diagonal with entries $g_{ii} = \|\partial\mathbf{S}(\mathbf{x})/\partial x_i\|^2$. I.e., the squared norm of the tangent vector along the i'th coordinate curve.

Proof: See Appendix B-A1. □

Remark 5: Proposition 1 is directly extendable to piecewise smooth $\mathcal{S}$ as one can integrate over each $\mathcal{S}_i$ as in (9), then sum all k contributions afterwards (like in [23] for $1{:}N$ mappings).

Eqn. (9) states that weak noise distortion is lowered when the g_{ii}'s are increased (i.e., when the length of the tangent vectors of $\mathcal{S}$ are increased), which is obtained when $\mathcal{S}$ is stretched like a rubber-sheet. Bending or cutting of $\mathcal{S}$ into pieces does not affect weak noise distortion.

The concept is illustrated in Fig. 3(b) for the $1{:}N$ case when $\mathcal{S}$ is a curve. Stretching of the curve makes the distance

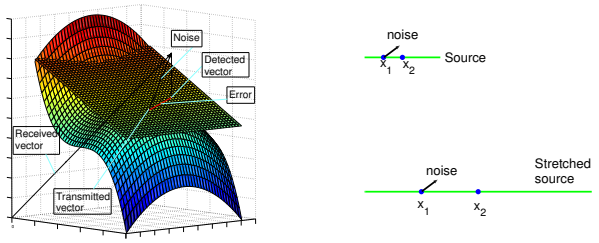

(a) (b)

Fig. 3. Kotel'nikovs weak noise concept. 3(a) Approximation of ML estimate under (8). 3(b) Error reduction for $1{:}N$ mappings.

between points in source space (x_1 and x_2) appear larger relative to a given noise vector. Equivalently, the more the source is stretched at the transmitter trough $\mathcal{S}$, the more the noise will be attenuated at the receiver, lowering distortion. This result implies that the source space should be stretched indefinitely. However, as will be seen in Section III-A2,

under a channel power constraint this cannot be done without introducing large errors.

The following corollary is a special case of Proposition 1:

Corollary 1: Shape-preserving mapping

When $\mathbf{S}$ has a diagonal metric G with $g_{ii}(\mathbf{x}) = g_{jj}(\mathbf{x}) = \alpha, \forall \mathbf{x}, i, j$, and with α a constant, then

$$\bar{\varepsilon}^2_{wn} = \frac{\sigma_n^2}{\alpha^2}. \tag{10}$$

That is, all source vectors are equally scaled when mapped through $\mathbf{S}$, and so the noise will affect all $\mathbf{x}$ equally.

Proof: Insert $g_{ii}(\mathbf{x}) = g_{jj}(\mathbf{x}) = \alpha$ in (9). □

A shape-preserving mapping can be seen as an amplification factor α from source to channel. Although a shape-preserving mapping leads to simple analysis, its not necessarily optimal in general, as shown in [50, 294-297].

In order to determine the error made in the distortion estimate under linear approximation, we need to consider 2nd order Taylor expansion. We have the following proposition:

Proposition 2: Weak noise error under 2nd order Taylor approximation

Under 2nd order Taylor approximation, the special case of $1{:}N$ mappings (curves) has an error in the absence of anomalies given by

$$\begin{aligned} \varepsilon^2_{wn} &\approx \frac{\sigma_n^2}{\|\mathbf{S}_0'\|^2}\left(1 + \frac{1}{4}\sigma_n^2 \frac{\|\mathbf{S}_0''\|^2}{\|\mathbf{S}_0'\|^4}\right) \\ &= \frac{\sigma_n^2}{\|\mathbf{S}_0'\|^2}\left(1 + \frac{1}{4}\sigma_n^2 \kappa^2(x_0)\right), \end{aligned} \tag{11}$$

valid for any S-K mapping $\mathbf{S}(x) \in C^n$, $n \geq 2$. The last equality is true under scaled arc-length parametrization. Further, for any continuous dimension expanding S-K mapping as defined in Definition 3, with LoC coordinate curves, the error is given by

$$\begin{aligned} \varepsilon^2_{wn}(\mathbf{x}_0) &\approx \frac{\sigma_n^2}{M}\sum_{i=1}^{M}\left\{\frac{1}{g_{ii}(\mathbf{x}_0)}\left(1 + \frac{\sigma_n^2}{4}\frac{b_{ii}^2(\mathbf{x}_0)}{g_{ii}^2(\mathbf{x}_0)}\right)\right\} \\ &= \frac{\sigma_n^2}{M}\sum_{i=1}^{M}\left\{\frac{1}{g_{ii}(\mathbf{x}_0)}\left(1 + \frac{\sigma_n^2}{4}\kappa_i^2(\mathbf{x}_0)\right)\right\}. \end{aligned} \tag{12}$$

Here, $\kappa_i = b_{ii}/g_{ii}$ is the curvature along coordinate curve i with b_{ii} the diagonal components of the SFF (see Appendix A-B).

Proof: See Appendix B-A2. □

Remark 6: We only treat 2nd order Taylor approximation here to simplify the analysis. It will be seen in Section III-B that higher order terms are even less influential as σ_n is raised to a power twice that of the order, which at high SNR ($\sigma_n << 1$) leads to a negligible contribution. For piecewise smooth $\mathcal{S}$, one evaluate (12) for each $\mathcal{S}_i$, then sum all k contributions.

In the absence of anomalies, one can characterize distortion for S-K mappings in general without choosing a specific $\mathcal{S}$ in advance, as it is expressed solely w.r.t. FFF and SFF components, making it easier to evaluate the distortion analytically for such mappings.

From (12) alone a linear mapping seems convenient as $\kappa_i = 0, \forall i$. However, at high SNR linear mappings perform poorly, and with (12) in mind, one would seek nonlinear mappings with the smallest possible $\kappa_i(\mathbf{x})$. Therefore the weak noise regime, as defined next, is a good approximation for any *reasonably* chosen mapping at high SNR.

Definition 4: Weak noise regime, dimension expansion

With $\mathbf{x}_0$ the transmitted vector and $\mathbf{S}(\mathbf{x}_0)$ its representation on the channel, we say that we are in the *weak noise regime* whenever the 2nd order term in (12) (the term containing κ_i), is negligible compared to the 1st order term. That is, (8) is a close approximation to $\mathbf{S}$ at any point and (9) is an accurate approximation to the actual distortion in the absence of anomalies. □

Example 2: When is Definition 4 satisfied? There are at least three cases:

i) SNR$\to \infty$ ($\sigma_n \to 0$): The linear approximation in (8) is exact as $\mathcal{S}$ is locally Euclidean.

ii) When $\mathcal{S}$ is linear then $\kappa_i = 0, \forall i$. The same goes for HDA schemes composed of piecewise line- or (hyper) plane patches (as the HVQLC in Section V).

iii) Small maximal principal curvature $\kappa_{\max}$: The smaller $\kappa_{\max}$ is, the larger σ_n can be before (9) becomes inaccurate. This is inline with mappings obtained from numerical optimization algorithms, which tend to bend less and less the lower the SNR is [36], [51].

2) Anomalous distortion: With a channel power constraint, $\mathcal{S}$ must be constrained to lie within some $N-1$ sphere[2], $\mathbb{S}^{N-1}$. To make weak noise distortion small, $\mathcal{S}$ must be stretched, bent and twisted to "fit" within this sphere. As an example take the 1:2 case in Fig. 4. Take a decomposition of the noise $\mathbf{n}$ into a tangential component to $\mathcal{S}$, $\mathbf{n}_{wn} = \mathbf{n}_{||}$, and a normal component $\mathbf{n}_{an} = \mathbf{n}_{\perp}$, as depicted in Fig. 4(a). $\mathbf{n}_{wn}$ contributes to weak noise, whilst $\mathbf{n}_{an}$ contributes to anomalous errors, which occur whenever $\|\mathbf{n}_{an}\|$ crosses a certain boundary. Then the transmitted vector $\mathbf{S}(x_0)$, representing x_0, will be detected as the vector $\mathbf{S}(x_{err})$ on another arm (or *fold*) of the spiral in Fig. 4(b). This happens if the distance, Δ, between the spiral arms is chosen too small w.r.t. σ_n. Although $\mathbf{S}(x_{err})$ is close to $\mathbf{S}(x_0)$ in the channel space, x_{err}, is far away from x_0 in source space, leading to large decoding errors.

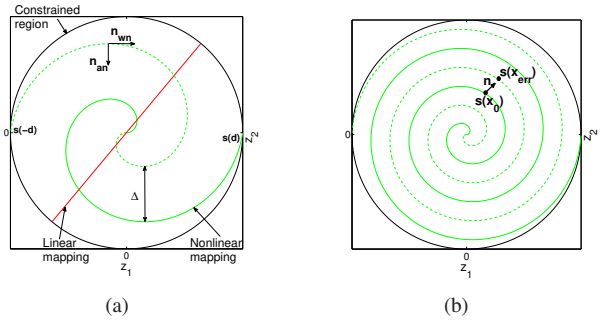

Fig. 4. Example of 1:2 S-K mappings (here $\pm d$ denote the boundary of $\mathcal{D}_s$). 4(a) Linear and nonlinear mappings. Negative source values are represented by dashed curve. 4(b) As the spiral arms, or *folds*, gets close, noise may take the transmitted vector $\mathbf{S}(x_0)$ closer to another fold of the spiral leading to large decoding errors.

[2]The definition of an N-sphere is $\mathbb{S}^N = \{\mathbf{y} \in \mathbb{R}^{N+1} | d(\mathbf{y}, 0) = \text{constant}\}$ [52, p.7], where d is the distance from any point $\mathbf{y}$ on $\mathbb{S}^N$ to the origin of $\mathbb{R}^{N+1}$. E.g. the *sphere* embedded in $\mathbb{R}^3$ is denoted $\mathbb{S}^2$.

To quantify anomalous distortion in general, the concept of a *canal surface* is needed:

Definition 5: Canal surface
With $\mathbf{S}(x)$, a curve in $\mathbb{R}^N$, the corresponding *canal surface*, S_c, is the *envelope* to the family, F, of congruent $N-1$ spheres, $\mathbb{S}^{N-1}$, of radius r with center on $\mathbf{S}(x)$, given by the equation

$$H(\mathbf{z},x) = (\mathbf{z}-\mathbf{S}(x))\cdot(\mathbf{z}-\mathbf{S}(x)) - r^2 = 0. \quad (13)$$

I.e., (13) defines a hyper-surface in $\mathbb{R}^N$, with $\mathbf{z}\in\mathbb{R}^N$, the channel variables. □

The following definition is an extension of [47, p. 263].

Definition 6: Characteristic and characteristic intersection
Consider the equations:

$$\begin{aligned} &H(\mathbf{z},x)=0, \quad \frac{\partial H(\mathbf{z},x)}{\partial x} = -2\dot{\mathbf{S}}(x)\cdot(\mathbf{z}-\mathbf{S}(x)) = 0, \\ &\frac{\partial^2 H(\mathbf{z},x)}{\partial x^2} = -2\ddot{\mathbf{S}}(x)\cdot(\mathbf{z}-\mathbf{S}(x)) + 2 = 0. \end{aligned} \quad (14)$$

The two first equations define the *characteristic* of S_c, an $N-2$ sphere lying in the space normal to $\mathbf{S}$. All three equations defines the *characteristic intersection* of S_c, an $N-3$ sphere.□

If a solution to (14) does not exists for any x, the canal surface will not intersect itself at any point, and it can be used to bound the probability for anomalous errors by relating the noise variance σ_n^2 to the radius r (see Example 4 below).

Example 3: In $\mathbb{R}^3$, with $\mathbf{S}(x)$ a space curve, the canal surface is a tube as shown in Fig. 5. The characteristic is a circle lying in the *normal plane* of $\mathbf{S}$ (see Appendix A-A), and the characteristic intersection is two points corresponding to the intersection of two circles (the characteristic at two points of $\mathbf{S}$). In $\mathbb{R}^4$, the characteristic is a sphere, and the characteristic intersection is a circle. In $\mathbb{R}^2$ the characteristic consists of two points and the characteristic intersection consist of one point corresponding to the value of $\mathbf{S}(x)$ where the points of the characteristic coincide.

A generalization for M:N mappings is straight forward:

Definition 7: Extended Canal surface
The *extended canal surface*, S_c, of an M-dimensional $\mathbf{S}$ embedded in $\mathbb{R}^N$ is the envelope of the congruent hyper-spheres $\mathbb{S}^{N-M}$ with radius r and center on $\mathbf{S}(\mathbf{x})$. We refer to an extended canal surface simply as "canal surface" in the following. □

We also need the following definition to properly define anomalous distortion:

Definition 8: Folds and minimum distance of $\mathcal{S}$
Let $\mathcal{S}$ have a canal surface with no characteristic intersection. Then any two points on $\mathcal{S}$ will reside on different *folds* of $\mathcal{S}$ whenever the straight line between them intersects the canal surface in one- or several points.

Given that $\mathbf{x}_0$ is transmitted, then $\Delta_{min}(\mathbf{x}_0)$ is the *minimum distance* from $\mathbf{S}(\mathbf{x}_0)$ to the closest point on another fold in Euclidean distance, denoted $\mathbf{S}(\mathbf{x}_{err})$. □

To bound the anomalous error probability one can consider the coordinate curve as being the LoC along the maximal principal curvature κ_{max}. Then the following Lemma provides conditions for a non-intersecting canal surface:

Lemma 1: Consider M:N dimension expanding $\mathcal{S}$ with $\rho_{\min} = 1/\kappa_{\max}$ and $\kappa_{\max}$ the maximal principal curvature of $\mathcal{S}$ at any point $\mathbf{x}_0$. With r, the radius of the hyper-sphere $\mathbb{S}^{N-M}$ from Definition 7, and Δ_{min} the minimum distance in Definition 8, then the canal surface, S_c, in Definition 7 will not intersect itself at any point if and only if i) $\Delta_{min} > 2r$ and ii) $\rho_{\min} > r$ for all points of $\mathcal{S}$. That is, the characteristic intersection does not exist at any point on $\mathcal{S}$.

Proof: See Appendix B-A3. □

Remark 7: Note that condition ii) is incorporated into condition i). The reason we explicitly state ii) is to constrain the curvature of $\mathcal{S}$ so that it can be removed from later analysis.

Example 4: 1:3 mapping: Fig. 5 depicts the canal surface surrounding a curve, $\mathbf{S}(x)$, in $\mathbb{R}^3$. The radius of the canal

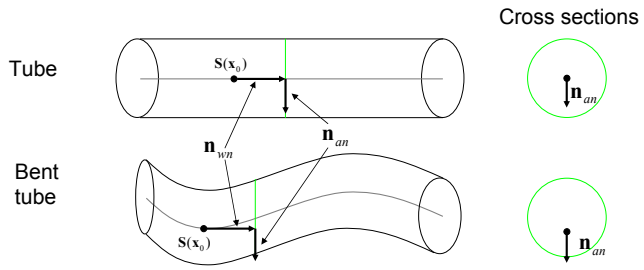

Fig. 5. Canal Surfaces for: (Top) Straight line, $\mathbb{L}\times\mathbb{S}^1$. (Bottom) Nonlinear curve, $\mathbf{S}\times\mathbb{S}^1$.

surface is linked to the noise vector $\mathbf{n}_{an} = \mathbf{n}_\perp$. Bending of the tube can increase the probability for anomalous errors, implying that straight lines have the lowest probability for such errors. However, according to Lemma 1, one can circumvent this if the radius of curvature of $\mathbf{S}$ is small enough. The significant probability mass of the normalized noise vector, $\mathbf{n}_{an}$, is located within a circle of radius $\rho_n = \sqrt{2b_n^2\sigma_n^2/3}$ (see Section IV-A), with b_n related to the variance of $\mathbf{n}_{an}$ (with $b_n > 4$ about 99.99% of the probability mass is included when the dimension of $\mathbf{n}_{an}$ is small). Therefore, if i) is satisfied, and if $\rho_{min} \geq r = \rho_n \geq \sqrt{2b_n^2\sigma_n^2/3}$, no characteristic intersection exist and the tube in Fig. 5 will not intersect itself.

We provide a definition of anomalous distortion valid in the vicinity of the optimal operational SNR. That is, we only consider jumps to the nearest point on another fold, $\mathbf{S}(x_{err})$, from a given transmitted point, $\mathbf{S}(\mathbf{x}_0)$ (jumps across several folds may happen as σ_n grows, but this is far from optimal). Fig. 4 shows the terminology used in the following definition.

Definition 9: Anomalous distortion
Let $\mathbf{x}_0$ denote the transmitted vector and $\mathbf{S}(\mathbf{x}_0)$ its representation in the channel space. Let $\mathbf{n}_{an}$ denote the $K(\leq N)$ dimensional component of a decomposition of the noise $\mathbf{n}$ pointing in the direction of the closest point, $\mathbf{S}(\mathbf{x}_{err})$, on any other fold of $\mathbf{S}$ from $\mathbf{S}(\mathbf{x}_0)$ (see Fig. 4(b)). $\mathbf{x}_{err}(\mathbf{x}_0)$ is reconstruction in the case of this anomaly and $\Delta_{min}(\mathbf{x}_0)$ is the distance between $\mathbf{S}(\mathbf{x}_0)$ and $\mathbf{S}(\mathbf{x}_{err})$. Let $\rho_{an} = \|\mathbf{n}_{an}\|$ with $f_{\rho_{an}}(\rho_{an})$ its pdf (see (15) in Section IV-A). The probability that $\mathbf{x}_0$ is detected as $\mathbf{x}_{err}$ is then

$$P_{an}(\mathbf{x_0}) = \int_{\Delta_{min}(\mathbf{x}_0)/2}^{\infty} f_{\rho_{an}}(\rho_{an})\mathrm{d}\rho_{an}. \quad (15)$$

The anomalous distortion close to the optimal operational SNR is then defined as

$$\bar{\varepsilon}_{an}^2 = E_{\mathbf{x}}\{P_{an}(\mathbf{x})\|\mathbf{x} - \mathbf{x}_{err}(\mathbf{x})\|^2\}. \tag{16}$$

□

Remark 8: To lower $P_{an}(\mathbf{x_0})$, Δ_{min} should be chosen larger. There is thus a tradeoff between reducing weak noise distortion, obtained by decreasing Δ_{min}, and anomalous distortion. This tradeoff results in one optimal point for a fixed Δ_{min}. If σ_n changes, then Δ_{min} must be adapted to maintain optimality. This is inline with Ziv's results in [32].

B. M:N Dimension Reducing S-K mappings.

Results presented in this section are extensions of [2]. Fig. 1(b) shows a block diagram for the dimension reducing communication system under consideration. From Definition 3, a continuous dimension reducing $\mathcal{S}$ is an N dimensional subset of the source space $\mathcal{D}_s \subseteq \mathbb{R}^M$, that can be realized by the parametrization $\mathbf{S}(\mathbf{z})$ in (3), with the channel signal $\mathbf{z}$ acting as parameters. In that sense, $\mathcal{S}$ is a representation of the channel in source space.

To reduce the dimension of a source under a channel power constraint in general, its information content must be reduced. The source vectors $\mathbf{x}$ are approximated by their projection onto $\mathcal{S}$, a lossy operation denoted $\mathbf{q}(\mathbf{x}) \in \mathcal{S} \subset \mathcal{D}_s \subseteq \mathbb{R}^M$. The dimension is subsequently changed from M to N by a lossless operator $\mathbf{d}_r : \mathbf{S} \to \mathcal{D}_c \subseteq \mathbb{R}^N$, with $\mathcal{D}_c$ as in Definition 1.The total operation is named *projection operation*, and denoted $\mathbf{p} = \mathbf{d}_r \circ \mathbf{q} : \mathbf{x} \in \mathcal{D}_s \mapsto \mathbf{p}(\mathbf{x}) \in \mathcal{D}_c$. The vector $\mathbf{z} = \mathbf{p}(\mathbf{x})$ is transmitted over the AWGN channel. The ML-decoder will now produce the estimate $\hat{\mathbf{x}} = \mathbf{S}(\mathbf{z} + \mathbf{n})$. The noise $\mathbf{n}$ leads to displacements of the projected source vector along $\mathcal{S}$. With a continuous $\mathcal{S}$, the distortion due to channel noise will be gradually increasing with σ_n^2, i.e. no anomalous errors will occur. The concept is illustrated for a 2:1 mapping in Fig. 6(b).

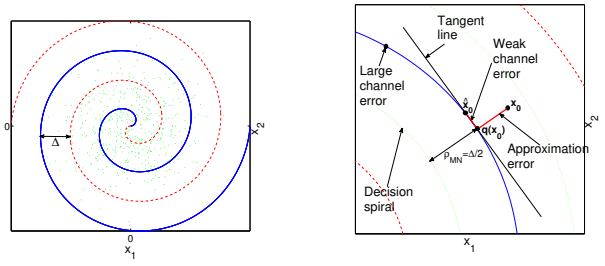

(a) (b)

Fig. 6. 2:1 dimension reducing S-K mapping. 6(a) Covering of source-space, $\mathcal{D}_s$, with a curve: Dashed curve represent negative channel values. Green dots are $\mathbf{x}$ drawn from Gaussian pdf. 6(b) Local behavior. Curve segments are close to osculating circles.

There are two contributions to the total distortion for continuous $\mathcal{S}$: *approximation distortion* from the projection operation, and *channel distortion* resulting from channel noise mapped through $\mathcal{S}$ at the receiver. However, anomalous errors may also occur if $\mathcal{S}$ is piecewise continuous.

1) Channel distortion: The received vector $\hat{\mathbf{z}} = \mathbf{z} + \mathbf{n}$ is mapped through $\mathcal{S}$ to reconstruct $\mathbf{x}$. When noise is sufficiently small, distortion can be modelled by considering a linear approximation $\mathbf{S}_{lin}(\mathbf{z}_0)$ of $\mathbf{S}(\mathbf{z}) \in C^1$ at $\mathbf{z}_0$

$$\mathbf{S}_{lin}(\mathbf{z}_0 + \mathbf{n}) = \mathbf{S}(\mathbf{z_0}) + J(\mathbf{z_0})\mathbf{n}. \tag{17}$$

The following proposition provides the exact distortion under linear approximation:

Proposition 3: Minimum weak channel distortion
For any continuous i.i.d. Gaussian channel of dimension N and any continuous dimension reducing S-K mapping $\mathbf{S} \in \mathcal{S}$, where $S_i \in C^r,\ r \geq 1,\ i = 1, ..., M$, the distortion due to channel noise under the linear approximation in (17) is given by

$$\bar{\varepsilon}_{ch}^2 = \frac{\sigma_n^2}{M} \iint \cdots \int_{\mathcal{D}_c} \sum_{i=1}^{N} g_{ii}(\mathbf{z}) f_{\mathbf{z}}(\mathbf{z}) \mathrm{d}\mathbf{z}, \tag{18}$$

where $f_{\mathbf{z}}(\mathbf{z})$ is the channel pdf, and g_{ii} the diagonal components of the metric tensor of $\mathbf{S}$.

Proof: See Appendix B-B1. □

Remark 9: For piecewise smooth $\mathcal{S}$, one applies (18) over each $\mathcal{S}_i$, then sum all k contributions.

The name *weak channel distortion* is due to Definition 10 given below. Proposition 3 states that weak channel distortion increases in magnitude when $\mathcal{S}$ is stretched as the g_{ii}'s increases. To keep the channel distortion small, $\mathcal{S}$ should be stretched minimally. The opposite is sought in the dimension expansion case as an increase of g_{ii} leads to larger attenuation of noise at the receiver side. The following corollary is a special case of Proposition 3:

Corollary 2: Shape-preserving mapping
When $\mathbf{S}$ has a diagonal metric with $g_{ii}(\mathbf{z}) = g_{jj}(\mathbf{z}) = \alpha, \forall z, i, j$, and α constant, then

$$\bar{\varepsilon}_{ch}^2 = \frac{N\sigma_n^2}{M}\alpha^2. \tag{19}$$

I.e. all channel vectors are equally scaled when mapped through $\mathbf{S}$, and so noise will affect all source vectors $\mathbf{x}$ equally.

Proof: Insert $g_{ii}(\mathbf{z}) = g_{jj}(\mathbf{z}) = \alpha$ in (18). □

Under Corollary 2, $\mathcal{S}$ can be seen as an amplification α from channel to source at the receiver.

As the channel noise becomes larger, (18) becomes inaccurate as illustrated in Fig. 6(b). To determine the error under linear approximation, we consider 2nd order Taylor expansion:

Proposition 4: Error under 2nd order Taylor approximation
Under 2nd order Taylor approximation, in the special case of M:1 mappings, the error due to channel noise is given by

$$\begin{aligned}\varepsilon_{ch}^2(z_0) &= \sigma_n^2\|\mathbf{S}_0'\|^2 + \frac{3\sigma_n^4}{4}\frac{\|\mathbf{S}_0''\|^2}{\|\mathbf{S}_0'\|^4} \\ &= \|\mathbf{S}_0'\|^2\sigma_n^2 + \frac{3\sigma_n^4\kappa^2(x_0)}{4},\end{aligned} \tag{20}$$

valid for any S-K mapping $\mathbf{S}(z) \in C^n$, $n \geq 2$. The last equality is true under scaled arc-length parametrization. For any continuous dimension reducing S-K mapping in Definition 3,

with LoC coordinate curves, the error is given by

$$\begin{aligned}\varepsilon_{ch}^2(\mathbf{z}_0) &\approx \frac{\sigma_n^2}{M}\sum_{i=1}^{N}\left(g_{ii}(\mathbf{z}_0)+\frac{3\sigma_n^2}{4}\kappa_i^2(\mathbf{z}_0)\right)\\ &= \frac{\sigma_n^2}{M}\sum_{i=1}^{N}\left(g_{ii}(\mathbf{z}_0)+\frac{3\sigma_n^2}{4}\frac{b_{ii}^2(\mathbf{z}_0)}{g_{ii}^2(\mathbf{z}_0)}\right).\end{aligned} \tag{21}$$

Proof: See Appendix B-B2. □

Remark 10: Comparing with dimension expansion in Proposition 2 we see that distortion is scaled by the components of the SFF (or curvature), b_{ii}, in a similar manner. However, the scaling w.r.t. g_{ii} is opposite, corresponding to the results in (9) and (18).

Remark 11: From the proof of Proposition 4, Appendix B-B2, Eq. (88), we have

$$\begin{aligned}\varepsilon_{ch}^2(z_0) &= \sigma_n^2\|\dot{\mathbf{S}}(z_0)\|^2+\frac{3\sigma_n^4}{4}\|\ddot{\mathbf{S}}(z_0)\|^2+\frac{5\sigma_n^6}{12}\|\dddot{\mathbf{S}}(z_0)\|^2\\ &= \sigma_n^2+\frac{3}{4}\kappa_0^2\sigma_n^4+\frac{5}{12}\kappa_0^2\tau_0^2\sigma_n^6,\end{aligned} \tag{22}$$

for the channel error under 3rd order Taylor expansion. The last equality is a *canonical representation* [47, p.48], valid for any curve $\mathbf{S}\in C^r$, $r\geq 3$, where τ_0 the *torsion* of $\mathbf{S}$ (see Appendix A-A). This shows that higher order terms become smaller as σ_n decreases, at least for curves with small κ_0 and τ_0. Referring to Section III-A, this is the reason why we did not consider Taylor expansion beyond 2nd order there.

Definition 10: Weak noise regime, dimension reduction
Let $\mathbf{z}_0$ denote the transmitted vector and $\mathbf{S}(\mathbf{z}_0)$ its representation in the source space. We are in the *weak noise regime* whenever the second order term in (21) is negligible compared to the 1st order term. That is, (17) is a close approximation to $\mathbf{S}$ and (18) is an accurate approximation to the actual distortion due to channel noise. □

Remark 12: Generally the error in the ML-estimate increases with κ_{max}. However, for continuous mappings, κ_{max} must be non-zero in order to cover the sources space and thereby keep the approximation distortion low. One should therefore choose a mapping that fills the source space with the smallest possible κ. Alternatively, one may consider a scheme consisting of parallel lines or (hyper) planes where $\kappa_i=0$, at the expense of introducing anomalous errors. Therefore the weak noise regime is a good approximation for any reasonably chosen mappings at high SNR.

2) Approximation distortion: Approximation distortion results from the lossy operation $\mathbf{q}$. Its magnitude depends on the average distance source vectors have to $\mathcal{S}$. In order to make the approximation distortion as small as possible, $\mathcal{S}$ should cover the source space so that any $\mathbf{x}$ is as close to it as possible. Covering of the source space is obtained by stretching, bending and twisting the transformed channel space $\mathcal{S}$ inside the subset of the source space with significant probability mass (an example for the 2:1 case is provided in Fig. 6(a)). This is in conflict with the requirement of reducing channel distortion in which the stretching of $\mathcal{S}$ should be minimized. This tradeoff leads to a single optimal point, inline with [32].

Since approximation distortion is structure dependent, one cannot find a closed form expression for it in general. However, one can find a general expression valid for certain special cases that becomes exact as the dimension of the mapping becomes large.

Definition 11: Uniform S-K mapping
For an S-K mapping where at each point, $P\in\mathcal{S}$, there is a fixed distance Δ to the closest point on another fold of $\mathcal{S}$, is a *uniform S-K mapping*. The maximal approximation error from $\mathbf{x}$ to $\mathcal{S}$ will then be $\Delta/2$ for any $\mathbf{x}$ to any point of $P\in\mathcal{S}$.□

Remark 13: For a uniform $\mathcal{S}$, any vector being approximated to any point of $\mathcal{S}$ will be confined within a canal surface, S_c, as in Definition 7, but now with radius $r=\Delta/2$ and $\mathbf{S}(\mathbf{z})$ its center, and with the roles of $\mathbf{z}$ and $\mathbf{x}$ exchanged in equations (13) and (14).

The 2:1 S-K mapping shown in Fig. 6(a) is a uniform mapping (except close to the origin). For uniform S-K mappings, a similar distortion lower bound as that found for vector quantizers in [53] can be derived for small Δ, i.e., a *sphere bound* [54]. We have the following proposition:

Proposition 5: Sphere bound for approximation distortion
For a uniform $\mathcal{S}$ with distance Δ between closest points on neighboring folds, the approximation distortion for sufficiently small Δ is bounded by

$$\bar{\varepsilon}_q^2 \geq \frac{M-N}{4M(M-N+2)}\Delta^2. \tag{23}$$

Equality is obtained when $M=N+1$, and generally as $M,N\to\infty$, with $N/M=r$ constant.

Proof: See Appendix B-B3. □

Remark 14: Uniform mappings with $\bar{\varepsilon}_q^2$ bounded by (23) exist. For $M=N+1$, where (23) is exact, an example is parallel N-dimensional planes with distance Δ embedded in $\mathbb{R}^{N+1}$. The 3:2 HVQLC in Section V-A3, depicted in Fig. 2 to the upper left, is an example of this construction. Another is concentric N-spheres with radii $r=n\cdot\Delta$, $n\in\mathbb{N}$ (the 2:1 spiral in Fig. 6(a) is similar to this). For 3:1 case, place parallel lines in $\mathbb{R}^3$ such that each line have distance Δ to each of its nearest neighbors. With the lines oriented along x_3-axis, one wold obtain a lattice in the x_1,x_2-plane, and (23) serve as a lower bound. This construction, generalized to $\mathbb{R}^M$ for $M>3$ was treated in [45] for Gaussian multiple access channel. There, this mappings was also generalized to higher dimensions using hyper planes, analyzing its asymptotic performance.

IV. Asymptotic analysis for S-K mappings

We investigate how S-K mappings perform as their *dimensionality* (or *block-length*) increases. I.e., letting M,N increase while $r=N/M\in\mathbb{Q}^+$ is kept constant. Ultimately, can S-K mappings obtain OPTA as $M,N\to\infty$, and what conditions on $\mathcal{S}$ are needed to do so? We consider Gaussian sources here.

When constructing mappings based on (hyper) surfaces, one method is to construct several parallel and independent systems based on curves (i.e., 1:N or M:1 mappings), each one representing a coordinate curve on the resulting surface. This approach was taken in [7] and is a simple way of constructing higher dimensional mappings. However, one cannot

obtain optimal performance at high SNR in this way: Take a $(m+n)$:2 mapping when $M > N$ and a 2:$(m+n)$ mapping when $M < N$, both realized as two parametric curve-based systems in parallel. A m:1 and n:1 mapping when $M > N$ and a 1:m and 1:n mapping when $M < N$. Then we have

Proposition 6: Sub-optimality of decomposable mappings Any $(m+n)$:2 or 2:$(m+n)$ mapping composed of lower dimensional sub-mappings will always follow SDR$\sim$ SNR$^{\tilde{r}}$ as SNR$\to\infty$, with $\tilde{r}$, the dimension change factor of the sub-system with highest distortion. Therefore, such mappings will diverge from OPTA at high SNR.

Proof: See Appendix C-1. □

Remark 15: A result for M:N mappings follows from Proposition 6 using several such systems in parallel with power allocation over all sub-systems (water filling [55, p.277]).

Decomposable mappings should be avoided if one seeks a scheme approaching OPTA at high SNR. However, as will be seen in Section V, such mappings can be applicable in lower SNR regions.

The asymptotic result provided in the following do not refer to a particular $\mathcal{S}$, as such the results are non-constructive. However, the results provide conditions for $\mathcal{S}$ to *potentially* obtain OPTA in the limit $M, N \to \infty$. By "potential" we mean that any (global) geometrical structure satisfying all conditions should obtain OPTA if properly optimized. That is, when optimal choice of coordinates and other parameters are determined.

A. Asymptotic analysis for dimension expanding S-K mappings.

We determine under which conditions dimension expanding S-K mappings may achieve OPTA for $\forall r \in \mathbb{Q}[1,\infty)$ in the limit $M, N \to \infty$. The results presented are extensions of [3].

We start with a proposition concerning anomalous distortion as $M, N \to \infty$:

Proposition 7: Asymptotic anomalous distortion Take normalized noise vectors $\tilde{\mathbf{n}} = \mathbf{n}/\sqrt{N}$. With Δ_{min} as in Definition 8, let $\mathbf{n}_{an}$ be the $K(\leq N)$ dimensional sub-vector of $\tilde{\mathbf{n}}$ pointing in the direction of the closest point on another fold of $\mathcal{S}$ along which Δ_{min} is measured. Then $\bar{\varepsilon}^2_{an} \to 0$ as $K, N \to \infty$ if $\Delta_{min} > 2\sqrt{K/N}\sigma_n$, $\forall \mathbf{x}_0$.

Proof: By definition, $\tilde{\mathbf{n}}$ has mean length σ_n. It is shown in [43, pp.324-325] that the variance of $\|\tilde{\mathbf{n}}\|$ decreases as N increases and that $\lim_{N\to\infty}\|\tilde{\mathbf{n}}\| = \sigma_n$ with probability one. For $\mathbf{n}_{an}$, a $K(<N)$ dimensional subset of $\tilde{\mathbf{n}}$, we get $\|\mathbf{n}_{an}\| = \sqrt{K/N}\sigma_n$ with probability one. □

Remark 16: Proposition 7 is equivalent to having a non-intersecting canal surface as in Lemma 1. I.e., $1/\kappa_{max} \geq \rho_n \geq \sqrt{b_n^2\sigma_n^2(N-M)/N}$, with $K = N - M$, where $b_n \to 1$ as $M, N \to \infty$.

Proposition 7 is the key to performance gain through increased mapping dimensionality: Consider Definition 9. The distribution of $\rho = \|\mathbf{n}_{an}\|$, $\mathbf{n}_{an} \in \mathbb{R}^K$, is given by [56, p. 237]

$$f_\rho(\rho) = \frac{2(\frac{K}{2})^{\frac{K}{2}}\rho^{K-1}}{\Gamma(\frac{K}{2})\sigma_n^K} e^{-\frac{\frac{K}{2}\rho^2}{\sigma_n^2}}, \qquad K \geq 1, \tag{24}$$

where $\Gamma(\cdot)$ is the *Gamma function* [57]. Fig. 7(a) shows (24) for selected values of K. Note that the probability mass of

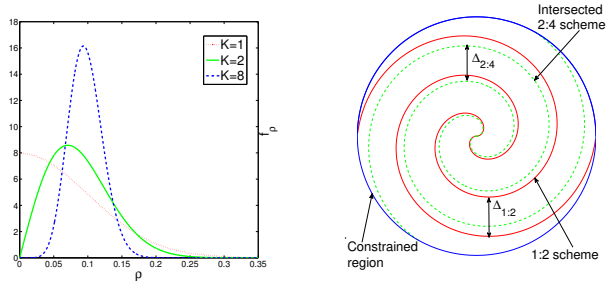

(a) (b)

Fig. 7. (a) Pdf of $\rho = \|\mathbf{n}_{an}\|$ when $\sigma_n = 0.1$. (b) Performance improvement from increased mapping dimensionality for $r = 2$: The dashed curve is an intersection of a surface in $\mathbb{R}^4$. As $\Delta_{2:4} < \Delta_{1:2}$, it is possible to obtain a gain for the 2:4 mapping.

ρ becomes more located around σ_n as N increases. For S-K mappings, a gain can potentially be obtained when increasing dimensionality as Δ_{min} can be reduced: Consider $r = 2$, which can be accomplished by both 1:2 and 2:4 mappings. Take a 2:4 mapping with diagonal G with $g_{11} = g_{22}$, both chosen optimally. The 2:4 mapping can then be "packed" more densely in the channel space as $f_\rho(\rho)$ narrows. That is, $\Delta_{2:4} < \Delta_{1:2}$ as Fig. 7(b) illustrates (note that the intersected 2:4 mapping in the figure is just an illustration, not an actual 2:4 mapping.). The g_{ii}'s can therefore be made larger with the 2:4 mapping, effectively reducing $\bar{\varepsilon}^2_{wn}$ and thereby the gap to OPTA. We provide a mapping obtaining such a gain for the $r = 2$ case in Section V-B3.

Remark 17: Linear mappings do not introduce anomalous errors, so they cannot benefit from increased dimensionality.

According to Proposition 7, anomalous errors can be avoided as $M, N \to \infty$ if $\Delta_{min} \geq 2\sqrt{K/N}\sigma_n$, which is is the same as satisfying Lemma 1. To determine the optimal $\mathcal{S}$, we must determine the smallest obtainable $\bar{\varepsilon}^2_{wn}$ under this condition without violating a channel power constraint.

As proving the existence of general hyper surfaces satisfying a distortion criterion is hard, if at all possible, we use a geometrical argument and consider how large volume the transformed source will occupy in the channel space, a generalization of results presented in [43, pp.666-674]. In order to determine the volume $\mathcal{S}$ occupies in the channel space it must be enclosed within an entity of N-dimensional volume. Arguments in [43, pp. 670-672] state that for 1:N mappings this is an $N-1$ dimensional *tube*, $\mathcal{S} \times \mathbb{S}^{N-2}$, with constant radius $\rho_{MN} \geq \|\mathbf{n}_{an}\| > \sqrt{b_{NM}^2\sigma_n^2(N-1)/N}$ ($b_{NM} \to 1$ as $N \to \infty$), with the signal curve at its center. This is a canal surface after Definition 5 with characteristic $\mathbb{S}^{N-2}$, a $N-2$ sphere with radius ρ_{MN}. Locally this canal surface can be approximated by $\mathbb{L} \times \mathbb{S}^{N-2}$, with $\mathbb{L}$ a line-segment. Referring back to Example 4, we locally have $\mathbb{L} \times \mathbb{S}^{N-2}$ when we are in the weak noise regime of Definition 4. Then, for $M : N$ mappings, one can consider extended canal surfaces in Definition 7. Thus, $\mathcal{S}$ should be enclosed within $\mathcal{S} \times \mathbb{S}^{N-M-1}$, which can locally be approximated

by $\mathbb{B}^M \times \mathbb{S}^{N-M-1}$ if we are in the weak noise regime of Definition 4. Here, $\mathbb{S}^{N-M-1}$ is a hyper sphere with radius $\rho_{MN} \geq \sqrt{b_{NM}^2 \sigma_n^2 (N-M)/N} = \sqrt{1-r^{-1}} b_{NM} \sigma_n$ and $\mathbb{B}^M$ is an M-dimensional *ball* of radius ρ_M, which size corresponds to the *stretching* of $\mathcal{D}_s$ through $\mathcal{S}$.

Definition 12: Local $\mathbb{B}^M \times \mathbb{S}^{N-M-1}$ regime
We say we are in the *local* $\mathbb{B}^M \times \mathbb{S}^{N-M-1}$ *regime* whenever: i) Definition 4 is satisfied. ii) $\Delta_{min} = 2\rho_{MN} \geq 2\sqrt{1-r^{-1}} b_{NM} \sigma_n$ at every point of $\mathcal{S}$. iii) Lemma 1 is satisfied, i.e., the canal surface $\mathcal{S} \times \mathbb{S}^{N-M-1}$ has no characteristic intersection. □

Example 5: Definition 12 is satisfied for the 1:3 mapping in Fig. 5 when the cylinder is a valid model locally along the whole curve.

Remark 18: For fixed SNR there is an optimal ρ_{MN}, inline with [32]: If σ_n increases the performance will deteriorate due to anomalous errors, while if σ_n decreases there will be non-utilized space available to stretch $\mathcal{S}$, implying sub-optimal $\bar{\varepsilon}_{wn}^2$. In the latter case the slope of SDR vs SNR will follow that of a linear system according to (12) as the first term dominates.

We have the following proposition:

Proposition 8: Minimum asymptotic distortion for dimension expanding S-K mappings
Assume that $f_{\mathbf{x}}(\mathbf{x})$ is Gaussian. Any non-decomposable shape preserving dimension expanding $\mathcal{S}$ satisfying Definition 12, will in the limit $M, N \to \infty$, for any $r = N/M \in \mathbb{Q}([1,\infty))$, have anomalous distortion $\bar{\varepsilon}_{an}^2 \to 0$ and potentially obtain weak noise distortion given by

$$\bar{\varepsilon}_{wn_{min}}^2 = \sigma_x^2 \left(1 + \frac{P_N}{\sigma_n^2}\right)^{-r}. \tag{25}$$

Proof: See Appendix C-2. □

Remark 19: Summary of conditions that $\mathcal{S}$ must satisfy to obtain the distortion in (25):

1. Definition 4 should be satisfied: $\mathcal{S}$ should be nearly flat within a hyper-sphere of radius σ_n. The larger σ_n is, the smaller κ_{max} should be, so that the 1st term in (11) dominates.
2. At any point of $\mathcal{S}$, $\Delta_{min} > 2\sqrt{(1-r^{-1})}\sigma_n$ to avoid anomalous errors. That is, the canal surface $\mathcal{S} \times \mathbb{S}^{N-M-1}$ should satisfy Lemma 1.
3. $\mathcal{S}$ should fill the channel space as densely as possible while satisfying 1 and 2 above for a given power constraint in order to stretch (amplify) the source as much as possible and thereby minimize $\bar{\varepsilon}_{wn}^2$. I.e., a $\mathcal{S}$ with $\rho_{MN} = \Delta_{min}$ =constant to optimally utilize the channel space.
4. $\mathcal{S}$ can be shape preserving (Corollary 1). This condition was chosen to simplify the proof of Proposition 8. It may therefore be that more general $\mathcal{S}$ can obtain OPTA.

Example 6: What S-K mapping would satisfy the conditions in Remark 19? The *parallel planes mapping* illustrated in Fig. 2 and discussed in Remark 14 (but now residing in $\mathcal{D}_c$) is a potential candidate. The special case of 1:2 is depicted in Fig 8. The mapping in Fig. 8(a) potentially fulfill all condition as $\kappa = 0$ and it fills the channel space properly with constant $\Delta_{min} = 2\rho_{MN}$. We will consider this mapping in Section V-B3, where we show that it can achieve OPTA as $M, N \to \infty$. For a fully continuous mapping,

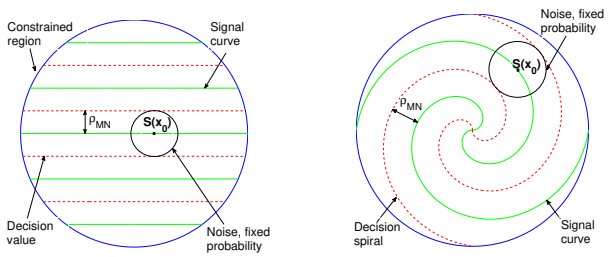

(a) (b)

Fig. 8. Structures that potentially satisfy the conditions of Proposition 8. $\Delta_{min} = 2\rho_{MN}$ should decrease with increasing SNR. (a) Parallel line segments (HDA system) (b) Archimedes spiral.

consider the spiral in Fig. 8(b): It satisfies 2-4, but also 1 as long as $\kappa << \sigma_n^2$. That is, the spiral must have smaller curvature as the SNR drops, obtained by choosing Δ_{min} lager, inline with earlier efforts [5]. The question is if higher dimensional generalizations satisfying the above conditions can be constructed.

B. Dimension reducing S-K mappings.

We determine under which conditions dimension reducing S-K mappings may achieve OPTA for $\forall r \in \mathbb{Q}[0,1)$ as $M, N \to \infty$.

Again we need to enclose $\mathcal{S}$ within a canal surface. By similar reasoning as in Section IV-A, we obtain the canal surface $\mathcal{S} \times \mathbb{S}^{M-N-1}$, now residing in the source space. This canal surface can locally be approximated as $\mathbb{B}^N \times \mathbb{S}^{M-N-1}$, with $\mathbb{B}^N$ a ball with radius ρ_N, a local representation of the transformed channel space in source space, and $\mathbb{S}^{M-N-1}$, a hyper-sphere with radius ρ_{MN}, corresponding to the decision borders for approximation to a uniform $\mathcal{S}$ (Definition 11).

Definition 13: Local $\mathbb{B}^N \times \mathbb{S}^{M-N-1}$ regime
We say we are in the *local* $\mathbb{B}^N \times \mathbb{S}^{M-N-1}$ *regime* whenever: i) Definition 10 is satisfied ii) Definition 11 is satisfied with $\Delta = 2\rho_{MN}$, where ρ_{MN} is the radius of $\mathbb{S}^{M-N-1}$. □

Condition i) states that $\mathcal{S}$ must be approximately flat inside a sphere of radius $\alpha\sqrt{b_N}\sigma_n$ at any point, where α is the amplification factor in (19). Condition ii) ensures uniformity (Definition 11). Note that both i) and ii) will be satisfied iff $\mathcal{S} \times \mathbb{S}^{M-N-1}$ has no characteristic intersection, which limits the maximal principal curvature κ_{max}. Take the 3:1 case: we then have the canal surface in Fig. 5, but where $\mathbf{n}_{an}$ now corresponds to the approximation error $\mathbf{x}_0 - \mathbf{q}(\mathbf{x}_0)$ and $\mathbf{n}_{wn}$ corresponds to the channel error $\mathbf{S}(\hat{\mathbf{x}}_0) - \mathbf{q}(\mathbf{x}_0)$.

To determine optimal performance, the free parameter Δ must be determined. Different from the expansion case, Δ is not directly related to the noise variance and has to be found through a minimization process determining the optimal balance between the two distortion terms $\bar{\varepsilon}_q^2$ and $\bar{\varepsilon}_{ch}^2$ (see Eq.(114), Appendix C-3). We have the Proposition.

Proposition 9: Minimum asymptotic distortion for dimension reducing S-K mappings
Assume that $f_{\mathbf{x}}(\mathbf{x})$ is Gaussian. Any non-decomposable shape

preserving dimension reducing S-K mapping satisfying Definition 13, will in the limit $M, N \to \infty$, for any $r = N/M \in \mathbb{Q}([0,1])$, potentially obtain the distortion

$$D_{min} = \bar{\varepsilon}_q^2 + \bar{\varepsilon}_{ch}^2 = \sigma_x^2 \left(1 + \frac{P_N}{\sigma_n^2}\right)^{-r}. \quad (26)$$

Proof: See Appendix C-3. □

Remark 20: Summary of conditions that $\mathcal{S}$ should satisfy to obtain the distortion in (26):

1. Definitions 10 and 13 must be satisfied: $\mathcal{S}$ should be approximately flat within a sphere of radius $\alpha\sigma_n$, implying that larger σ_n necessitates smaller curvature κ_{max}.

2. For fixed approximation distortion, the canal surface of $\mathcal{S}$ should cover the source space with the least possible stretching and curvature to minimize channel distortion.

3. $\mathcal{S}$ can be uniform (Definition 11) and shape-preserving (Corollary 2). These were chosen to simplify the proof of Proposition 9. More general mappings may therefore obtain OPTA.

Example 7: What $\mathcal{S}$ satisfies these conditions? The mapping in Fig 6(a) satisfies 2-3 in the finite dimensional case. However, as in the expansion case, $\kappa << \sigma_n^2$, if point 1 should be satisfied. A mapping similar to the one shown in Fig. 8(a), now residing in the source space, satisfies all these conditions. By making sure that that the ends of each line/plane are close in the channel space, anomalous errors are avoided. We proved that the generalization of this approach to an M:1 mapping of arbitrary dimensionality, i.e., the *parallel planes mapping* mentioned in Remark 14, can achieve OPTA when $M, N \to \infty$ at high SNR (see [58], Proposition 1).

Lastly, we state a condition on Δ following from the proof of Proposition 9, which will be important for mapping construction in Section V:

Corollary 3: For any uniform dimension reducing $\mathcal{S}$, then $\bar{\varepsilon}_{ch}^2 \sim \Delta^{-(M-N)/N}$ to obtain the same slope as OPTA as SNR$\to \infty$.

Proof: Follows from the proof of Proposition 9 in Appendix C, Eqn (113). □

Example 8: Take a uniform 3:2 mapping where $\bar{\varepsilon}_a^2 \sim \Delta^2$ according to Proposition 5. Then we need $\bar{\varepsilon}_{ch}^2 \sim 1/\Delta$, in order to obtain SDR $\sim$ SNR$^{2/3}$ as SNR$\to \infty$.

V. Mapping Construction

Construction of 1:N or M:1 mappings follow more or less directly from results and conditions derived for curves throughout this paper as illustrated in [5]. However, when it comes to (hyper) surfaces some more care needs to be taken. We mainly consider surfaces in $\mathbb{R}^3$, if not otherwise stated, in order to obtain simple and explicit results.

Earlier investigations [40, pp. 88-89] indicated that a diagonal G with $g_{ii}(x_i)$ =constant $\forall i$, is convenient as it avoids nonlinear distortion, providing a shape preserving mapping[3] (see Corollary 1 and 2). Further, for general (source) distributions it can be convenient to choose

$$G(x_1, x_2) = \text{diag}[g_{11}(x_1), g_{22}(x_2)] \quad (27)$$

[3]A diagonal G arises naturally from (9) and (18) as only the g_{ii}'s (and not the g_{ij}'s) contribute.

where $g_{ii}(x_i)$ can be optimized for the source pdf for each coordinate curve on $\mathcal{S}$ (see [50, pp.296-297] for 1:N mappings). However, Proposition 6 and Corollary 3 reveal that the metric in (27) is not sufficient for a mapping to follow the same slope as OPTA curve as SNR$\to \infty$.

Coordinate curves on $\mathcal{S}$ where g_{ii} only depends on x_i are possible for certain sub-families of surfaces: An *isometric mapping* between two surfaces $\mathcal{S}$ and $\mathcal{S}^*$ is length preserving, i.e., $g_{\alpha\beta} = g^*_{\alpha\beta}$, under the same choice of coordinates [47, pp.176-177]. Any $\mathcal{S}$ that has a metric like (27) can be mapped isometrically to the Euclidean plane, and Theorem 59.3 in [47, p.189] states that this has to be a *developable surface*:

Definition 14: Developable surface in $\mathbb{R}^3$:
Consider a *ruled surface* (RS), obtained by a set of straight lines, $\mathbf{z}(\ell)$, named *generators* interrelated through a space curve $\mathbf{y}(\ell)$, named *indicatrix* [47, p.181], as $\mathbf{S}(\ell, t) = \mathbf{y}(\ell) + t\mathbf{z}(\ell)$. $\mathbf{z}$ is a unit vector linearly independent of the tangent vector $\dot{\mathbf{y}}$, i.e., $\dot{\mathbf{y}} \times \mathbf{z} \neq 0$. $\mathbf{y}(\ell)$, acts like the *trajectory* for a straight line through space, and both $\mathbf{z}$ and $\mathbf{y}$ are coordinate curves on $\mathcal{S}$. The RS is a developable surface (DS) $\Leftrightarrow |\dot{\mathbf{y}}\ \mathbf{z}\ \dot{\mathbf{z}}| = 0$ according to Theorem 58.1 in [47, p.182]).□

For any DS, g_{ii} can be made constant equal to 1 $\forall x_i$, by arc-length parametrization of $\mathbf{y}$. An example of DS is shown in Fig. 9(a) in Section V-A1.

Remark 21: As all DS can be seen as a straight line (a 1:1 system) moved along a curve $\mathbf{y}$ (a M:1 or 1:N system), any DS will diverge from OPTA as SNR grows large, including the higher dimensional mappings proposed in [7].

To avoid the problem of non-optimal slope one has to widen the set of mappings beyond DS, keeping a similar type of G as in (27). The most direct generalization are surfaces that can be mapped in an *angle preserving* way (or *conformally*), to the Euclidean plane. The metric between two surfaces $\mathcal{S}$ and $\mathcal{S}^*$ are then proportional, i.e. $g^*_{\alpha\beta} = \eta(u^1, u^2) g_{\alpha\beta}$ [47, pp. 193-194]. A subset of such surfaces are shape preserving, for example when η is a constant.

Remark 22: Another condition for an S-K mapping to minimize channel power and reduce the effect of noise is to construct the mapping so that source vectors with highest probability are allocated to channel representations with low power [59, p.103]. Also, the condition in Corollary 3 is important to consider for dimension reducing mappings.

In the following we illustrate the results of this paper with focus on 3:2 and 2:3 mappings. We also provide an example on the effect of dimensionality increase in the $r = 2$ case.

A. Examples on 3:2 mappings

Three 3:2 mappings selected based on intuition obtained through previous sections are evaluated: The first two are selected from the *Encyclopedia of Analytical Surfaces* [60] as likely candidates for well-performing mapping based on the criteria of this paper: One DS-based mapping as well as a non-decomposable mapping. The third is a piecewise smooth (HDA) mapping specifically constructed to satisfy all requirements for obtaining the slope of OPTA at high SNR.

To evaluate performance of the example mappings we compare them with OPTA and *block pulse amplitude modulation*

(BPAM) [37], the optimal linear mapping. Obviously, any meaningful choice of nonlinear mapping should rise well above BPAM as the SNR increases. At the end of the section all suggested schemes are compared to existing mappings.

1) Right Cylinder with Archimedes Spiral Directrix (RCASD): Fig. 9(a) depicts the RCASD in the source space. Its parametric equation is given by [60, p. 51]

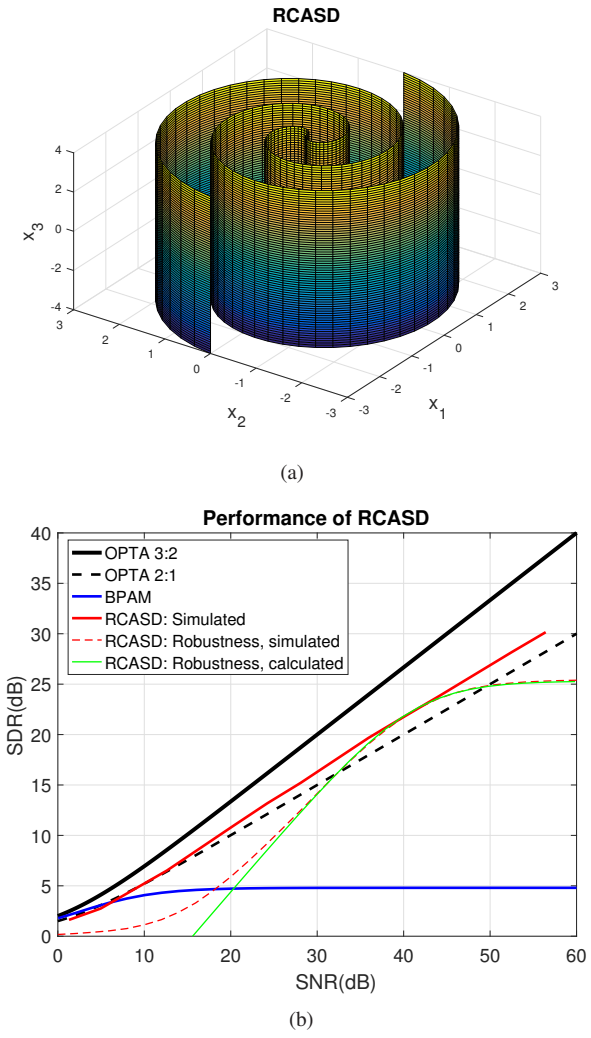

(a)

(b)

Fig. 9. (a) RCASD in source space with LoC coordinate grid. (b) Performance of RCASD compared to OPTA and BPAM.

$$\mathbf{S}(\mathbf{z}) = \big[\pm a\varphi(z_1)\cos(\varphi(z_1)), \pm a\varphi(z_1)\sin(\varphi(z_1)), \alpha_2 z_2\big], \tag{28}$$

with α_2 some amplification factor and $a = \Delta/\pi$, where $\pm$ refers to positive and negative channel values. Δ is the smallest distance between the two "spiral surfaces", or folds, seen in Fig. 9(a). The RCASD is a DS with Archimedes spiral as directrix (a 2:1 sub-mapping treated in [5]).

The components of FFF are

$$\begin{aligned} g_{11} &= \left(\frac{\Delta}{\pi}\right)^2 \big(\varphi'(z_1)\big)^2\big(1+\varphi^2(z_1)\big), \\ g_{22} &= \alpha_2^2,\ g_{12} = g_{21} = 0, \end{aligned} \tag{29}$$

and the components of the SFF are

$$\begin{aligned} b_{11} &= -a(\varphi'(z_1))^2 \frac{2+\varphi^2(z_1)}{\sqrt{1+\varphi^2(z_1)}}, \\ b_{12} &= b_{21} = b_{22} = 0. \end{aligned} \tag{30}$$

The components in (29) are computed as $g_{\alpha\beta} = \mathbf{S}_\alpha \cdot \mathbf{S}_\beta$, and the components of the SFF are computed using Eq.(43) in [46, p.4]. With (29) and (30), one can from Theorem 2 in Appendix A-B, conclude that the coordinate curves are LoC as $g_{12} = b_{12} = 0$. Therefore (20) describes the 2nd order behavior of this mapping.

Evaluation of curvature: With LoC coordinates, the principal curvatures are found from the fundamental forms as:

$$\kappa_1 = \frac{b_{11}}{g_{11}} = -\frac{2+\varphi^2(z_1)}{a(\sqrt{1+\varphi^2(z_1)})^{3/2}},\ \kappa_2 = \frac{b_{22}}{g_{22}} = 0. \tag{31}$$

By choosing

$$\varphi(z_1) = \pm\sqrt{\alpha_1 z_1/(\eta\Delta)}, \tag{32}$$

with α_1 some amplification factor, one approximates arc-length parametrization along the directrix as shown in [5]. Evaluation of κ_1 as function of the free parameters Δ and α_1 is provided in [46, p.23], Fig. 18(a). Generally, the curvature is relatively small for this mapping. By inserting optimized parameters for 30dB SNR found by the optimization procedure below, i.e., $\Delta^* = 0.608$ and $\alpha_1^* = 3.33$, one obtains $|\bar{\kappa}_1| < 1$ averaged over the relevant range of z_1. By considering the distortion terms in (12), with total transmission power 1, then $\sigma_n^2 = 0.001$, and one can see that the 1st order term is in the order of about $10^{-3}/(10^{-3})^2 = 1000$ over the 2nd order term. Therefore, RCASD is a mapping following Definition 4 at high SNR.

Optimization of RCASD as 3:2 mapping: The RCASD's performance is made scalable with SNR through the factor $a = \Delta/\pi$ where Δ is adapted to the noise variance σ_n^2.

Distortion: With $\hat{z}_i = z_i + n_i$ mapped through (28), the channel distortion is computed from (18). With φ as in (32), $g_{11} \approx \alpha_1^2,\ \forall z_1, z_2$. Similarly, since $x_3 = \alpha_2 z_2$, then $g_{22} = \alpha_2^2$, and so G is diagonal with constant g_{ii}'s, which was one of the criteria sought. Therefore

$$\begin{aligned} \bar{\varepsilon}_{ch}^2 &= \frac{\sigma_n^2}{3}\iint \sum_{i=1}^{2} g_{ii}(\mathbf{z}) f_{\mathbf{z}}(\mathbf{z})\mathrm{d}\mathbf{z} \\ &= \frac{\sigma_n^2}{3}\big(\alpha_1^2+\alpha_2^2\big) f_{\mathbf{z}}(\mathbf{z})\mathrm{d}\mathbf{z} = \frac{\sigma_n^2\big(\alpha_1^2+\alpha_2^2\big)}{3}. \end{aligned} \tag{33}$$

From Fig. 9(a) one can see that we have a uniform S-K mapping (Definition 11), implying that Eq. (23) with $N = 2$ and $M = 3$ applies exactly as $M = N + 1$,

$$\bar{\varepsilon}_q^2 = \Delta^2/36. \tag{34}$$

Power: The Archimedes' spiral directrix was applied as 2:1 mapping in [5]. With φ as in (32) it was shown that a Laplace distribution over z_1 is obtained with variance $\sigma_{y_1}^2 = 2(2\eta\sigma_x^2\pi/(\Delta\alpha_1))^2,\ \eta = 0.16$, at high SNR. As $z_2 = x_3/\alpha_3$, z_2 has a Gaussian distribution with variance $\sigma_{z_2}^2 = \sigma_x^2/\alpha_2^2$. Therefore, the total channel power becomes

$$P_t = \frac{1}{2}\left(2\left(\frac{2\eta\sigma_x^2\pi}{\Delta\alpha_1}\right)^2 + \frac{\sigma_x^2}{\alpha_2^2}\right). \tag{35}$$

Optimization: With constraint $C_t = P_{\max} - P_t(\Delta, \alpha_1, \alpha_2) \geq 0$, the following objective function is obtained,

$$\mathcal{L}(\Delta, \alpha_1, \alpha_2) = \bar{\varepsilon}_q^2(\Delta) + \bar{\varepsilon}_{ch}^2(\alpha_1, \alpha_2) - \lambda C_t(\Delta, \alpha_1, \alpha_2). \quad (36)$$

The optimal parameters are found by a numerical approach, as in [40, pp. 87].

The performance of the optimized RCASD is shown in Fig. 9(b) (red curve). The RCASD improves with SNR, rising well above BPAM as SNR increases, and is also robust to varying SNR, having both graceful improvement and degradation for a fixed set of parameters (red dashed curve). The calculated performance is also shown (green curve) in order to demonstrate the accuracy of the theory in Section III-B. The distortion contributions in Section III-B is observed from the robustness graphs: $\bar{\varepsilon}_q^2$ dominates above the optimal SNR, whereas below, $\bar{\varepsilon}_{ch}^2$ dominates. Simulated and calculated performance correspond well, confirming that RCASD follows Definition 10, inline with the curvature evaluation above. However, the slope at high SNR follows that of 2:1 OPTA (black dashed curve) which is expected from Proposition 6 as the RCASD is decomposable into a 2:1- and 1:1 system.

2) Snail Surface: The *snail surface* is non-decomposable and covers a spherical subset of the source space properly.Its parametrization has components [60, p. 280]

$$\begin{aligned} S_1(z_1, z_2) &= a\varphi(z_1)\sin(\varphi(z_1))\cos(\alpha_2 z_2 + \phi), \\ S_2(z_1, z_2) &= b\varphi(z_1)\cos(\varphi(z_1))\cos(\alpha_2 z_2 + \phi), \\ S_3(z_1, z_2) &= -c\varphi(z_1)\sin(\alpha_2 z_2 + \phi), \end{aligned} \quad (37)$$

which are valid for $0 \leq z_1 \leq k\pi$, $-\pi \leq z_2 \leq \pi$. To include negative values of z_1, i.e., $-k\pi \leq z_1 \leq 0$, one flips the sign of all components in (37), and obtain a *double* snail surface (DSS),as depicted in Fig. 10(a). By choosing $\psi = \pi/2$ and $a = b = c = 2\Delta/\pi$ one obtains a spherical symmetry which leads to a (close to) uniform S-K mapping (Definition 11), and so (34) approximates $\bar{\varepsilon}_q^2$. ϕ will be decided later. For a general $\varphi(z_1)$, the metric tensor is found to be [46]

$$\begin{aligned} g_{11} &= (a\varphi'(z_1))^2\big(1 + \varphi^2(z_1)\cos^2(\alpha_2 z_2 + \phi)\big), \\ g_{22} &= a^2\alpha_2^2\varphi^2(z_1), \;\; g_{12} = g_{21} = 0. \end{aligned} \quad (38)$$

By inserting $\varphi(z_1) = \alpha_1 z_1$ in (38) one observes that $g_{ii} \sim z_1^2$, $i = 1, 2$, and so $\bar{\varepsilon}_{ch}^2$ increases with z_1^2. One can compensate this for both g_{ii} components simultaneously by choosing $\varphi \sim \sqrt{z_1}$. As the RCASD also has $g_{11} \sim z_1^2$ when $\varphi(z_1) = \alpha_1 z_1$, and that DSS scales with Δ like RCASD, it makes sense to use (32) for DSS as well, the choice of η being arbitrary.

Evaluation of curvature: The components of the SFF, as derived in [46, p.23], are

$$\begin{aligned} b_{11} &= -\frac{a(\varphi'(z_1))^2\varphi^2(z_1)\cos^3\theta}{\sqrt{1 + \varphi^2(z_1)\cos^2\theta}}, \\ b_{22} &= -\frac{a\alpha_2^2\varphi^2(z_1)\cos\theta}{\sqrt{1 + \varphi^2(z_1)\cos^2\theta}}, b_{12} = \frac{a\alpha_1\alpha_2\varphi^2(z_1)\sin\theta}{\sqrt{1 + \varphi^2(z_1)\cos^2\theta}}, \end{aligned} \quad (39)$$

with $\theta = \alpha_2 z_2 + \phi$. As the coordinates are not LoC, the principal curvatures are the roots of (69) in Appendix A-B

$$\kappa_{1/2} = \frac{1}{2}\left(\frac{b_{11}}{g_{11}} + \frac{b_{22}}{g_{22}} \pm \sqrt{\left(\frac{b_{11}}{g_{11}} + \frac{b_{22}}{g_{22}}\right)^2 - 4\frac{b_{11}b_{22} - b_{12}^2}{g_{11}g_{22}}}\right). \quad (40)$$

Evaluation of κ_i as function of the free parameters Δ, α_1 and α_2 is provided in [46, p.23], Fig. 18(b). Not surprisingly, the curvature is larger than for RCASD in general, particularly when Δ is large and α_1 is small (corresponding to low SNR case). However, when Δ is small and α_1 is large, corresponding to high SNR case, the curvature is relatively small: By inserting optimized parameters for 30dB SNR found by the optimization procedure below ($\Delta^* = 0.539$, $\alpha_1^* = 4.76$, $\alpha_2^* = 2.57$) one obtains average maximal curvature $|\bar{\kappa}_2| < 1$ averaged over the relevant range of z_1 [46, p.23]. Similar to the RCASD, the DSS can be considered to follow Definition 4 at high SNR.

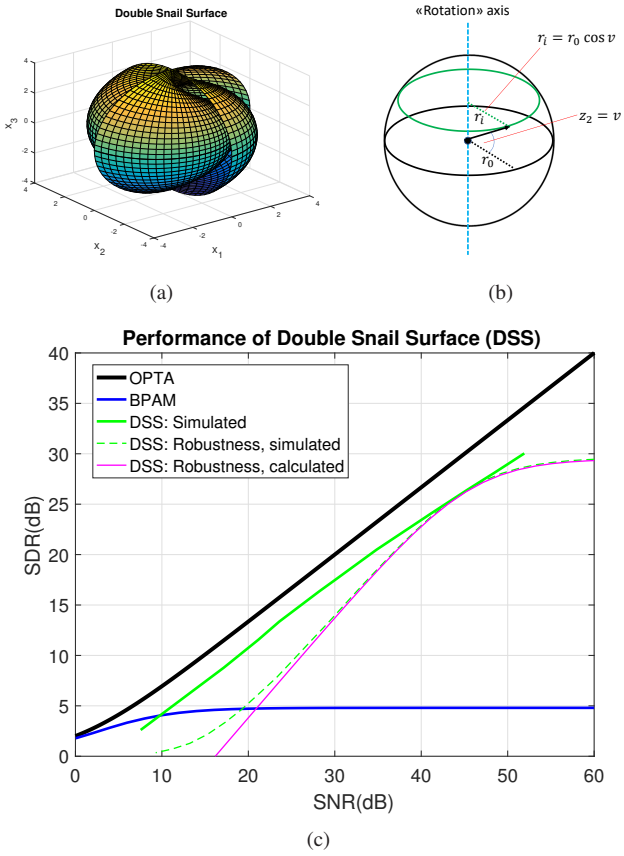

Fig. 10. (a) The DSS ($a = b = c = 2\Delta/\pi$). (b) Virtual spherical shell applied to compute the channel pdf of z_2. (c) Performance of Double Snail Surface (DSS) compared to OPTA and BPAM.

Optimization of DSS as 3:2 mapping:

Channel Power and Density Function: To evaluate the channel input from DSS it is convenient to analyze variation over each channel separately (see [46] p.21-22 for more details).

Take channel 1 first: It was argued in [46, p.21] that the mapping from DSS to z_1 can be approximated as the *radius*, $\rho = \sqrt{x_1^2 + x_2^2 + x_3^2}$, tracing out points inside a sphere as z_1 and z_2 vary over their domains. Then, with Δ small, one can approximate the mapping $\mathbf{x} \to z_1$ as a continuous function

$h:\mathbb{R}^3\to\mathbb{R}$. This assumption becomes more accurate as SNR grows, i.e., as Δ decreases. By choosing $\varphi=(\gamma z_1)^n$, $n\in\mathbb{Q}^+$, then $z_1=h(x_1,x_2,x_3)=\pm\gamma a^{-n}(x_1^2+x_2^2+x_3^2)^{n/2}=\pm\gamma a^{-n}\rho^n=\ell(\rho)$, and we have:

Lemma 2: At high SNR, with $\varphi=(\gamma z_1)^n$, the pdf for z_1 when $\mathcal{S}$ is a DSS, is approximated by

$$f_{z_1}(z_1)=\frac{na^3\gamma^3|z_1|^{3n-1}}{\sqrt{2\pi}\sigma_x^3}e^{-\frac{a^2\varphi^2(z_1)}{2\sigma_x^2}}. \tag{41}$$

Proof: See Appendix D-1. □

Now assume that $\varphi(z_1)$ is given by (32), then $\gamma=\sqrt{\alpha_1/(\eta\Delta)}$, and thus

$$f_{z_1}(z_1)=\frac{a^3\alpha_1^{3/2}\sqrt{|z_1|}}{2\sqrt{2\pi}\sigma_x^3(\eta\Delta)^{3/2}}e^{-\frac{a^2\alpha_1|z_1|}{2\sigma_x^2\eta\Delta}}. \tag{42}$$

According to [61, p.87,154] a Gamma distribution has the form $f_\Gamma(x)=u(x)x^{c-1}e^{-\frac{x}{b}}/(\Gamma(c)b^c)$ with second moment $\mathrm{E}\{x^2\}=c(c+1)b^2$. Therefore (42) is a *double Gamma distribution* with $c=3/2$ and $b=(2\eta\Delta\sigma_x^2)/(a^2\alpha_1)$. Since (42) has zero mean, the power on channel 1 becomes

$$P_1=\mathrm{Var}\{z_1\}=\frac{15(\eta\Delta\sigma_x^2)^2}{a^4\alpha_1^2}=\frac{15(\eta\pi^2\sigma_x^2)^2}{16\alpha_1^2\Delta^2}. \tag{43}$$

Now take channel 2: z_2 makes out a circle which "rotates" about the x_3 axis when z_1 varies (see [46], Fig. 15(b) for illustration). The circle's radius is given by $2\Delta z_1/\pi$. If $\phi=0$, the rotation axis is at $\pi/2$. The radius of the rotating circle does not affect the pdf of z_2 as $z_2\in[-\pi,\pi]$, independent of z_1. From the perspective of z_2, as the joint pdf of $\mathbf{x}$ is spherically symmetric, we have a uniform mass distribution over a virtual spherical shell of arbitrary radius, r_0, as depicted in Fig. 10(b). To find the probability mass associated with different values of z_2, one considers the sum of all points along circles resulting from the intersections of this virtual sphere by planes perpendicular to the rotation axis (the green circle in Fig. 10(b)). The radius, r_i, of this circle is $r_i=r_0\cos(\upsilon)$, where $\upsilon=z_2$ is the angle from the equatorial plane, $\upsilon=\pi/2-\varrho$, and ϱ the polar angle. The circumference as a function of z_2 is $O(z_2)=2\pi r_0\cos(z_2)$. Since r_0 is arbitrary, one can set $r_0=1/(2\pi)$ implying that $f_{z_2}(z_2)\sim|\cos(z_2)|,\ z_2\in[-\pi,\pi]$. To avoid high probability for the largest channel amplitude values, one can set $\phi=\pi/2$ to obtain zero probability there. Then a *sine distribution* results. To normalize, as $\int_0^\pi\sin(z_2)\mathrm{d}z_2=2$, then

$$f_{z_2}(z_2)=\frac{\alpha_2}{4}|\sin(\alpha_2 z_2)|. \tag{44}$$

Since $f_{z_2}(z_2)$ is proportional to *Gilberts sine distribution* $f_x(x)=\sin(2x)$, which according to [62] has variance $E\{x^2\}=(\pi^2/4-1)/2$, the power for channel 2 becomes

$$P_2=\mathrm{Var}\{z_2\}=\frac{2}{\alpha_2^2}\left(\frac{\pi^2}{4}-1\right). \tag{45}$$

Distortion: Using (38), we obtain

$$\begin{aligned}I_2&=\iint g_{22}(\mathbf{z})f_{\mathbf{z}}(\mathbf{z})\mathrm{d}\mathbf{z}\\&=2(a\alpha_2)^2\frac{\alpha_1}{\eta\Delta}\int_{-\infty}^{\infty}z_1f_{z_1}(z_1)\mathrm{d}z_1=3\alpha_2^2\sigma_x^2.\end{aligned} \tag{46}$$

The last equality comes from the fact that z_1 is gamma distributed, therefore the integral in (46) becomes [61, p.154] $bc/2=3\eta\Delta\sigma_x^2/(a^2\alpha_1)$. Further, we have (see [46] for details),

$$I_1=\iint g_{11}(\mathbf{z})f_{\mathbf{z}}(\mathbf{z})\mathrm{d}\mathbf{z}=\frac{\alpha_1\Delta}{\eta\pi^2}E\{z_1^{-1}\}+\frac{2\alpha_1^2}{3\pi^2\eta^2}. \tag{47}$$

Through power series expansion one can show that $E\{z_1^{-1}\}\approx 4(1+\mathrm{Var}\{z_1\})$ up to 3rd order. Inserting this into (47), the channel distortion results from (18),

$$\begin{aligned}\bar{\varepsilon}_{ch}^2&=\frac{\sigma_n^2\left(I_1+I_2\right)}{3}\approx\\&\frac{\sigma_n^2}{3}\left(\frac{4\alpha_1\Delta}{\eta\pi^2}\left(1+\frac{15(\eta\pi^2\sigma_x^2)^2}{16\alpha_1^2\Delta^2}\right)+\frac{2\alpha_1^2}{3\pi^2\eta^2}+3\alpha_2^2\sigma_x^2\right).\end{aligned} \tag{48}$$

Optimization: With constraint $C_t=P_{\max}-P_t(\Delta,\alpha_1,\alpha_2)\geq 0$, we get a similar objective function as in (36).

The performance of the optimized DSS is plotted in Fig. 10(c). Comparing with Fig. 9(b) its clear that DSS has better performance than the RCASD at high SNR, which is expected from Proposition 6. The DSS is also noise robust (green dashed curve), and the magenta line confirms that the theoretical model derived for DSS above is quite accurate. However, one can see that the gap to OPTA increases somewhat above 40dB, the reason being that $\bar{\varepsilon}_{ch}^2\sim 1/\Delta^2$ instead of $\bar{\varepsilon}_{ch}^2\sim 1/\Delta$, which is required according to Corollary 3. Therefore, the DSS will eventually diverge from OPTA (albeit at a higher SNR than a decomposable mapping). One option that has not yet been investigated that may lead to the right slope is a change of coordinates curves on DSS.

3) 3:2 Hybrid Vector Quantizer Linear Coder (HVQLC): We construct a mapping satisfying all criteria for obtaining SDR$\sim$ SNR$^{2/3}$ as SNR$\to\infty$. A piecewise smooth (HDA) approach is taken: Consider approximating $\mathbf{x}$ to planes parallel to x_1,x_2-plane in $\mathbb{R}^3$ with distance Δ between them, like the *parallel planes* mapping suggested in Remark 14, depicted in Fig. 2, but now residing in $\mathcal{D}_s$. This is a uniform $\mathcal{S}$, and so $\bar{\varepsilon}_q^2\sim\Delta^2$ from Proposition 5. With parallel planes $G=\alpha I$, with α some scaling factor. To obtain a non-decomposable mapping, we map each plane onto the channel ($\mathcal{D}_c$) with its center placed on Archimedes spiral, thereby obtaining a *mix* of several sources on each channel. A spiral is chosen for two reasons: i) The condition $\bar{\varepsilon}_{ch}^2\sim 1/\Delta$ in Corollary 3 is obtained, as shown in Proposition 10. ii) To easily scale the mapping with SNR: By choosing φ as in (32), an equal distance, Δ, between the spiral arms as well as between the centroids along each arm results. I.e., a uniform VQ on a disc, as illustrated in [40, p.90]. The block diagram for the 3:2 HVQLC is depicted in Fig. 11(a). Q_Δ is a uniform scalar quantizer producing an index, i, mapped to two values through the 1:2 spiral, then scaled before transmission. The received $\hat{z}_1$ is projected to the closest (discrete) point on the spiral to reproduce the indices. x_1 and x_2 are scaled, then transmitted.

Optimization of 3:2 HVQLC:

Distortion: A drawback of this mapping is that it introduces anomalous errors when centroids are mis-detected. This happens with probability $Pr\{\|\mathbf{y_{12}}+\mathbf{n}\|\geq\Delta/(2\alpha_3)\}$, where $\mathbf{y_{12}}=[x_1\ x_2]/\alpha$. The error is bounded by $2b_x\sigma_x$,

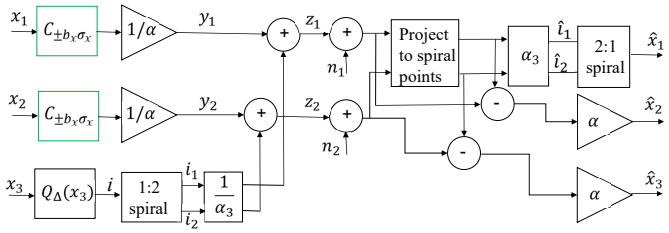

(a)

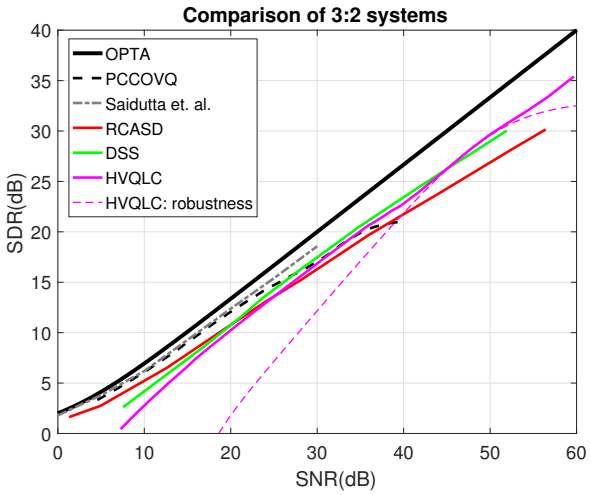

(b)

Fig. 11. (a) 3:2 HVQLC block diagram. The limitation operation, $C_{\pm b_x\sigma_x}$, in green blocks are optional. (b) Performance of all suggested 3:2 schemes compared to key mappings in literature.

with b_x depending on the *limiting* of x_1 and x_2 described below. The pdf of $\mathbf{y_{12}}+\mathbf{n}$ is the product the distributions of $x_i+n_i \sim \mathcal{N}(0,\sigma_y^2+\sigma_n^2)$, $i=1,2$ [61, pp.181-182]. The variable $w=\|\mathbf{y_{12}}+\mathbf{n}\|$ is then Rayleigh distributed [61, pp. 202-203], $f_w(w)=w/(\sigma_y^2+\sigma_n^2)\exp(-w^2/2(\sigma_y^2+\sigma_n^2))$. Therefore the anomalous distortion becomes

$$\begin{aligned}\bar{\varepsilon}_{an}^2 &= 4b_x^2\sigma_x^2 Pr\left\{w\geq\frac{\Delta}{2\alpha_3}\right\}\\ &= 4b_x^2\sigma_x^2\int_{\Delta/(2\alpha_3)}^{\infty} f_w(w)\mathrm{d}w = 4b_x^2\sigma_x^2 e^{-\frac{\Delta^2}{8\alpha_3^2(\sigma_x^2/\alpha^2+\sigma_n^2)}}.\end{aligned} \tag{49}$$

In order to obtain a mapping where anomalous errors happen with low probability one will either condition Δ/α_3 to be small, or limit x_1 and x_2 at some value by the green blocks in Fig. 11(a). By limiting x_i at the value $b_x\sigma_x$, one introduces a distortion [63]

$$\bar{\varepsilon}_\kappa^2=\frac{4}{3}\int_{b_x\sigma_x}^{\infty}(x_i-b_x\sigma_x)^2 f_x(x_i)\mathrm{d}x_i,\ i=1,2. \tag{50}$$

By limiting each source separately, the HVQLC will result in parallel planes in $\mathcal{D}_s\subseteq\mathbb{R}^3$, whereas by limiting $\sqrt{x_1^2+x_2^2}$, parallel discs will be obtained.

To make the probability of anomalous errors small, the following constraint is needed

$$\frac{\Delta}{\alpha_3}>\frac{2b_x\sigma_x}{\alpha}+2b_n\sigma_n. \tag{51}$$

The probability is adjusted with b_x. With $b_x>4$ then 99.99% of all source values are included.

As mentioned above, $g_{ii}=\alpha^2$ and so the channel distortion becomes $\bar{\varepsilon}_{ch}^2=2\sigma_n^2\alpha^2/3$. We also have a uniform $\mathcal{S}$. Therefore, the total distortion becomes

$$D_t=\frac{\Delta^2}{36}+\frac{2\sigma_n^2\alpha^2}{3}+4b_x^2\sigma_x^2 e^{-\frac{\Delta^2}{8\alpha_3^2(\sigma_x^2/\alpha^2+\sigma_n^2)}}. \tag{52}$$

Power: Since x_1 and x_2 are scaled Gaussians, their transmission power becomes $P_1+P_2=2\sigma_x^2/\alpha^2$. As x_3 is mapped through a discretisized version of the 1:2 mapping in [5], the same power expression applies for small Δ, or high SNR (a term in [5] is removed as x_3 takes values over $\mathbb{R}$. In [5] the source was in the range $[-1,1]$): $P_3\approx 2\Delta\sigma_x/(\eta\sqrt{2\pi^5}\alpha_3^2)$. The fact that $P_3\sim\Delta/\alpha_3^2$ makes $\bar{\varepsilon}_{ch}^2\sim 1/\Delta$ as required by Corollary 3. The total power is then

$$P_t=\frac{2\sigma_x^2}{\alpha^2}+\frac{2\Delta\sigma_x}{\eta\sqrt{2\pi^5}\alpha_3^2}. \tag{53}$$

*Optimization:*To determine optimal performance we consider the Lagrangian

$$\mathcal{L}(\Delta,\alpha,\alpha_3)=D_t(\Delta,\alpha)-\lambda_1 C_1(\Delta,\alpha,\alpha_3)-\lambda_2 C_2(\Delta,\alpha,\alpha_3), \tag{54}$$

where $C_1=P_{\max}-(P1+P2+P3)$ and $C_2(\Delta,\alpha,\alpha_3)=\Delta-2b_x\sigma_x\alpha_3/\alpha-2b_n\sigma_n\alpha_3$. The slight difference from the constraint in (51) is to obtain better numerical stability when solving (54).

The optimized performance of HVQLC (with no limitation of $\mathbf{x}$), is shown in Fig. 11(b), magenta curve. The HVQLC seem to follow the OPTA slope at high SNR and it is noise robust (magenta dashed curve) despite of the anomalous errors. But anomalies are likely the reason why HVQLC has a larger distance to OPTA than DSS for SNR <40 dB.

High SNR analysis: We prove that 3:2 HVQLC has the same slope as OPTA as SNR$\to\infty$.

Proposition 10: 3:2 *HVQLC at high SNR.* At high SNR the SDR of 3:2 HVQLC follows

$$\mathrm{SDR}=\left(\frac{9\eta\sqrt{\pi^5}}{8b_x^2}\right)^{\frac{2}{3}}\mathrm{SNR}^{\frac{2}{3}}. \tag{55}$$

Proof: See Appendix D-2. □

From (55), with $\sigma_x=1$, $b_x=4$ and $\eta=0.16$, the loss from OPTA becomes $\mathrm{SDR}_{\text{loss}}=-10\lg(9\cdot 0.16\sqrt{\pi^5}/(8\cdot 16))^{2/3}\approx 4.7$dB, corresponding to the gap seen in Fig. 11(b).

4) Comparison of different 3:2 schemes: The performance of all 3:2 mappings proposed are compared in Fig. 11(b). We also include the performance of the 3:2 mapping of Saidutta et. al. [8] found by deep learning, i.e., *variational auto encoders* (VAE), as well as *power constrained channel optimized vector quantizer* (PCCOVQ) [36], [64]. PCCOVQ is a numerically optimized discrete mapping replicating continuous (or piecewise smooth) mappings when the number of source- and channel symbols in the mapping is large. Approaching the VAE or PCCOVQ is a good indication of a well performing mapping as these are properly optimized structures.

Not surprisingly, Saidutta's VAE mapping (gray dash-dot curve) and PCCOVQ (black dashed curve) have superior

performance in the SNR range they have been optimized for[4]. However, the proposed mappings are only about 1dB away from the reference systems. The RCASD is best at low SNR, the DSS is best between 20 and 45 dB, while the HVQLC is best from 45dB and above. The HVQLC is the only system that does not diverge from OPTA at high SNR. Although DS-based mappings, like RCASD, diverge from OPTA at high SNR, decomposable mappings have their *virtue* as a simple alternative that perform well at lower SNR.

Although the mappings proposed are inferior to the two optimized schemes, the loss is small, and they have the advantage of having a fixed geometrical structure that only needs to be scaled in order to adapt to varying SNR, thus lowering complexity. Its is also noteworthy that widely different configurations provide well performing mappings. However, any such configuration will need to comply with the conditions presented in Sections III and IV.

B. Examples on 2:3 *mappings and the gain from dimensionality increase when* $r = 2$

First we analyze two 2:3 mappings: i) A piecewise smooth scheme, *hybrid vector quantizer linear coders* (HVQLC) suggested in [40, pp. 89-93]. ii) The RCASD treated in Section V-A1. Then we illustrate performance gain obtained by increasing mapping dimensionality when $r = 2$.

1) 2:3 *HVQLC:* This is a generalization of the hybrid scalar qunatizer linear coder (HSQLC) proposed in [24]. The block diagram is depicted in Fig. 12.

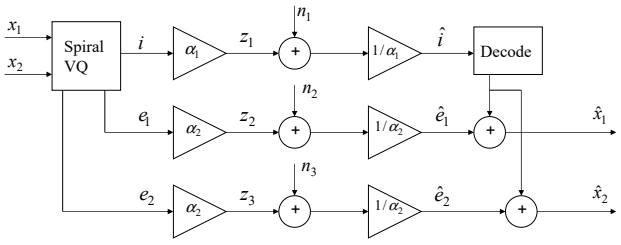

Fig. 12. 2:3 HVQLC block diagram.

Here VQ centroid indices are denoted by i, e_1 and e_2 denote the two error components from the VQ, and α_1, α_2 are scaling factors to adjust channel power. To make the VQ adaptable to varying SNR, its centroids are placed on Archimedes' spiral with distance δ between them, see [40, p.90] for illustration. Arc-length parametrization is chosen along the spiral for the same reason as for the 3:2 HVQLC. The scaled VQ indices are transmitted as PAM symbols on channel 1, while the scaled error components are transmitted on channels 2 and 3, leading to a "mix" of both sources on all three channels. Geometrically, the 2:3 HVQLC consists of planes parallel to the z_1, z_2-plane in channel domain $\mathcal{D}_c$, as illustrated in Fig. 2 to the upper left, (see also [40, p.90]), making it similar to 3:2 HVQLC (parallel planes in source domain $\mathcal{D}_s$).

[4]The reason why the PCCOVQ declines above 22dB is because 4096 symbols are used during optimization, a too small a number for high SNR.

Distortion: $\bar{\varepsilon}^2_{wn}$ can be found from (10), as the HVQLC is shape preserving. Only the error components e_1, e_2 contribute, and so $\bar{\varepsilon}^2_{wn} = \sigma_n^2/\alpha_2^2$.

As the VQ indices are scaled by α_1, the distance between each plane in channel space is α_1. Relating back to Section IV-A, then $\Delta_{min} = \alpha_1$. Therefore, the anomalous error probability is $p_{th} = Pr\{n_1 \geq \alpha_1/2\}$. Since n_1 is Gaussian, $p_{th} = (1 - \text{erf}(\alpha_1/2\sqrt{2}\sigma_n)$ (see [40, p.90]). The error made when anomalous errors occur is δ, as this is the distance to the nearest neighbor for any given centroid. Therefore,

$$\bar{\varepsilon}^2_{an} = \frac{\delta^2}{2}\left(1 - \text{erf}\left(\frac{\alpha_1}{2\sqrt{2}\sigma_n}\right)\right). \tag{56}$$

Power: As centroids are placed on the Archimedes' spiral in an equidistant manner, the pdf of z_1 will be a discretized version of the pdf for RCASD directrix. I.e., a discretized Laplace pdf. For small δ, its variance can be approximated by the variance of a Laplace pdf. Therefore, the power on channel 1 is approximated as

$$P_1 = \text{Var}\{z_1\} \approx 2\alpha_1^2\left(2\eta\frac{\pi^2}{\delta^2}\sigma_x^2\right)^2. \tag{57}$$

Generally, the right hand side will be somewhat smaller than the real power, but the smaller δ is (higher SNR) the better they coincide. Note particularly that $\sigma^2_{z_1} \sim 1/\delta^4$, different from the 3:2 RCASD directrix where $\sigma^2_{z_1} \sim 1/\delta^2$. The reason is that indices are sent on the channel and so the length measured along the spiral is independent of Δ. This difference in exponent is crucial to make HVQLC obtain the same slope as 2:3 OPTA.

For channels 2 and 3, assuming that δ is small, e_1 and e_2 are uniformly distributed over $(\delta/2) \times (\delta/2)$. Therefore, the power on channel 2 and 3 can be approximated by $P_2 = P_3 \approx \alpha_2^2\delta^2/12$. The total channel power is then

$$P_t = \frac{2}{3}\left(\left(2\alpha_1\eta\frac{\pi^2}{\delta^2}\sigma_x^2\right)^2 + \frac{\alpha_2^2\delta^2}{12}\right). \tag{58}$$

Optimization: The Lagrangian is $\mathcal{L}(\delta, \alpha_1, \alpha_2, \lambda) = \bar{\varepsilon}^2_{wn}(\alpha_2) + \bar{\varepsilon}^2_{th}(\delta, \alpha_1) - \lambda c_t(\delta, \alpha_1, \alpha_2)$, where $c_t(\delta, \alpha_1, \alpha_2) = P_{\text{max}} - P_t(\delta, \alpha_1, \alpha_2) \geq 0$, with $P_t(\delta, \alpha_1, \alpha_2)$ as in (58), and P_{max} the maximum power per channel. Numerical optimization is applied (see [40, p. 92]).

The performance of the optimized 2:3 HVQLC system is shown in Fig. 13(a) (green curve). The HVQLC is about 5dB from OPTA above 20dB SNR. It also seem to follow the slope of OPTA at high SNR, as will be shown in Proposition 11. Both simulated (green dashed curve) and calculated (magenta curve) robustness performance are shown, where the two distortion contributions can be seen: $\bar{\varepsilon}^2_{wn}$ dominates above the optimal SNR point and behaves like a linear scheme (having the same slope as BPAM) which is to be expected from Definition 4 and Proposition 1. Below the optimal SNR, $\bar{\varepsilon}^2_{an}$ dominates, and is observed to diverge faster from OPTA than $\bar{\varepsilon}^2_{wn}$. The theoretical model coincides well with simulations at high SNR.

High SNR analysis: We prove that 2:3 HVQLC has the same slope as OPTA as SNR$\rightarrow \infty$. To simplify one can eliminate anomalous errors by choosing α_1 sufficiently large. By letting

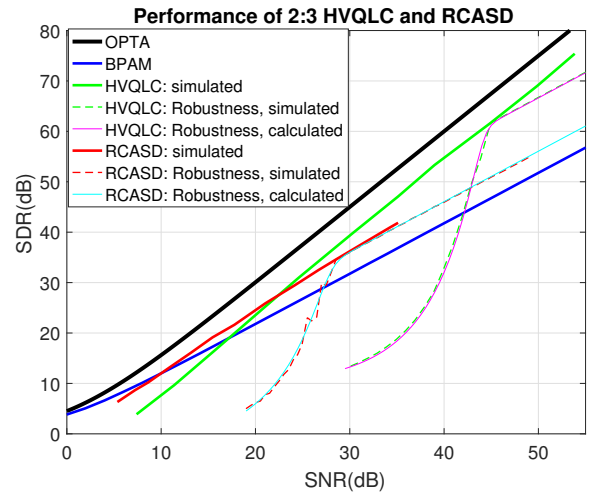

(a)

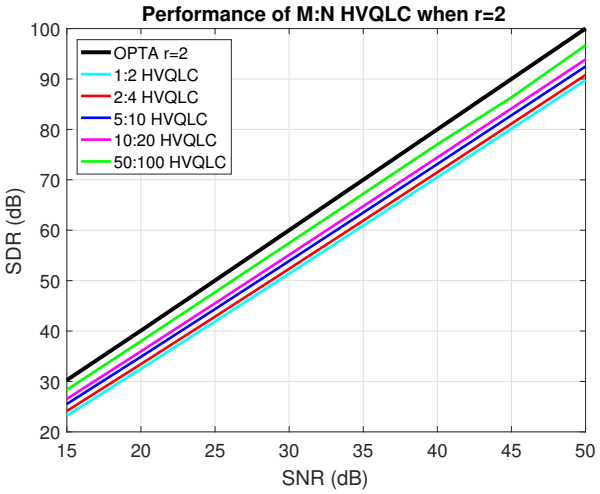

(b)

Fig. 13. Performance of: (a) 2:3 HVQLC and RCASD compared to OPTA and BPAM. (b) $r = 2$ HVQLC for selected M, N.

$\alpha_1 \geq 2b_n\sigma_n$, with $b_n > 4$, 99.99% of all noise events are included, and the total distortion can be approximated as $D_t \approx \sigma_n^2/\alpha_2^2$.

Proposition 11: 2:3 *HVQLC at high SNR.* At high SNR, the SDR of 2:3 HVQLC follows

$$\text{SDR} = \frac{7\sqrt{3}}{6\eta\pi^2 b_n}\text{SNR}^{\frac{3}{2}}. \tag{59}$$

Proof: See Appendix D-3. □

With $b_n = 4$, $\eta = 0.16$, the loss from OPTA is $\text{SDR}_{\text{loss}} = -10\lg(7\sqrt{3}/(6\eta\pi^2 b_n)) \approx 4.95$dB, corresponding to the performance gap seen in Fig. 13(a).

2) 2:3 RCASD: The parametrization is the same as in (32), but now as a function of $\mathbf{x}$. The distortion and power is easily derived using results from preceding sections and existing papers:

To compute $\bar{\varepsilon}_{wn}^2$ we assume arc-length parametrization and obtain the same G as for the 3:2 RCASD in Section V-A1. Then (9) is reduced to $\bar{\varepsilon}_{wn}^2 = 0.5\sigma_n^2(\alpha_1^{-2}+\alpha_2^{-2})$. Furthermore, $\bar{\varepsilon}_{an}^2$ is the same as for the 1:2 mapping in [5], Eqn.(25), scaled by 0.5.

The power on channels 1 and 2 are also the same as for the 1:2 mapping in [5], and is given by $P_1 + P_2 = 2\Delta\sigma_x\alpha_2/(\eta\sqrt{2\pi})$. As x_3 is scaled with α_3 and sent on channel 3, the power is $P_3 = \sigma_x^2\alpha_3^2$. Then $P_t = (P_1 + P_2 + P_3)/3$.

The performance of the optimized RCASD is shown in Fig. 13(a). As expected from Proposition 6, the RCASD diverges from OPTA, following the slope of a 1:1 system at high SNR. Between 10-22 dB SNR, the RCASD outperforms the HVQLC, and so a DS-based mapping is advantageous at low to medium SNR. The correspondence between the calculated and simulated robustness curves indicate that the theoretical model fits well with reality at high SNR.

3) M:N HVQLC for r = 2: The construction we consider here was briefly discussed in Example 6 as a potential candidate for obtaining OPTA in $r = 2$ case, satisfying all necessary conditions in Proposition 8. The approach is a generalization of the HSQLC treated in [24], using an M-dimensional uniform VQ instead of a scalar quantizer. We use a similar construction as for the 2:3 HVQLC in Fig. 12, except that the M VQ centroid values (not the indices) are sent directly on the first $M = N/2$ channels after scaling by α_1. The error from this quantization process is sent on the remaining $N/2$ channels after scaling by α_2.

As this is a shape preserving mapping, the weak noise distortion is given by (10), $\bar{\varepsilon}_{wn}^2 = \sigma_n^2/\alpha_2^2$. An anomalous error is, as for 2:3 HVQLC, equal to δ, but now scaled with $1/M$. The probability for this event is found by integrating (24) from $\alpha_1\delta/2$ to ∞, substituting $N = 2M$ so that $N-M = M$. From the integration rules of exponential functions, one can find a closed-form expression for the integrand $x^n e^{cx}$ as a series expansion. This expansion can be simplified by some straight forward rearrangements. Then the total distortion is

$$D_t = \bar{\varepsilon}_{wn}^2 + \bar{\varepsilon}_{an}^2 = \frac{\sigma_n^2}{\alpha_2^2} + \frac{\delta^2}{M}\frac{\left(\frac{M}{2}\right)^{M/2} e^{-\frac{M\delta^2}{\sigma_n^2}}}{\Gamma\left(\frac{M}{2}\right)} \sum_{i=0}^{M-1} \frac{i!\ \delta^{M-1-i}}{M^{i+1}(2\sigma_n)^{M-2(i+1)}}. \tag{60}$$

The pdf on the first $N/2$ channels can be approximated by a Gaussian distribution as $\delta \to 0$ (at high SNR). As the error of the VQ is sent on the remaining $N/2$ channels, the power is lower bounded by the sphere bound distortion for a M-dimensional VQ as stated in (90), Appendix B-B3. The power per channel therefore becomes

$$P_t \approx \frac{1}{2}\left(\alpha_1^2\sigma_x^2 + \alpha_2^2\frac{M\delta^2}{4(M+2)}\right). \tag{61}$$

A more realistic power expression for small block length is the error of a scalar quantizer on each channel. This is obtained by replacing the last term in (61) by $\alpha_2^2\delta^2/12$.

By setting up a similar Lagrangian as in Section V-B1, one can numerically determine the optimal parameters. We plot the optimized performance for HVQLC for selected values of M, N in Fig. 13(b). Its clear that the HVQLC benefits from increased dimensionality.

High SNR analysis: We provide a sphere bound for HVQLC valid at high SNR. To simplify, we eliminate anomalous

errors by choosing $\alpha_1 \geq 2b_{NM}\sigma_n$, with b_{NM} determined by integrating (24) from $b_{NM}\sigma_n$ to ∞ so a very small probability results. Then one can approximate $D_t \approx \sigma_n^2/\alpha_2^2$.

Proposition 12: Sphere bound for M:N HVQLC with $r = 2$ at high SNR: At high SNR, the SDR of $r = 2$ HVQLC has the sphere bound

$$\text{SDR} = \frac{1 + 2/M}{b_{NM}^2}\text{SNR}^2, \tag{62}$$

and so, as $b_{NM} \to 1$ when $M, N \to \infty$, the HVQLC obtains OPTA.

Proof: See Appendix D-4. □

C. Remarks for both 3:2 and 2:3 mappings:

From the analysis and simulations in Sections V-A and V-B it may appear that fully continuous mappings based on surfaces cannot obtain the slope of OPTA at high SNR. This is in contrast to S-K mappings realized by continuous curves where such divergence is not observed [5], [40], [39]. However, we have not yet investigated the optimal choice of coordinate system on non-decomposable mappings like DSS. Just as curve-based mappings will diverge from OPTA if φ is chosen non-wisely [40], it may be that the divergence observed for continuous surfaces is due to sub-optimal choice of coordinates on $\mathcal{S}$. Its worth noting the VAE-based 3:2 mapping in [8], a structure quite similar to the DSS, is continuous and seem to follow OPTA at high SNR. However its performance is only evaluated up to 30dB, where also DSS follows the slope of OPTA, so this is inconclusive. An intuitive choice of coordinate curves for dimension reducing mappings are *geodesics* (see [46, p.11] or [47, pp.162-168]) as they represent the path of minimum length between points on $\mathcal{S}$, and thereby reduces the g_{ii}'s. Determining the optimal coordinate system in general is difficult even for 2D surfaces, and should be followed up in future effort(s).

VI. Summary, discussion and extensions

In this paper a theoretical framework for analyzing and constructing continuous or piecewise smooth mappings used for joint source-channel coding, named named Shannon-Kotel'nikov (S-K) mappings, has been proposed for the case of memoryless sources and channels.

The distortion framework introduced describes S-K mapping behaviour in general, that is, without reference to a specific mapping realization. Also, the framework provides guidelines for construction of well-performing mappings for both low and arbitrary complexity and delay.

We showed that any S-K mapping which can be decomposed into combinations of lower dimensional sub-mappings cannot obtain the same slope as OPTA at high SNR. We also showed that the performance of S-K mappings has the potential to improve under certain criteria when their dimensionality (or block length) is increased, potentially obtaining OPTA when their dimensionality goes to infinity.

Further, the provided theory was applied to construct mappings for 2:3 and 3:2 cases as well as M:N case for $r = 2$. The mappings display decent performance. Albeit some of them are inferior to mappings found by deep learning, the loss is small (about 1dB), and the mappings found can easily be adapted to varying channel conditions simply by scaling one given structure, thereby reducing complexity. The M:N mapping was shown to obtain OPTA as $M, N \to \infty$.

The conditions stated throughout this paper can provide constraints on numerical approaches like [6], [65] that may provide mappings closer to the global optimum without having to input a pre-determined, close to optimal mapping. The conditions presented may also provide deeper understanding of why certain configurations are favored by deep learning approaches [8], [29].

Future extensions should deal with optimal global structure, low SNR case and optimal choice of coordinate curves for S-K mappings. The theory could also be extended to mutimodal source distributions, correlated sources and channels, as well as simple network structures. The case of a bivariate source transmitted on two channels has been treated in [66] and the case of multivariate sources communicated on a Gaussian multiple access channel has been treated in [45].

Appendix A
Concepts from differential geometry

A. Arc-length parametrization, differential geometry of curves and formula of Frenet.

Let $\mathbf{S} : u \in [a, b] \subseteq \mathbb{R} \to \mathbf{S}(u) \subset \mathbb{R}^N$ with $\mathbf{S}(u) \in C^1$ be a parametrization for the curve $\mathcal{C}$ w.r.t. $\ell(u)$, where $\ell(u)$ is the arc-length of $\mathbf{S}$ as defined in (4), and φ its inverse.

Theorem 1: Let $\mathbf{y}(\ell)$ be a parametrization of $\mathcal{C}$. Then $\mathbf{y}(\ell)$ and $\mathbf{S}(\varphi(u))$ will have the same image, and $\|\mathbf{y}'(\ell)\| = \|\mathbf{S}'(\varphi(\ell))\| \equiv 1, \quad \forall \ell$.

Proof 1: See[67, pp. 115-116]. □

There are n orthonormal vectors connected to any curve $\mathcal{C} : \mathbf{S}(u)$ in $\mathbb{R}^n$, and related to these are the *generalized curvatures* [68]. In this paper we will only need three of them. The *unit tangent vector* $\mathbf{t} = \dot{\mathbf{S}} = \mathbf{S}'/\|\mathbf{S}'\|$, the *unit principal normal vector* $\mathbf{p}_n = \dot{\mathbf{t}}/\|\dot{\mathbf{t}}\| = \ddot{\mathbf{S}}/\|\ddot{\mathbf{S}}\|$, and the *unit binormal vector* which in $\mathbb{R}^3$ is defined as $\mathbf{b} = \mathbf{t} \times \mathbf{p}_n$. In $\mathbb{R}^n$, $\mathbf{b}$ is found by a *Gram-Schmidt orthogonalization process* [69, pp. 172-173] involving the vectors $\mathbf{t}$, $\mathbf{p}_n$ and $\dddot{\mathbf{S}}$. $\mathbf{t}$, $\mathbf{p}_n$ and $\mathbf{b}$ define three mutually orthogonal planes. We consider two of them: i) *Osculating plane* spanned by $\mathbf{t}$ and $\mathbf{p}_n$. ii) *Normal plane* spanned by $\mathbf{p}_n$ and $\mathbf{b}$.

For a curve, $\mathbf{S}(u)$, the principal curvature w.r.t. arc-length is defined as $\kappa_0 = \|\ddot{\mathbf{S}}(u_0)\|$ [47, p. 34]. Then we also have $\mathbf{p}_n = (1/\kappa)\ddot{\mathbf{S}} = \rho\ddot{\mathbf{S}}$. The *torsion* [47, p. 37-40] is defined as $\tau(x) = -\mathbf{p} \cdot \mathbf{b}$. For a general parametrization we have [47, pp.35,39]

$$\kappa = \frac{\sqrt{\|\mathbf{S}'\|^2\|\mathbf{S}''\|^2 - (\mathbf{S}' \cdot \mathbf{S}'')^2}}{\|\mathbf{S}'\|^{\frac{3}{2}}}. \tag{63}$$

The principal curvature can locally be interpreted as a circle of radius $\rho = 1/\kappa$, named *radius of curvature*, lying in the osculating plane of $\mathbf{S}$. This is the *osculating circle* and its center is the *centre of curvature*. I.e., the curvature in a neighborhood of u_0 is equivalent to that of a circle with radius

ρ (illustration is given in [46], Fig. 3). When $\tau = 0, \forall u$, $\mathbf{S}$ will be confined to a plane, otherwise it will twist up into space.

The *Formula of Frenet* (FoF) [47, p. 41] relates the derivatives $\dot{\mathbf{t}}$, $\dot{\mathbf{p}}$ and $\dot{\mathbf{b}}$ to linear combinations of $\mathbf{t}$, $\mathbf{p}_n$, and $\mathbf{b}$ of curve $\mathcal{C}$ as follows:

$$\dot{\mathbf{t}} = \kappa \mathbf{p}_n, \quad \dot{\mathbf{p}_n} = -\kappa \mathbf{t} + \tau \mathbf{b}, \quad \dot{\mathbf{b}} = -\tau \mathbf{p}_n. \tag{64}$$

B. Surfaces, fundamental forms and curvature

To keep the introduction to curvature of surfaces short and informative, we mainly introduce concepts for 2D surfaces in $\mathbb{R}^3$. All relevant concepts are extendable to hyper surfaces in $\mathbb{R}^n$. However, as we do not need to explicitly evaluate particular components or values for the sake of this paper (with the exception of the metric tensor), we do not need the more elaborate and subtle generalized definitions. The reader may consult [48] for details.

1) Fundamental forms: **First fundamental form (FFF)**: Consider a hyper surface, $\mathcal{S}$, realized by (2) or (3). In order to measure lengths, angles and areas on $\mathcal{S}$, a metric is needed. A length differential of a curve $\mathcal{C} \in \mathcal{S}$ is given by [47, p.82]

$$\begin{aligned} \mathrm{d}\ell^2 &= (\mathbf{S}_1 \mathrm{d}u^1 + \mathbf{S}_2 \mathrm{d}u^2) \cdot (\mathbf{S}_1 \mathrm{d}u^1 + \mathbf{S}_2 \mathrm{d}u^2) \\ &= \mathbf{S}_1 \cdot \mathbf{S}_1 (\mathrm{d}u^1)^2 + 2\mathbf{S}_1 \cdot \mathbf{S}_2 \mathrm{d}u^1 \mathrm{d}u^2 + \mathbf{S}_2 \cdot \mathbf{S}_2 (\mathrm{d}u^2)^2. \end{aligned} \tag{65}$$

A generalization to M-dimensional surfaces is obtained by adding M "$\mathbf{S}_i \mathrm{d}u^i$-terms" in the above expression. The quantities $g_{\alpha\beta} = \mathbf{S}_\alpha \cdot \mathbf{S}_\beta$, $\alpha, \beta = 1, \cdots, m$, are components of a *2nd order covariant tensor* (see [47, pp.88-105] or [46] for definition) named *metric tensor*. By Einstein's summation convention, $\mathrm{d}\ell^2 = g_{\alpha\beta} \mathrm{d}u^\alpha \mathrm{d}u^\beta$, which is the *first fundamental form* (FFF). For a smooth embedding $\mathbf{S}$ in $\mathbb{R}^N$ ($M \leq N$) the metric tensor is a symmetric, positive definite $M \times M$ matrix $G = J^T J$ [52, pp.301-304], with J the *Jacobian* of $\mathbf{S}$, a $N \times M$ matrix with entries $J_{ij} = \partial S_i / \partial u_j$, $i \in 1, \cdots, N$, $j \in 1, \cdots, M$. I.e., g_{ii} is the squared norm of the tangent vector along the i'th coordinate curve of $\mathbf{S}$. All *cross terms*, g_{ij}, are inner products of tangent vectors along the i'th and j'th coordinate curve of $\mathbf{S}$.

Second fundamental form (SFF): For any point, P, of a curve $\mathcal{C}$ on $\mathcal{S} \subset \mathbb{R}^3$, the corresponding unit normal to $\mathbf{S} \in \mathcal{S}$, $\mathbf{N} = \mathbf{S}_1 \times \mathbf{S}_2 / \|\mathbf{S}_1 \times \mathbf{S}_2\|$, lies in the normal plane of $\mathcal{C}$ which also contains its principal normal $\mathbf{p}_n$. The angle between $\mathbf{N}$ and $\mathbf{p}_n$, denoted γ, depends on the geometry of both $\mathcal{C}$ and $\mathcal{S}$ in a neighborhood of P. Its shown in [47, pp.118-119] and [46] that $\kappa \cos\gamma = (\mathbf{S}_{\alpha\beta} \cdot \mathbf{N}) \dot{u}^\alpha \dot{u}^\beta$, with κ, the principal curvature of $\mathcal{C}$. The term in the parentheses,

$$b_{\alpha\beta} = \mathbf{S}_{\alpha\beta} \cdot \mathbf{N}, \ \alpha, \beta = 1, \cdots, N, \tag{66}$$

depends on $\mathcal{S}$ only (independent of $\mathcal{C}$), and $b_{\alpha\beta} = b_{\beta\alpha}$. The $b_{\alpha\beta}$'s are components of a 2nd order covariant tensor, where the quadratic form $b_{\alpha\beta} \mathrm{d}u^\alpha \mathrm{d}u^\beta$ is the *second fundamental form* (SFF). The SFF exist for hyper surfaces as well, but its definition is more elaborate.

2) Normal curvature, principal curvature, lines of curvature: Let t be any allowable parameter for curve $\mathcal{C}$. Then $\dot{u}^\alpha = (\mathrm{d}u^\alpha / \mathrm{d}t)(\mathrm{d}t / \mathrm{d}\ell) = u^{\alpha\prime} / \ell'$, and therefore

$$\begin{aligned} \kappa \cos\gamma = b_{\alpha\beta} \dot{u}^\alpha \dot{u}^\beta &= \frac{b_{\alpha\beta} u^{\alpha\prime} u^{\beta\prime}}{\ell'} \\ &= \frac{b_{\alpha\beta} u^{\alpha\prime} u^{\beta\prime}}{g_{\alpha\beta} u^{\alpha\prime} u^{\beta\prime}} = \frac{b_{\alpha\beta} \mathrm{d}u^\alpha \mathrm{d}u^\beta}{g_{\alpha\beta} \mathrm{d}u^\alpha \mathrm{d}u^\beta}. \end{aligned} \tag{67}$$

It is shown in [47, pp. 121-124] that $\kappa_n = \kappa \cos\gamma$ is the curvature at point $P \in \mathcal{S}$ of the *normal section* $\mathcal{C} \subset \mathcal{S}$, an intersection of $\mathcal{S}$ by a plane passing through both $\mathbf{t}$ of $\mathcal{C}$ and $\mathbf{N}$ of $\mathcal{S}$, named *normal curvature* at P. The *Theorem of Meusnier* [47, p.122] states that one can restrict treatment of curvature at any point $P \in \mathcal{S}$ to that of normal sections without loss of generality.

The directions where κ_n has extremal values can be determined (except when $b_{\alpha\beta} \sim g_{\alpha\beta}$). From (67) one can derive [47, pp.128-129],

$$(b_{\alpha\gamma} - \kappa_n g_{\alpha\gamma}) \mathrm{d}u^\alpha = 0, \ \gamma = 1, 2. \tag{68}$$

The roots of (68) are directions for which κ_n is extreme, named *principal directions of normal curvature* at P. The corresponding curvatures, κ_1 and κ_2, are the *principal curvatures* of $\mathcal{S}$, corresponding to the maximal and minimal curvature of $\mathcal{S}$ at P, respectively. It is proven in [47, p.129] that the roots of (68) are real and the principal directions are orthogonal at every point. Further, a curve on $\mathcal{S}$ whose direction at every point is a principal direction is a *line of curvature* (LoC) of $\mathcal{S}$. One may always choose coordinates u^1, u^2 on $\mathcal{S}$ so that the LoC are allowable (see [46, p. 2]). Then [47, p.130]:

Theorem 2: The coordinate curves of any allowable coordinate system on $\mathcal{S}$ coincide with the LoC $\Leftrightarrow$ $g_{12} = 0$ and $b_{12} = 0$, at any point where those coordinates are allowable.

Proof: See [47, p.130]. □

Under LoC coordinates, (68) leads to $\kappa_i = b_{ii} / g_{ii}$. For general coordinates, with B the matrix of $b_{\alpha\beta}$, κ_i are the roots of [47, p. 130]

$$\kappa_i^2 - b_{\alpha\beta} g^{\alpha\beta} \kappa_i + \det(B) / \det(G) = 0. \tag{69}$$

Here $g^{\alpha\beta}$ is the *contravariant metric tensor* (see [46, pp.3-4]) defined so that $g_{\alpha\beta} g^{\alpha\beta} = \delta_\alpha^\beta$. Note that the κ_i's as defined above are also valid for M-dimensional surfaces, i.e., $i = 1, \cdots, M$.

APPENDIX B
PROOFS FOR SECTION III

A. Proofs for Section III-A

1) Proof, Proposition 1: For $\mathbf{S} \in \mathcal{S}$, assume that $S_i \in C^1(\mathbb{R}^M)$, $i = 1, .., N$. The tangent space at $\mathbf{x}_0$ is given by (8). Applying ML detection, then $\mathbf{S}(\mathbf{x}_{ML}) = \mathbf{S}(\mathbf{x}_0) + P_{proj}\mathbf{n}$ (see Fig. 3(a)), where P_{proj} is a projection matrix given by [69, p.158]

$$\begin{aligned} P_{proj} &= J(\mathbf{x}_0)(J(\mathbf{x}_0)^T J(\mathbf{x}_0))^{-1} J(\mathbf{x}_0)^T \\ &= J(\mathbf{x}_0) G(\mathbf{x}_0)^{-1} J(\mathbf{x}_0)^T. \end{aligned} \tag{70}$$

Setting $\mathbf{S}_{\text{lin}}(\mathbf{x}) = \mathbf{S}(\mathbf{x}_{ML})$, with $\mathbf{S}_{\text{lin}}$ as in (8) and from (70), we get $J(\mathbf{x}_0)(\mathbf{x}_{\text{ML}} - \mathbf{x}_0) = J(\mathbf{x}_0) G(\mathbf{x}_0)^{-1} J(\mathbf{x}_0)^T \mathbf{n}$. Multiplying both sides from the left with J^T, with G is invertible,

then $(\mathbf{x}_{\rm ML}-\mathbf{x}_0)=G(\mathbf{x}_0)^{-1}J(\mathbf{x}_0)^T\mathbf{n}$. The MSE given that $\mathbf{x}_0$ was transmitted is then

$$\varepsilon_{wn}^2=\frac{1}{M}E\{(\mathbf{x}_{\rm ML}-\mathbf{x}_0)^T(\mathbf{x}_{\rm ML}-\mathbf{x}_0)\}. \tag{71}$$

Lemma 3: With ML detection, the minimum MSE in (71) is achieved with a diagonal G

$$\varepsilon_{wn}^2=\frac{\sigma_n^2}{M}\sum_{i=1}^{M}\frac{1}{g_{ii}}, \tag{72}$$

where g_{ii} are the diagonal components of G at $\mathbf{x}_0$. □

Lemma 3 implies that the smallest possible weak noise MSE is obtained with orthogonal coordinate curves. Expectation over $\mathcal{D}_s$ gives the wanted result. □

Proof, Lemma 3: Consider the MSE in (71). To avoid matrix multiplication, the N-dimensional noise vector $\mathbf{n}$ is, without loss of generality, replaced by its M dimensional projection $\mathbf{n}_P$, which is also Gaussian since P_{proj} is a linear transformation [69, p.117]. Let $J=J(\mathbf{x}_0)$. Assume that a hypothetical inverse $\mathbf{B}=J^{-1}$ exists. Let $\mathbf{S}_t$ denote the (M-dimensional) tangent space of $\mathbf{S}$ at $\mathbf{x}_0$. Under Definition 4 the linear approximation to $\mathbf{S}^{-1}$ can be applied, and so $\hat{\mathbf{x}}=\mathbf{S}^{-1}(\mathbf{S}_t(\mathbf{x}_0)+\mathbf{n}_P)\approx\mathbf{S}^{-1}(\mathbf{S}_t(\mathbf{x}_0))+\mathbf{B}\mathbf{n}_P=\mathbf{x}_0+\mathbf{B}\mathbf{n}_P$. Then, Eqn. (71) becomes $\varepsilon_{wn}^2=E\{\mathbf{n}_P^T\mathbf{B}^T\mathbf{B}\mathbf{n}_P\}/M=\mathbf{b}_i^T\mathbf{b}_jE\{n^in^j\}/M$, using Einstein summation convention in the last equality, where $\mathbf{b}_i$ column vector no. i of $\mathbf{B}$. With i.i.d. noise, $E\{n_in_j\}=\sigma_n^2\delta_{ij}$, then

$$\begin{aligned}\varepsilon_{wn}^2&=\frac{1}{M}E\{\mathbf{n}_P^T\mathbf{B}^T\mathbf{B}\mathbf{n}_P\}\\&=\frac{\sigma_n^2}{M}\sum_{i=1}^{M}\mathbf{b}_i^T\mathbf{b}_i=\frac{\sigma_n^2}{M}\sum_{i=1}^{M}\|\mathbf{b}_i\|^2.\end{aligned} \tag{73}$$

Since $\mathbf{B}=J^{-1}$, and since any orthogonal matrix has an inverse, the above result implies that the basis of the tangent space of $\mathcal{S}$ can be chosen orthogonal without any loss. An orthogonal J results in a diagonal G (see Appendix A-B1). Therefore G^{-1}, as well as G^{-n}, are also diagonal with elements $1/g_{ii}$. With G^{-2} diagonal, $E\{n_in_j\}=\sigma_n^2\delta_{ij}$, and with (73) in mind, (71) leads to

$$\begin{aligned}\bar{\varepsilon}_{wn}^2&=\frac{1}{M}E\{(G^{-1}J^T\mathbf{n})^T(G^{-1}J^T\mathbf{n})\}\\&=\frac{1}{M}E\{(J^T\mathbf{n})^TG^{-2}(J^T\mathbf{n})\}=\frac{\sigma_n^2}{M}\sum_{i=1}^{M}\frac{1}{g_{ii}^2}\|J_i\|^2,\end{aligned} \tag{74}$$

where J_i is column vector no. i of J and $\|J_i\|^2\equiv g_{ii}$. □

2) Proof, Proposition 2: The ML-estimate of this problem, using 2'nd order Taylor approximation, has no simple solution [46]. However, we can apply the analysis for *pulse-position modulation* (PPM) in [43, pp. 703-704]. Geometrically, PPM is a curve on a hyper sphere where the arc between any two coordinate axes is like the circle segment depicted in Fig. 14. As the curvature of any curve can be described locally by the osculating circle, the analysis done for PPM is also valid locally for any 1:N mapping under arc-length parametrization. In the following, the curve segment in Fig. 14 is named *circle approximation*.

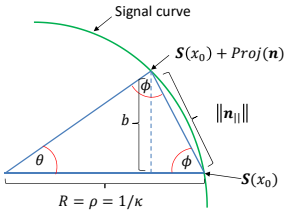

Fig. 14. Circle approximation for calculation of error up to 2nd order.

We divide the noise into the components $\text{Proj}(\mathbf{n})=\mathbf{n}_{||}$, i.e., the projection onto the closest point on the circle in Fig. 14, and its normal, $\mathbf{n}_\perp$. For the circle approximation $R(x)=\rho(x)=1/\kappa(x)=1/\|\ddot{\mathbf{S}}_0\|$ iff $\mathbf{t}=\|\dot{\mathbf{S}}_0\|=1$. In polar coordinates, $\mathbf{S}(x)\approx[R(x),\theta(x)]=[\rho,\theta]$. Then $R(x)=R=\rho,\ \forall x$ and we have $\mathbf{S}=[R\cos(\theta(x)),R\sin(\theta(x))]$. Then

$$\frac{\mathrm{d}\mathbf{S}}{\mathrm{d}x}=\left[R\sin(\theta(x))\frac{\mathrm{d}\theta(x)}{\mathrm{d}x},-R\cos(\theta(x))\frac{\mathrm{d}\theta(x)}{\mathrm{d}x}\right]. \tag{75}$$

By taking the norm we find that $\|\mathrm{d}\mathbf{S}/\mathrm{d}x\|^2=R^2(\mathrm{d}\theta(x)/\mathrm{d}x)^2$. From this we get

$$\frac{\mathrm{d}\theta(x)}{\mathrm{d}x}=\frac{1}{R}\left\|\frac{\mathrm{d}\mathbf{S}}{\mathrm{d}x}\right\|=\frac{\|\mathbf{S}_0'\|}{\rho}=\alpha\kappa=\alpha\|\ddot{\mathbf{S}}_0\|. \tag{76}$$

That is, $\mathrm{d}\theta(x)/\mathrm{d}x\sim\kappa$. The two last equalities in (76) are valid under scaled arc-length parametrization. To determine the ML estimate for the circle approximation, rewrite (76) as $\mathrm{d}x=\mathrm{d}\theta(x)/(\|\mathbf{S}_0'\|\|\mathbf{S}_0''\|)=\mathrm{d}\theta(x)\rho(x_0)/\|\mathbf{S}_0'\|$. Then

$$x_0-\hat{x}_{ML}=\frac{\rho(x_0)}{\|\mathbf{S}_0'\|}\theta=\frac{\theta}{\kappa(x_0)\|\mathbf{S}_0'\|}. \tag{77}$$

θ must be expressed in terms of $\mathbf{n}_{||}$ and ρ (or κ). In Fig. 14 we have a right-legged triangle where $\phi=(\pi-\theta)/2$, and with $b=\rho\sin(\theta)$ its right normal. Therefore $\sin(\phi)=b/\|\mathbf{n}_{||}\|\Rightarrow\|\mathbf{n}_{||}\|=b/\sin(\phi)=\rho\sin(\theta)/\sin(\phi)$. Furthermore, $\sin(\phi)=\sin(\pi/2-\theta/2)=\cos(\theta/2)$. Since $\sin 2y=2\sin y\cos y$, with $y=\theta/2$, then $\sin(\theta)=2\sin(\theta/2)\cos(\theta/2)$, implying that $\|\mathbf{n}_{||}\|=2\rho\sin(\theta/2)$. Therefore $\theta=2\sin^{-1}(\|\mathbf{n}_{||}\|/(2\rho(x_0)))$. By the expansion [70, p. 117] $\sin^{-1}(x)=x+x^3/(2\cdot3)+x^5 1\cdot3/2\cdot4\cdot5+\cdots$, we get, up to two terms

$$\theta\approx\frac{\|\mathbf{n}_{||}\|}{\rho(x_0)}\left(1+\frac{\|\mathbf{n}_{||}\|^2}{24\rho^2(x_0)}\right). \tag{78}$$

One can then compute the error up to second order from (77) and (78)

$$\begin{aligned}\varepsilon_{wn}^2&=E\{(x-\hat{x}_{ML})^2|x=x_0\}=E\left\{\left(\frac{\rho(x_0)}{\|\mathbf{S}_0'\|}\theta\right)\right\}\\&=\frac{\rho^2(x_0)}{\|\mathbf{S}_0'\|^2}E\left\{\left(\frac{\|\mathbf{n}_{||}\|}{\rho(x_0)}\left(1+\frac{\|\mathbf{n}_{||}\|^2}{24\rho^2(x_0)}\right)\right)^2\right\}\\&=\frac{1}{\|\mathbf{S}_0'\|^2}E\left\{\|\mathbf{n}_{||}\|^2+\frac{2\|\mathbf{n}_{||}\|^4}{24\rho^2(x_0)}+\frac{\|\mathbf{n}_{||}\|^6}{24^2\rho^4(x_0)}\right\}.\end{aligned} \tag{79}$$

The noise, $\mathbf{n}_{||}$, under the circle approximation, is following a *von-Mises* distribution [71]. As the mean of $\mathbf{n}$ will always be on the circle above, the variance becomes $\sigma_{vm}^2=2(1-I_1(\sigma_n^{-2})/I_0(\sigma_n^{-2}))$, where I_0 and I_1 are the 0th and 1st order *modified Bessel function of first kind*, respectively. When σ_n is

just a fraction of the radius of the (osculating) circle in Fig. 14, which is the case when high SNR is assumed, then $\sigma_n^2 \approx \sigma_{vm}^2$. For example, when $\sigma_n^2 = 0.1$ (about 31% of the radius of curvature) then $\sigma_{vm}^2 = 0.103$, the difference becoming rapidly smaller as σ_n^2 decreases. Under the assumption that $\mathbf{n}_{||}$ is nearly Gaussian, then, since $E\{n^a\} = 1 \cdot 3 \cdots (a-1)\sigma_n^a$, a even, and zero otherwise [61, p.148], we get

$$\begin{aligned}\varepsilon_{wn}^2 &= \frac{\sigma_n^2}{\|\mathbf{S}_0'\|^2}\left(1 + \frac{\sigma_n^2}{4\rho^2(x_0)} + \frac{5\sigma_n^4}{48\rho^4(x_0)}\right) \\ &= \frac{\sigma_n^2}{\|\mathbf{S}_0'\|^2}\left(1 + \frac{1}{4}\sigma_n^2\kappa^2(x_0) + \frac{5}{48}\sigma_n^4\kappa^4(x_0)\right).\end{aligned} \tag{80}$$

In general, κ is given by (63). Under scaled arc-length parametrization, $\|\mathbf{S}'(x_0)\| = \alpha\|\dot{\mathbf{S}}(x_0)\| = \alpha$, $\forall x_0$, then (63) reduces to $\kappa(x_0) = \|\mathbf{S}_0''\|/\|\mathbf{S}_0'\|^2$. Then the error can be expressed in terms of the derivatives of $\mathbf{S}$ as

$$\varepsilon_{wn}^2 = \frac{\sigma_n^2}{\|\mathbf{S}_0'\|^2}\left(1 + \frac{1}{4}\sigma_n^2\frac{\|\mathbf{S}_0''\|^2}{\|\mathbf{S}_0'\|^4} + \frac{5}{48}\sigma_n^4\frac{\|\mathbf{S}_0''\|^4}{\|\mathbf{S}_0'\|^8}\right). \tag{81}$$

As will be shown in Lemma 1, one should let $\sigma_n^2 << \rho^2(x_0)$ to avoid larger errors (at least at high SNR). At high SNR ($\sigma_n^2 << 1$) one can therefore make the approximation

$$\begin{aligned}\varepsilon_{wn}^2 &\approx \frac{\sigma_n^2}{\|\mathbf{S}_0'\|^2}\left(1 + \frac{1}{4}\sigma_n^2\kappa^2(x_0)\right) \\ &= \frac{\sigma_n^2}{\|\mathbf{S}_0'\|^2}\left(1 + \frac{1}{4}\sigma_n^2\frac{\|\mathbf{S}_0''\|^2}{\|\mathbf{S}_0'\|^4}\right)\end{aligned} \tag{82}$$

At high SNR $\mathbf{S}$ can be significantly stretched, i.e., $\|\mathbf{S}_0'\| = \alpha >> 1$, and the 1st order term in (11) will dominate more and more over the 2nd order term. As shown in Section B-B2, higher order terms will contribute even less, and so the circle approximation above will do.

To see that the circle approximation above is valid locally for any $1{:}N$ mapping, consider a general curve in polar coordinates. The product rule gives

$$\begin{aligned}\frac{\mathrm{d}\mathbf{S}}{\mathrm{d}x} = \Big[&R'(x)\cos(\theta(x)) + R(x)\sin(\theta(x)), \\ &R'(x)\sin(\theta(x)) - R(x)\cos(\theta(x))\Big].\end{aligned} \tag{83}$$

Locally, $R'(x)$ is small if the curvature of $\mathbf{S}$ changes slowly with x. Therefore, the smaller the derivative $\kappa'(x)$, the more accurate the circle approximation is. As will become clear in Lemma 1, it is not convenient to use a curve (or surface in general) with a rapidly changing curvature.

For generalization to surfaces, consider first $2{:}N$ mappings. Assume that x_1 and x_2 are parameters in a LoC coordinate representation. Then, according to Theorem 2 in Section A-B2, $g_{12} = b_{12} = 0$, therefore the curvature is $\kappa_i(\mathbf{x}_0) = b_{ii}(\mathbf{x}_0)/g_{ii}(\mathbf{x}_0)$, $i = 1, 2$. Since x_1, x_2, n_1 and n_2 are independent and i.i.d., and we have two orthogonal coordinate curves,

$$\begin{aligned}\varepsilon_{wn}^2(\mathbf{x}_0) &\approx \frac{\sigma_n^2}{2}\sum_{i=1}^{2}\left\{\frac{1}{g_{ii}(\mathbf{x}_0)}\left(1 + \frac{\sigma_n^2}{4}\kappa_i^2(\mathbf{x}_0)\right)\right\} \\ &= \frac{\sigma_n^2}{2}\sum_{i=1}^{2}\left\{\frac{1}{g_{ii}(\mathbf{x}_0)}\left(1 + \frac{\sigma_n^2}{4}\frac{b_{ii}^2(\mathbf{x}_0)}{g_{ii}^2(\mathbf{x}_0)}\right)\right\},\end{aligned} \tag{84}$$

which is a straight forward generalization of the result for $1{:}N$ mappings. For $M{:}N$ mappings, the generalization follows directly as we have M orthogonal curves forming a coordinate grid, and the result is obtained by letting the sum in (84) run from 1 to M. □

3) Proof, Lemma 1: Condition i) is obvious, and can be seen directly from Fig. 4(b).

Condition ii): We begin with $1{:}N$ mappings. From (14) we have $\partial H/\partial x = -2\dot{\mathbf{S}}\cdot(\mathbf{z}-\mathbf{S}) = 0$, implying that $(\mathbf{z}-\mathbf{S}) \perp \dot{\mathbf{S}}$, and $\partial^2 H/\partial x^2 = -2\ddot{\mathbf{S}}(x)\cdot(\mathbf{z}-\mathbf{S}(x)) + 2 = -2\kappa_s\mathbf{p}_n\cdot(\mathbf{z}-\mathbf{S}) + 2 = 0$. The last equality is due to the FoF (64). Also, $\kappa_s = 1/\rho_s$. From (14), $\|\mathbf{z}-\mathbf{S}\| = r$.

$\Rightarrow$: Since $\|\mathbf{p}_n\cdot(\mathbf{z}-\mathbf{S})\| = \|\mathbf{z}-\mathbf{S}\| = r$, this condition follows from $-2\rho_s^{-1}\mathbf{p}_n\cdot(\mathbf{z}-\mathbf{S}) + 2 = 0$.

$\Leftarrow$: If $\rho_s > r$ $\forall x$, the last equation in (14) will not have a real solution.

With the definition of principal curvature in Appendix A-B2 it is straight forward to extend the proof to $M{:}N$ mappings (canal hyper surfaces): The result follows directly from $1{:}N$ case by letting a curve $\mathcal{C}$ be LoC with maximal principal curvature for all points of $\mathcal{S}$. That is, $\mathcal{C}$ is always in the direction of the maximal curvature on $\mathcal{S}$. □

B. Proofs Section III-B

1) Proof Proposition 3: Under Definition 10, the received signal $\hat{\mathbf{x}} = \mathbf{S}(\hat{\mathbf{z}})$ can be approximated by (17), where $J(\mathbf{z}_0)\mathbf{n}$ contributes to the distortion. The MSE per source component given that $\mathbf{z}_0$ was transmitted is then

$$\begin{aligned}\varepsilon_{ch}^2 &= \frac{1}{M}E\big\{(J(\mathbf{z}_0)\mathbf{n})^T(J(\mathbf{z}_0)\mathbf{n})\big\} \\ &= \frac{1}{M}E\bigg\{\left(\frac{\partial S_1}{\partial z_1}n_1 + \cdots + \frac{\partial S_1}{\partial z_N}n_N\right)^2 + \cdots \\ &\quad + \left(\frac{\partial S_M}{\partial z_1}n_1 + \cdots + \frac{\partial S_M}{\partial z_N}n_N\right)^2\bigg\}.\end{aligned} \tag{85}$$

Since noise on each sub-channel is independent, $E\{n_i n_j\} = \sigma_n^2\delta_{ij}$. After some rearrangement,

$$\begin{aligned}\varepsilon_{ch}^2 &= \frac{\sigma_n^2}{M}\bigg(\left[\left(\frac{\partial S_1}{\partial z_1}\right)^2 + \cdots + \left(\frac{\partial S_M}{\partial z_1}\right)^2\right] + \cdots \\ &\quad + \left[\left(\frac{\partial S_1}{\partial z_N}\right)^2 + \cdots + \left(\frac{\partial S_M}{\partial z_N}\right)^2\right]\bigg) \\ &= \frac{\sigma_n^2}{M}\big(g_{11} + g_{22} + \cdots + g_{NN}\big) = \frac{\sigma_n^2}{M}\sum_{i=1}^{N} g_{ii}.\end{aligned} \tag{86}$$

Expectation w.r.t. $\mathbf{z}$ gives the wanted result. □

2) Proof, Proposition 4: With z_0 transmitted, and noise n, we have:

$$\mathbf{S}(z_0+n) \approx \mathbf{S}(z_0) + n\mathbf{S}'(z_0) + \frac{n^2}{2}\mathbf{S}''(z_0) + \frac{n^3}{3!}\mathbf{S}'''(z_0), \tag{87}$$

from the 3rd order Taylor expansion. From this we can derive the *channel distortion* as

$$\varepsilon_{ch}^2(z_0) = E\left\{\left\|n\mathbf{S}'(z_0) + \frac{n^2}{2}\mathbf{S}''(z_0) + \frac{n^3}{3!}\mathbf{S}'''(z_0)\right\|^2\right\}. \tag{88}$$

To expand this expression and take the expectation, it is advantages to use arc-length parametrization (see Appendix A-A).

Then, $\dot{\mathbf{S}}\cdot\ddot{\mathbf{S}}=0$, $\dot{\mathbf{S}}\cdot\dddot{\mathbf{S}}=0$ and $\ddot{\mathbf{S}}\cdot\dddot{\mathbf{S}}=0$ [47, pp. 36-37]. With this in mind, using the fact that $E\{n^a\}=1\cdot 3\cdots(a-1)\sigma_n^a$, a even, and zero otherwise [61, p.148], the expectation in (88) can be found from straight forward calculations

$$\varepsilon_{ch}^2(z_0)=\sigma_n^2\|\dot{\mathbf{S}}(z_0)\|^2+\frac{3\sigma_n^4}{4}\|\ddot{\mathbf{S}}(z_0)\|^2+\frac{5\sigma_n^6}{12}\|\dddot{\mathbf{S}}(z_0)\|^2, \quad (89)$$

where $\|\dot{\mathbf{S}}(x_0)\|=1$ according to Theorem 1 in Appendix A-A. The first term in (89) dominates when σ_n is small if κ and τ are sufficiently small (see Eq. (22)).

Consider scaled arc-length parametrization, i.e., $\|\mathbf{S}'(z_0)\|=\alpha\|\dot{\mathbf{S}}(z_0)\|=\alpha$, $\forall z_0$. Then (63) reduces to $\kappa(z_0)=\|\mathbf{S}_0''\|/\|\mathbf{S}_0'\|^2$ (since $\mathbf{S}_0'\perp\mathbf{S}_0''$, still) and the channel error can be expressed up to 2nd order in terms of the signal curves derivatives as in (20).

For general hyper surfaces the Taylor expansion is a complicated expression, making it hard to draw conclusions. It is more convenient to consider LoC: By choosing LoC as coordinates on a M:2 mapping $\mathcal{S}$, then a direct generalization of the M:1 case results. Assume that z_1 and z_2 are along the LoC. Then, according to Theorem 2, $g_{12}=b_{12}=0$. Therefore $\kappa_i(\mathbf{z}_0)=b_{ii}(\mathbf{z}_0)/g_{ii}(\mathbf{z}_0)$ with g_{ii} and b_{ii} evaluated w.r.t. the channel variables z_i. Then (21) follows. □

3) Proof, Proposition 5: Consider an m-dimensional vector quantizer (VQ) with equal distance among each neighboring centroid, Δ, i.e., a *uniform* VQ. The distortion is then lower bounded by assuming $m-1$-spheres as Voronoi regions [53], [54], i.e., a sphere bound. Let the radius of these spheres be ρ_m. Then we have

Lemma 4: The distortion for an m-dimensional uniform VQ is lower bounded by[5]

$$\bar{\varepsilon}_a^2\geq E\{\|\mathbf{x}-\mathbf{q}(\mathbf{x})\|^2\}=\frac{m}{4(m+2)}\Delta^2, \quad (90)$$

when Δ is small, with $\mathbf{q}(\mathbf{x})$, the centroids of the VQ. □

As the decision borders of a uniform VQ become spherical as $m\to\infty$ [54], [72], equality is obtained in (90) as $m\to\infty$ when Δ is sufficiently small and when $m=1$.

The bound (90) must be modified to entail S-K mappings. Assuming a uniform $\mathcal{S}$, then for each point P on $\mathcal{S}$, all points in the $M-N$ dimensional space orthogonal to $\mathcal{S}$ at P, which will be approximated onto P, will for large M,N, lie within an $M-N-1$-sphere, $\mathbb{S}^{M-N-1}$, with radius $\Delta/2$. This sphere corresponds to the characteristic of the canal surface for $\mathcal{S}$, acting as decision borders for the approximation from $\mathbb{R}^M$ to $\mathcal{S}$. From (14), the characteristic is in the space normal to $\mathcal{S}$ at any point. As the decision borders for any point, P, is an $M-N-1$ sphere, the approximation to an N-dimensional uniform S-K mapping results in the same distortion as that of an $M-N$ dimensional VQ. By substituting $m=M-N$ in (90), dividing by M to obtain distortion per source component, the wanted result is obtained. Further, as $M=N+1$ corresponds to $m=1$ in (90), equality is obtained. □

Proof, Lemma 4: Consider first the special case of high dimensional VQ with spherical Voronoi regions of unit radius $\rho_m=1$, and with one centroid at the origin. If the source variance $\sigma_x>>\rho_m$, then the pdf of $\|\mathbf{x}-\mathbf{q}(\mathbf{x})\|$, $f_{\mathbf{q}}$, will be approximately uniform [53]. Then one may consider an arbitrary centroid to quantify $\bar{\varepsilon}_a^2$. Let $\mathbf{q}(\mathbf{x})=0$ for simplicity, and let B_m denote the volume contained within the relevant Voronoi region (see (97) for analytical expression). Then $f_{\mathbf{q}}=1/B_m, q\in[0,\rho_m]$, and 0 otherwise. Then

$$\bar{\varepsilon}_a^2=\int\cdots\int_{B_m}\|\mathbf{x}\|^2 f_{\mathbf{q}}\mathrm{d}\mathbf{x}=\frac{1}{B_m}\int\cdots\int_{B_m}\|\mathbf{x}\|^2\mathrm{d}\mathbf{x}. \quad (91)$$

From [53, p. 375], we have that the moment of inertia

$$\int\cdots\int_{B_m}\|\mathbf{x}\|^2\mathrm{d}\mathbf{x}=\frac{m}{m+1}B_m. \quad (92)$$

Therefore $\bar{\varepsilon}_a^2=m/(m+1)$. As the quantization error scales with the radius of the Voronoi regions, ρ_m, the distortion $\bar{\varepsilon}_a^2$, will scale with $\rho_m^2=\Delta^2/4$. □

Appendix C
Proofs for Section IV

1) Proof, Proposition 6: Take the dimension reduction case: The minimal distortion for an n:1 system is found by solving (1) w.r.t. D_t, setting $N=1,M=n$,

$$D_{n:1}=\left(\frac{\sigma_x^2}{1+P_{n:1}/\sigma_n^2}\right)^{\frac{1}{n}}. \quad (93)$$

For an m:1 system, simply substitute n with m in (93). With P_t, the total power of the $(m+n)$:2 system, one can allocate power to the two sub-systems through a factor $\kappa\in[0,1]$ so that $P_{n:1}=\kappa P_t$. Let SNR$=P_t/\sigma_n^2$ and use the fact that $1+x\approx x$ as x becomes large. Then,

$$\begin{aligned}&\lim_{\mathrm{SNR}\to\infty}D_{t(m+n:2)}=\\&\lim_{\mathrm{SNR}\to\infty}\frac{\sigma_x^2}{m+n}\left[\left(1+\kappa\mathrm{SNR}\right)^{\frac{1}{n}}+\left(1+(1-\kappa)\mathrm{SNR}\right)^{\frac{1}{m}}\right]\\&=\frac{\sigma_x^2}{m+n}\lim_{\mathrm{SNR}\to\infty}\left[\frac{1}{\kappa^{1/n}\mathrm{SNR}^{1/n}}+\frac{1}{(1-\kappa)^{1/m}\mathrm{SNR}^{1/m}}\right].\end{aligned} \quad (94)$$

According to the laws of limits $\lim_{x\to\infty}\kappa x=\kappa\lim_{x\to\infty}x$, and so the power allocation factor(s) can be moved outside the limit. Then, for $m>n$ since $\mathrm{SNR}^{1/m}$ grows more slowly than $\mathrm{SNR}^{1/n}$, $D_{t(m+n:2)}$ will be dominated by the second term in (94) as SNR$\to\infty$.

In the expansion case, a similar derivation leads to

$$\begin{aligned}&\lim_{\mathrm{SNR}\to\infty}D_{t(2:m+n)}=\\&\frac{\sigma_x^2}{m+n}\lim_{\mathrm{SNR}\to\infty}\left[\frac{1}{\kappa\mathrm{SNR}^n}+\frac{1}{(1-\kappa)\mathrm{SNR}^m}\right].\end{aligned} \quad (95)$$

If $m>n$, the first term in (95) dominates as SNR$\to\infty$. □

2) Proof, Proposition 8: Assume the channel- and noise vectors are normalized with N. With power constrained Gaussian channel, the received vector will lie within an $N-1$ sphere of radius

$$\rho_N=\sqrt{P_N+b_N^2\sigma_n^2}, \quad (96)$$

with high probability. P_N and σ_n^2 denote channel power and noise variance per dimension, respectively. With b_N one takes

[5]Note that (90) differs from the bound derived in [53], since that bound was made invariant with respect to size of the quantizer cells. Here we need the distortion to scale with the cell size so it can depend on the SNR.

into consideration that ρ_N exceeds $\sqrt{P_N+\sigma_n^2}$ for finite N, so $b_N \to 1$ as $N \to \infty$. Let B_n denote the volume inside an $(n-1)$- sphere of unit radius [73]

$$B_n = \frac{\pi^{\frac{n}{2}}}{\Gamma\big(n/2+1\big)}. \tag{97}$$

To satisfy the power constraint then $\text{Vol}(\mathcal{S}^M \times \mathbb{S}^{N-M-1}) \leq B_N \rho_N^N$. Under Definition 12 we have $\mathbb{B}^M \times \mathbb{S}^{N-M-1}$ locally for all points on $\mathcal{S}$. With Gaussian pdf, $\mathbf{x}$ is distributed over $\mathcal{D}_s$ like an M-ball. Further, under Definition 4, in the absence of anomalies, the act of $\mathcal{S}$ is simply a stretching of $\mathcal{D}_s$ (as bending, or cutting, of $\mathcal{S}$ does not affect $\bar{\varepsilon}_{wn}^2$), and thereby the stretching of an M-ball. If $\mathcal{S}$ is shape preserving (Corollary 1), the stretching is the same for all $\mathbf{x} \in \mathcal{D}_s$, and so, equivalent to an amplification factor. Under Definition 12, we can identify this amplification with the radius ρ_M of $\mathbb{B}^M$. Then $\text{Vol}(\mathcal{S}^M \times \mathbb{S}^{N-M-1}) \leq B_N \rho_N^N$ becomes identical to

$$B_M \rho_M^M B_{N-M} \rho_{MN}^{N-M} \leq B_N \rho_N^N, \tag{98}$$

where ρ_{MN} is the canal hyper surface radius and ρ_M is the radius of the stretched source space $\mathcal{D}_s$. Further, assume the same decomposition of $\mathbf{n}$ as in Section III-A2 (see Fig. 4(a)), the M-dimensional tangent to $\mathcal{S}$, $\mathbf{n}_{wn}$ and the $N-M$ dimensional normal $\mathbf{n}_{an}$. To avoid anomalous errors, Proposition 7 states that $\rho_{MN} \geq \|\mathbf{n}_{an}\| = \sqrt{((N-M)/N) b_{NM}^2 \sigma_n^2}$, where $b_{NM} \to 1$ as $M, N \to \infty$. When M, N is large enough, (98) can be written ($b_N = b_{NM} = 1$ as $M, N \to \infty$)

$$B_M \rho_M^M B_{N-M} \left(\frac{N-M}{N}\sigma_n^2\right)^{\frac{N-M}{2}} \leq B_N (P_N+\sigma_n^2)^{\frac{N}{2}}. \tag{99}$$

As explained above, with shape preserving $\mathcal{S}$, $\bar{\varepsilon}_{wn}^2$ is determined by ρ_M. Solving (99) w.r.t. ρ_M,

$$\rho_M \leq \sqrt[M]{\tilde{B}}\sigma_n \left(\frac{1}{1-M/N}\right)^{\frac{N-M}{2M}} \left(1+\frac{P_N}{\sigma_n^2}\right)^{\frac{N}{2M}}, \tag{100}$$

where from (97)

$$\begin{aligned} \tilde{B} &= \frac{B_N}{B_M B_{N-M}} \\ &= \Gamma\left(\frac{N-M}{2}+1\right)\Gamma\left(\frac{M}{2}+1\right)\Big/\Gamma\left(\frac{N}{2}+1\right). \end{aligned} \tag{101}$$

Eqn. (101) can be expressed through the *Beta function* using [57, p. 9]

$$\mathcal{B}(\varrho,\varsigma) = \int_0^1 t^{\varrho-1}(1-t)^{\varsigma-1}\mathrm{d}t = \frac{\Gamma(\varrho)\Gamma(\varsigma)}{\Gamma(\varrho+\varsigma)}, \tag{102}$$

and the *Functional relation* $\Gamma(a+1) = a\Gamma(a)$ [57, p. 3]. Letting $\varrho = (N-M)/2+1$ and $\varsigma = M/2+1$, using the above relations, we obtain

$$\tilde{B} = \left(\frac{N}{2}+1\right)\mathcal{B}\left(\frac{N-M}{2}+1, \frac{M}{2}+1\right) = \left(\frac{N}{2}+1\right)\mathcal{B}_{(N,M)}. \tag{103}$$

As M of N noise components ($\mathbf{n}_{wn}$) contribute to weak noise distortion, we get

$$\bar{\varepsilon}_{wn}^2 = \frac{E\{\|\mathbf{n}_{wn}\|^2\}}{\rho_M^2} = \frac{M\sigma_n^2}{N\rho_M^2}, \tag{104}$$

from (10). With $\rho_{MN} > \|\mathbf{n}_{an}\|$, $\bar{\varepsilon}_{an}^2 = 0$ from Proposition 7. Then $\bar{\varepsilon}_{wn}^2$ is the total distortion D_t. Assume a fixed $r = N/M$. Substituting $M = N/r$ and inserting (100) into (104) then

$$D_t = \frac{1}{r}\left(1-\frac{1}{r}\right)^{r-1}\left(\frac{N}{2}+1\right)^{-\frac{2r}{N}}\mathcal{B}_{(N,r)}^{-\frac{2r}{N}}\left(1+\frac{P_N}{\sigma_n^2}\right)^{-r}, \tag{105}$$

where

$$\mathcal{B}_{(N,r)} = \int_0^1 t^{\frac{N}{2r}(r-1)}(1-t)^{\frac{N}{2r}}\mathrm{d}t. \tag{106}$$

What is left to show is then

$$\lim_{N\to\infty}\left(\frac{N}{2}+1\right)^{-\frac{2r}{N}}\mathcal{B}_{(N,r)}^{-\frac{2r}{N}} = r\left(1-\frac{1}{r}\right)^{1-r}. \tag{107}$$

Using the product rule for limits [74, p.68], the first term on the left in (107) is eliminated since its limit equals 1. Further, using Hölders inequality [75, p. 135-136], we get

$$\mathcal{B}_{(N,r)} \leq \left\|t^{\frac{N}{2r}(r-1)}(1-t)^{\frac{N}{2r}}\right\|_\infty, \tag{108}$$

with equality as $N \to \infty$. By differentiation one find that $t_{max} = 1-1/r$ maximizes the norm in (108), and so, as $N \to \infty$,

$$\mathcal{B}_{(N,r)} = \left(1-\frac{1}{r}\right)^{\frac{N}{2r}(r-1)}\left(\frac{1}{r}\right)^{\frac{N}{2r}}, \tag{109}$$

Raising both sides of (109) to the power $-2r/N$ gives the wanted result. To include σ_x, sets $\rho_M = \alpha\sigma_x$, solve (100) with respect to α, and substitute α for ρ_M in (104). □

3) Proof, Proposition 9: To make $\bar{\varepsilon}_q^2$ small, the canal surface $\mathbf{S} \times \mathbb{S}^{M-N-1}$ should *cover* the source space. Under Definition 12, then locally we have $\mathbb{B}^N \times \mathbb{S}^{M-N-1}$ for all points on $\mathcal{S}$. Under the same reasoning as in the proof of proposition 8, we have

$$B_N \rho_N^N B_{M-N} \rho_{MN}^{M-N} \geq B_M \rho_M^M. \tag{110}$$

$\rho_M = \|\mathbf{x}\| = \sqrt{M b_M^2 \sigma_x^2}$ is the radius of the source-space, $\rho_N = \alpha\sqrt{N(P_N + b_N^2\sigma_n^2)}$ is the radius of the stretched channel space (these are not normalized here), where α is an amplification factor, $\rho_{MN} = \Delta/2$ is the canal surface radius, and $b_M, b_N \to 1$ as $M, N \to \infty$. As in Appendix C-2 these are set to one in what follows. Inserting into (110) and solving w.r.t. α, we obtain

$$\alpha \geq \sqrt{\frac{M^{\frac{M}{N}}}{N}}\tilde{B}^{\frac{1}{N}}\left(\frac{\Delta}{2}\right)^{-\frac{M-N}{N}}\sigma_x^{\frac{M}{N}}\sigma_n^{-1}\left(1+\frac{P_N}{\sigma_n^2}\right)^{-\frac{1}{2}}, \tag{111}$$

where

$$\tilde{B} = \left(\frac{M}{2}+1\right)\mathcal{B}\left(\frac{M-N}{2}+1, \frac{N}{2}+1\right) = \left(\frac{M}{2}+1\right)\mathcal{B}_{(M,N)}, \tag{112}$$

derived in a similar way as in Appendix C-2. Assuming a shape preserving mapping and inserting (111) into (19), an expression for $\bar{\varepsilon}_{ch}^2$ is found. Furthermore, $\bar{\varepsilon}_q^2$ and $\bar{\varepsilon}_{ch}^2$ can be considered independent under Definition 13 as they are perpendicular, thus

$$\begin{aligned} D_t = \bar{\varepsilon}_q^2 + \bar{\varepsilon}_{ch}^2 &= \frac{M-N}{4M(M-N+2)}\Delta^2 + \\ &M^{\frac{M}{N}-1}\tilde{B}^{\frac{2}{N}}\left(\frac{\Delta}{2}\right)^{-2\frac{M-N}{N}}\sigma_x^{2\frac{M}{N}}\left(1+\frac{P_N}{\sigma_n^2}\right)^{-1}. \end{aligned} \tag{113}$$

This is a convex function in Δ, and so a unique minimum exists. Differentiating (113) with respect to Δ, equating to zero and solving for Δ, we obtain

$$\Delta_{opt} = M^{\frac{M-N}{2M}}\left(\frac{4M(M-N+2)}{M-N}\right)^{\frac{N}{2M}} \left(\frac{M-N}{N}\right)^{\frac{N}{2M}} 2^{1-\frac{N}{M}}\tilde{B}^{\frac{1}{M}}\sigma_x\left(1+\frac{P_N}{\sigma_n^2}\right)^{-\frac{N}{2M}}. \tag{114}$$

Inserting (114) and (112) into (113) and using the relation $N = Mr$, with $r \in \mathbb{Q}[0,1]$, we get

$$D_t = \left(1+\frac{r}{1-r}\right)\left(\frac{1-r}{1-r+2/M}\right)^{1-r} \left(\frac{1-r}{r}\right)^{r}\left(\frac{M}{2}+1\right)^{\frac{2}{M}}\mathcal{B}_{(M,r)}^{\frac{2}{M}}\sigma_x^2\left(1+\frac{P_N}{\sigma_n^2}\right)^{-r}. \tag{115}$$

where

$$\mathcal{B}_{(M,r)} = \int_0^1 t^{\frac{M}{2}(1-r)}(1-t)^{\frac{Mr}{2}}\mathrm{d}t. \tag{116}$$

We get rid of two terms as

$$\lim_{M\to\infty}\left[\left(\frac{M}{2}+1\right)^{\frac{2}{M}}, \left(\frac{1-r}{1-r+2/M}\right)^{1-r}\right] = [1,1], \tag{117}$$

using the product rule for limits [74, p.68]. From Hölders inequality [75, p. 135-136], $\mathcal{B}_{(M,r)} \leq (1-r)^{\frac{M}{2}(1-r)}r^{\frac{Mr}{2}}$, with equality when $M \to \infty$, and so

$$\lim_{M\to\infty}\left(1+\frac{r}{1-r}\right)\left(\frac{1-r}{r}\right)^{r}\mathcal{B}_{(M,r)}^{\frac{2}{M}} = \left(1+\frac{r}{1-r}\right)\left(\frac{1-r}{r}\right)^{r}(1-r)^{(1-r)}r^r = 1 \tag{118}$$

□

Appendix D
Proofs for Section V

1) Proof, Lemma 2: The cumulative distribution is given by a straight forward generalization of the $h : \mathbb{R}^2 \to \mathbb{R}$ case in [61, pp. 180-181]. With $\mathbf{x} = (x_1, \cdots, x_3)$

$$F_{z_1}(z_1) = p_r\{\mathbf{x} \in \mathcal{D}_{Z_1}^+ \cup \mathcal{D}_{Z_1}^-\} = \iiint_{\mathcal{D}_{Z_1}^+\cup\mathcal{D}_{Z_1}^-} f_{\mathbf{X}}(\mathbf{x})\mathrm{d}\mathbf{x}, \tag{119}$$

where $f_{\mathbf{X}}(\mathbf{x})$ is the 3D i.i.d. Gaussian distribution and

$$\mathcal{D}_{Z_1}^+ = \big\{\mathbf{x}\big|\|\mathbf{x}\|^n \leq \rho^n, z_1 \geq 0\big\}, \quad \mathcal{D}_{Z_1}^- = \big\{\mathbf{x}\big|\|\mathbf{x}\|^n \geq -\rho^n, z_1 < 0\big\}. \tag{120}$$

Then $f_{z_1}(z_1) = \mathrm{d}F_{z_1}/\mathrm{d}z_1$. As $f_{z_1}(z_1)$ is symmetric about the origin for the DSS, one can consider $\mathcal{D}_{Z_1}^+$ only. Since $\mathcal{D}_{Z_1}^+$ is spherical, it is convenient to integrate in spherical coordinates [76]

$$f_{z_1}(z_1) = \frac{1}{2}\frac{\mathrm{d}}{\mathrm{d}z_1}\int_0^{2\pi}\int_0^{\pi}\int_0^{a\varphi(z_1)} f_\rho(\rho)\rho^2\sin(\theta)\mathrm{d}\rho\mathrm{d}\theta\mathrm{d}\phi, \tag{121}$$

where $f_\rho(\rho) = \exp(-\rho^2/(2\sigma_x^2))/((2\pi)^{3/2}\sigma_x^2)$. The integrals over θ, ϕ become $I_{(\theta,\phi)} = \pi$, and

$$\frac{\mathrm{d}}{\mathrm{d}z_1}\int_0^{a\varphi(z_1)} f_\rho(\rho)\rho^2\mathrm{d}\rho = \frac{1}{(2\pi)^{3/2}\sigma_x^3}\frac{\mathrm{d}}{\mathrm{d}z_1}\int_0^{a\varphi(z_1)} e^{-\frac{\rho^2}{2\sigma_x^2}}\rho^2\mathrm{d}\rho = \frac{na^3\gamma^3 z_1^{3n-1}}{(2\pi)^{3/2}\sigma_x^3}e^{-\frac{a^2\varphi^2(z_1)}{2\sigma_x^2}}. \tag{122}$$

Using absolute value to include negative values, the wanted result is obtained. □

2) Proof, Proposition 10: With b_x sufficiently large, the probability for anomalies becomes small due to the constraint in (51), and the last term in (52) becomes negligible. A constant gap to OPTA at high SNR then implies that

$$D_t = \Delta^2/36 + 2\sigma_n^2\alpha^2/3 = C\cdot\mathrm{SNR}^{-\frac{2}{3}}, \tag{123}$$

with C some constant. We show that such a constant exists, complying with the optimization problem in (54) with D_t as in (123). Let $\beta = \eta\sqrt{2\pi^5}$. As α_3 does not occur explicitly in (123), we eliminate it by equating the constraints in (54) to zero and solving w.r.t. α_3. Then

$$\alpha_3^2 = \frac{\Delta\sigma_x\alpha^2}{\beta(P_t\alpha^2)} = \frac{\Delta^2\alpha^2}{(2b_x\sigma_x + 2b_n\sigma_n\alpha)^2}. \tag{124}$$

From this an equation for α results, $(4b_n^2\sigma_n^2 - P_t\Delta\beta)\alpha^2 + 8b_xb_n\sigma_n\alpha + (4b_x^2 + \Delta\beta) = 0$ (assuming $\sigma_x = 1$). With SNR$= P_t/\sigma_n^2$, the solution is

$$\alpha = \frac{-4b_x \pm \sqrt{\Delta\beta(4\mathrm{SNR}b_xb_n^{-2} + \Delta\beta b_n^{-2}\mathrm{SNR} - 4)}}{b_n\sigma_n(4 - \Delta\beta b_n^{-2}\mathrm{SNR})} \underset{\mathrm{SNR}\to\infty}{\approx} \frac{\pm\sqrt{\Delta\beta\mathrm{SNR}(4b_x^2+\Delta\beta)}}{\Delta\beta\sigma_n\mathrm{SNR}}, \tag{125}$$

where we used $x + \text{constant} \to x$ for large x in the last step. Only the positive solution is viable

$$\bar{\varepsilon}_{ch}^2 = \frac{2\sigma_n^2}{3}\alpha^2 = \frac{2}{3}\frac{4b_x^2+\Delta\beta}{\Delta\beta\mathrm{SNR}}. \tag{126}$$

The distortion contributions should *balance* at high SNR [77], i.e., $\bar{\varepsilon}_{ch}^2 = \bar{\varepsilon}_q^2$, and so $\Delta^2/36 = (C/2)\mathrm{SNR}^{-\frac{2}{3}}$. Therefore $\Delta = 3\sqrt{2}\mathrm{SNR}^{-\frac{1}{3}}$, and from (123) and (126),

$$D_t = 2\bar{\varepsilon}_{ch}^2 = \frac{4}{3}\cdot\frac{4b_x^2 + 3\beta\sqrt{2C}\mathrm{SNR}^{-\frac{1}{3}}}{3\beta\sqrt{2C}\mathrm{SNR}^{-\frac{1}{3}}\mathrm{SNR}} = C\cdot\mathrm{SNR}^{-\frac{2}{3}}. \tag{127}$$

Therefore

$$\frac{4b_x^2}{3\sqrt{2C}\beta\mathrm{SNR}^{-\frac{1}{3}}} = \frac{3C}{4}\mathrm{SNR}^{\frac{1}{3}} - \beta \underset{\mathrm{SNR}\to\infty}{\approx} \frac{3C}{4}\mathrm{SNR}^{\frac{1}{3}}. \tag{128}$$

Solving (128) w.r.t. C, then $C = (16b_x^2/(9\sqrt{2}\beta))^{2/3}$. □

3) Proof, Proposition 11: The Lagrangian for the problem is now

$$\mathcal{L}(\delta,\alpha_2,\lambda) = \frac{\sigma_n^2}{\alpha_2^2} + \lambda_1\left(\frac{\zeta^2\alpha_1^2}{\delta^4} + \frac{\alpha_2^2\delta^2}{12} - P_t\right) + \lambda_2(2b_n\sigma_n - \alpha_1), \tag{129}$$

where $\zeta = 2\eta\pi^2\sigma_x^2$. Equality constraints are assumed, $P_t = 0.5(P_1 + P_2)$ and $\alpha_1 = 2b_n\sigma_n$, as all the power should be

used, and HVQLC should fill the channel space as properly as possible under the given constraints. Solving (58) w.r.t. α_2 we get $\alpha_2 = 12(3P_t/2 - \zeta^2\alpha_1^2/\delta^4)/\delta^2$. Then,

$$\text{SDR} = \frac{\sigma_x^2}{D_t} = \frac{\sigma_x^2\alpha_2^2}{\sigma_n^2} = \frac{12\sigma_x^2}{\sigma_n^2\delta^2}\left(\frac{3P_t}{2} - \frac{\zeta^2\alpha_1^2}{\delta^4}\right) \tag{130}$$

The constrained problem over $\delta, \alpha_1, \alpha_2$ is then converted to an unconstrained problem over δ. By solving $\partial\text{SDR}/\partial\delta = 0$ we get $\delta^* = \sqrt[4]{12\zeta^2 b_n^2/\text{SNR}}$, with $\text{SNR} = P_t/\sigma_n^2$. By inserting this into (130), we get the wanted result. □

4) Proof, Proposition 12: The Lagrangian for the problem is now

$$\begin{aligned}\mathcal{L}(\delta, \alpha_2, \lambda) = \frac{\sigma_n^2}{\alpha_2^2} + \lambda_1\frac{1}{2}\left(\alpha_1^2\sigma_x^2 + \alpha_2^2\frac{M\delta^2}{4(M+2)}\right) - P_t\Bigg) \\ + \lambda_2(2b_{NM}\sigma_n - \alpha_1).\end{aligned} \tag{131}$$

Equality constraints are assumed for the same reason as for 2:3 HVQLC. Solving (61) w.r.t. α_2 and inserting into $D_t = \sigma_n^2/\alpha_2^2$,

$$D_t = \frac{\sigma_n^2}{\alpha_2^2} = \frac{\sigma_n^2\delta^4}{8(1+2/M)(P_t\delta^2 - 2b_{NM}^2\sigma_n^2\sigma_x^2)}. \tag{132}$$

The constrained problem over $\delta, \alpha_1, \alpha_2$ is then converted to an unconstrained problem over δ. By solving $\partial D_t/\partial\delta = 0$ we get $(\delta^*)^2 = 4b_{NM}^2\sigma_n^2\sigma_x^2/P_t$. This implies that $\alpha_1 = 1$, and so $\Delta_{min} = \delta$. By inserting this into (132), with $\text{SNR} = P_t/\sigma_n^2$, we get the wanted result. That $b_{NM} \to 1$ in the limit follows from Proposition 7. □

ACKNOWLEDGMENT

The authors would like to thank the Editor, Vinod Prabhakaran, and the anonymous reviewers for giving us solid feedback that greatly helped improve our manuscript. Our appreciation also goes to Michael Gastpar who gave us highly valuable advice on how to lift the results of this paper to a necessary level of precision and rigor. The authors would also like to thank Yurii Lyubarskii at Dept. of Mathematical Sciences, NTNU, for helpful discussions on mathematical concepts in the early stages of this research.

REFERENCES

[1] P. A. Floor and T. A. Ramstad, "Noise analysis for dimension expanding mappings in source-channel coding," in *7th Workshop on Signal Processing Advances in Wireless Communications*. Cannes, France: IEEE, Jul. 2006.

[2] ——, "Dimension reducing mappings in joint source-channel coding," in *Nordic Signal Processing Symposium*. Reykjavik, Iceland: IEEE, Jun. 2006.

[3] ——, "Optimality of dimension expanding Shannon-Kotel'nikov mappings," in *Information Theory Workshop*. Tahoe City, CA, USA: IEEE, Sep. 2007.

[4] M. Skoglund, N. Phamdo, and F. Alajaji, "Hybrid digital-analog source-channel coding for bandwidth compression/expansion," *IEEE Trans. Information Theory*, vol. 52, no. 8, pp. 3757–3763, Aug. 2006.

[5] F. Hekland, P. A. Floor, and T. A. Ramstad, "Shannon-Kotel'nikov mappings in joint source-channel coding," *IEEE Trans. Commun.*, vol. 57, no. 1, pp. 94–105, Jan. 2009.

[6] E. Akyol, K. B. Viswanatha, K. Rose, and T. A. Ramstad, "On zero-delay source-channel coding," *IEEE Trans. Information Theory*, vol. 60, no. 12, pp. 7473–7489, Dec. 2014.

[7] Y. Hu, J. Garcia-Frias, and M. Lamarca, "Analog joint source-channel coding using non-linear mappings and MMSE decoding," *IEEE Trans. Commun.*, vol. 59, no. 11, Nov 2011.

[8] Y. M. Saidutta, A. Abdi, and F. Fekri, "Joint source-channel coding over additive noise analog channels using mixture of variational autoencoders," *IEEE Journal on Selected Areas in Communications*, vol. Early Access, May 2021.

[9] R. E. Blahut, *Principles and practice of information theory*, first (reprint) ed. Addison-Wesley, 1991.

[10] T. J. Goblick, "Theoretical limitations on the transmission of data from analog sources," *IEEE Trans. Information Theory*, vol. 11, no. 10, pp. 558–567, Oct. 1965.

[11] T. Berger and D. W. Tufts, "Optimum pulse amplitude modulation part I: Transmitter-receiver design and bounds from information theory," *IEEE Trans. Information Theory*, vol. IT-13, no. 2, pp. 196–208, Apr. 1967.

[12] T. A. Ramstad, "On joint source-channel coding for the non-white Gaussian case," in *7th Workshop on Signal Processing Advances in Wireless Communications*. Cannes, France: IEEE, Jul. 2006.

[13] J. Schalkwijk and L. Bluestein, "Transmission of analog waveforms through channels with feedback," *IEEE Trans. Information Theory*, vol. 13, pp. 617–619, 1967.

[14] A. N. Kim and T. A. Ramstad, "Bandwidth expansion in a simple Gaussian sensor network using feedback," in *2010 Data Compression Conference*, IEEE. Snowbird, Utah: IEEE, Mar. 2010, pp. 259–268.

[15] A. Ben-Yishai and O. Shayevitz, "The Gaussian channel with noisy feedback: improving reliability via interaction," in *2015 IEEE International Symposium on Information Theory (ISIT)*. IEEE, 2015, pp. 2500–2504.

[16] M. Gastpar, B. Rimoldi, and M. Vetterli, "To code, or not to code: Lossy source-channel communication revisited," *IEEE Trans. Information Theory*, vol. 49, no. 5, pp. 1147–1158, May 2003.

[17] V. Kostina and S. Verdú, "Lossy joint source-channel coding in the finite blocklength regime," *IEEE Transactions on Information Theory*, vol. 59, no. 5, pp. 2545–2575, May 2013.

[18] N. Merhav, "Threshold effects in parameter estimation as phase transitions in statistical mechanics," *IEEE Trans. Information Theory*, vol. 57, no. 10, pp. 7000–7010, Oct. 2011.

[19] ——, "Weak-noise modulation-estimation of vector parameters," *IEEE Transactions on Information Theory*, vol. 66, no. 5, pp. 3268–3276, May 2020.

[20] Y. Kochman and R. Zamir, "Analog mathching of colored sources to colored channels," *IEEE Trans. Information Theory*, vol. 57, no. 6, pp. 3180–3195, Jun. 2011.

[21] U. Mittal and N. Phamdo, "Hybrid digital-analog (HDA) joint source-channel codes for broadcasting and robust communications," *IEEE Trans. Information Theory*, vol. 48, no. 5, pp. 1082–1102, May 2002.

[22] V. M. Prabhakaran, R. Puri, and K. Ramchandran, "Hybrid digital-analog codes for source-channel broadcast of Gaussian sources over Gaussian channels," *IEEE Transactions on Information Theory*, vol. 57, no. 7, pp. 4573–4588, 2011.

[23] D. McRae, "Performance evaluation of a new modulation technique," *IEEE Trans. Information Theory*, vol. 19, no. 4, pp. 431–445, Aug. 1971.

[24] H. Coward and T. A. Ramstad, "Quantizer optimization in hybrid digital-analog transmission of analog source signals," in *Proc. IEEE Int. Conf. on Acoustics, Speech, and Signal Proc.*, vol. 5. Istanbul, Turkey: IEEE, Jun. 2000, pp. 2637–2640.

[25] M. Kleiner and B. Rimoldi, "Asymptotical optimal joint source-chanel coding with minimal delay," in *Globecom Communication Theory Symposium*. Honolulu, HI: IEEE, Dec. 2009.

[26] S.-Y. Chung, "On the construction of some capacity-approaching coding schemes," Ph.D. dissertation, Massachusetts Institute of Technology, Sep. 2000. [Online]. Available: http://wicl.kaist.ac.kr/pdf/sychung%20phd%20thesis.pdf

[27] T. A. Ramstad, "Shannon mappings for robust communication," *Telektronikk*, vol. 98, no. 1, pp. 114–128, 2002. [Online]. Available: http://www.telenor.com/telektronikk/volumes/pdf/1.2002/Page_114-128.pdf

[28] C. Thomas, C. May, and G. Welti, "Hybrid amplitude-and-phase modulation for analog data transmission," *IEEE Trans. Commun.*, vol. 23, no. 6, pp. 634–645, Jun. 1975.

[29] Z. Xuan and K. Narayanan, "Low-delay analog joint source-channel coding with deep learning," *IEEE Transactions on Communications*, vol. 71, no. 1, pp. 40–51, 2023.

[30] C. E. Shannon, "Communication in the presence of noise," *Proc. IRE*, vol. 37, pp. 10–21, Jan. 1949.

[31] V. A. Kotel'nikov, *The Theory of Optimum Noise Immunity*. New York: McGraw-Hill Book Company, Inc, 1959.

[32] J. Ziv, "The behavior of analog communication systems," *IEEE Transactions on Information Theory*, vol. 16, no. 5, pp. 587–594, 1970.

[33] V. A. Vaishampayan, "Combined source-channel coding for bandlimited waveform channels," Ph.D. dissertation, University of Maryland, 1989.

[34] V. A. Vaishampayan and S. I. R. Costa, "Curves on a sphere, shift-map dynamics, and error control for continuous alphabet sources," *IEEE Trans. Information Theory*, vol. 49, no. 7, pp. 1658–1672, Jul. 2003.

[35] J. M. Lervik, A. Fuldseth, and T. A. Ramstad, "Combined image subband coding and multilevel modulation for communication over power- and bandwidth limited channels," in *Proc. Workshop on Visual Signal Processing and Communications*. New Brunswick, NJ, USA: IEEE, Sep. 1994, pp. 173–178.

[36] A. Fuldseth and T. A. Ramstad, "Bandwidth compression for continuous amplitude channels based on vector approximation to a continuous subset of the source signal space," in *Proc. IEEE Int. Conf. on Acoustics, Speech, and Signal Proc.*, 1997.

[37] K.-H. Lee and D. P. Petersen, "Optimal linear coding for vector channels," *IEEE Trans. Commun.*, vol. COM-24, no. 12, pp. 1283–1290, Dec. 1976.

[38] X. Cai and J. W. Modestino., "Bandwidth expansion shannon mapping for analog error-control coding," in *40th Annual Conference on Information Sciences and Systems*. IEEE, Mar. 2006.

[39] F. Hekland, "On the design and analysis of Shannon-Kotel'nikov mappings for joint source-channel coding," Ph.D. dissertation, Norwegian University of Science and Engineering (NTNU), 2007.

[40] P. A. Floor, "On the theory of Shannon-Kotel'nikov mappings in joint source-channel coding," Ph.D. dissertation, Norwegian University of Science and Engineering (NTNU), 2008. [Online]. Available: https://ntnuopen.ntnu.no/ntnu-xmlui/handle/11250/249749

[41] T. A. Ramstad and K. Rose, "Optimization of sample-by-sample transmission of non-Gaussian signals over non-Gaussian channels," in *International Conference on Recent Advances in Telecommunications (RACE'08)*, Osmania University, Hyderabad, Dec. 2008.

[42] B. Chen and G. W. Wornell, "Analog error-correcting codes based on chaotic dynamical systems," *IEEE Trans. Commun.*, vol. 46, no. 7, pp. 881–890, Jul. 1998.

[43] J. M. Wozencraft and I. M. Jacobs, *Principles of Communication Engineering*. New York: John Wiley & Sons, Inc, 1965.

[44] N. S. Jayant and P. Noll, *Digital Coding of Waveforms*. Prentice-Hall Inc. Englewood Cliffs, 1984.

[45] P. A. Floor, A. N. Kim, T. A. Ramstad, I. Balasingham, N. Wernersson, and M. Skoglund, "On joint source-channel coding for a multivariate Gaussian on a Gaussian MAC," *IEEE Transactions on Communications*, vol. 63, no. 5, pp. 1824–1836, May 2015.

[46] P. A. Floor and T. A. Ramsted, "Tools for analysis of Shannon-Kotel'nikov mappings," 2022, arXiv:2107.08526v2 [cs.IT]. [Online]. Available: https://arxiv.org/abs/2107.08526v2

[47] E. Kreyszig, *Differential Geometry*. Dover Publications, Inc., 1991.

[48] M. Spivak, *A Comprehensive Introduction to Differential Geometry, Vol. 2*, 3rd ed. Publish or Perish, Houston Texas, Inc, 1999.

[49] C. Therrien, *Discrete Random Signals and Statistical Signal Processing*. Prentice Hall, 1992.

[50] D. J. Sakrison, *Communication Theory: Transmission of Waveforms and Digital Information*. New York: John Wiley & Sons, Inc, 1968.

[51] P. A. Floor, T. A. Ramstad, and N. Wernersson, "Power constrained channel optimized vector quantizers used for bandwidth expansion," in *International Symposium on Wireless Communication Systems*. Trondheim, Norway: IEEE, Oct. 2007.

[52] M. Spivak, *A Comprehensive Introduction to Differential Geometry, Vol. 1*, 3rd ed. Publish or Perish, Houston Texas, Inc, 1999.

[53] A. Gersho, "Asymptotically optimal block quantization," *IEEE Trans. Information Theory*, vol. 25, no. 4, pp. 373–380, Jul. 1979.

[54] J. H. Conway and N. J. A. Sloane, *Sphere Packings, Lattices and Groups*. Springer Verlag, 1999.

[55] T. M. Cover and J. A. Thomas, *Elements of Information Theory*. New York: Wiley, 2006.

[56] H. Cramér, *Mathematical Methods of Statistics*, first (reprint) ed. Princeton University Press, 1951.

[57] H. Bateman, *Higher Transcendental Functions*, F. O. Arthur Erdélyi, Wilhelm Magnus and F. G. Tricomi, Eds. McGraw-Hill book company, Inc, 1953, vol. One.

[58] P. A. Floor, A. N. Kim, T. A. Ramstad, and I. Balasingham, "On transmission of multiple Gaussian sources over a Gaussian MAC using a VQLC mapping," in *Information Theory Workshop (ITW)*. Lausanne, Switzerland: IEEE, Sept. 3rd-7th 2012.

[59] J. M. Lervik, "Subband image communication over digital transparent and analog waveform channels," Ph.D. dissertation, NTNU, 1996.

[60] S. N. Krivoshapko and V. N. Ivanov, *Encyclopedia of Analytical Surfaces*. Springer International Publishing Switzerland, 2015.

[61] A. Papoulis and S. U. Pillai, *Probability, Random Variables and Stochastic Processes*, 4th ed. New York: McGraw-Hill higher education, Inc, 2002.

[62] A. Edwards, "Gilberts sine distribution," *Teaching Statistics*, vol. 22, no. 3, pp. 70–71, 2000.

[63] P. A. Floor, A. N. Kim, N. Wernersson, T. Ramstad, M. Skoglund, and I. Balasingham, "Zero-delay joint source-channel coding for a bivariate Gaussian on a Gaussian MAC," *IEEE Trans. Commun.*, vol. 60, no. 10, Oct. 2012.

[64] A. Fuldseth, "Robust subband video compression for noisy channels with multilevel signaling," Ph.D. dissertation, Norwegian University of Science and Engineering (NTNU), 1997.

[65] M. S. Mehmetoglu, E. Akyol, and K. Rose, "Deterministic annealing-based optimization for zero-delay source-channel coding in networks," *IEEE Transactions on Communications*, vol. 63, no. 12, pp. 5089–5100, Dec. 2015.

[66] P. A. Floor, A. N. Kim, T. Ramstad, and I. Balasingham, "Zero delay joint source channel coding for multivariate Gaussian sources over orthogonal Gaussian channels," *Entropy*, vol. 15, no. 6, pp. 2129–2161, Jun. 2013.

[67] J. J. Callahan, *The Geometry of Spacetime: An Introduction to Special and General Relativity*, S. Axler, F. W. Gehring, and K. A. Ribet, Eds. New York: Springer-Verlag, Inc, 2000.

[68] Wikipedia contributors, "Frenet-serret formulas— Wikipedia, the free encyclopedia," [Online; accessed 11-October-2022]. [Online]. Available: https://en.wikipedia.org/wiki/FrenetSerret_formulas

[69] G. Strang, *Linear Algebra and its Applications*, 3rd ed. Harcourt Brace Jovanovich, 1988.

[70] K. Rottmann, *Mathematische Formelsammlung*. Bibliographisches Institut & F. A. Brockhaus, 1991.

[71] P. Jupp and K. Mardia, *Directional Statistics*, ser. Wiley Series in Probability and Statistics. Wiley, 2000.

[72] R. Zamir and M. Feder, "On lattice quantization noise," *IEEE Trans. Information Theory*, vol. 42, no. 4, pp. 1152–1159, Jul. 1996.

[73] Wikipedia contributors, "m-sphere— Wikipedia, the free encyclopedia," [Online; accessed 26-December-2020]. [Online]. Available: https://en.wikipedia.org/wiki/N-sphere#Closed_forms

[74] C. H. Edwards and D. E. Penney, *Calculus with analytic geometry*. Prentice-Hall, Inc., 1998.

[75] C. Gasquet and P. Witomski, *Fourier Analysis and Applications*, 1st ed., M. G. J.E. Marsden, L. Sirovich and W. Jäger, Eds. Springer-Verlag New York, Inc, 1999.

[76] W. D. Richter, "Generalized spherical and simplicial coordinates," *Journal of Mathematical Analysis and Applications*, vol. 336, pp. 1187–1202, 2007.

[77] F. Hekland, G. E. Øien, and T. A. Ramstad, "Using 2:1 Shannon mapping for joint source-channel coding," in *Proc. Data Compression Conference*, IEEE. Snowbird, Utah: IEEE Computer Society Press, Mar. 2005, pp. 223–232.